ROMA TRE
UNIVERSITÀ DEGLI STUDI

DIPARTIMENTO DI MATEMATICA E FISICA

Shaking the square box: a PCA approach to the Ising model

Tesi di dottorato in matematica

XXXIII Ciclo

Candidato:

Valentina Apollonio

Relatore di tesi:

Prof.ssa Elisabetta Scoppola

Coordinatore:

Prof. Angelo Felice Lopez

Anno Accademico 2020-2021

Dipartimento di Matematica e Fisica, Università Roma Tre

Largo San Leonardo Murialdo 1, 00146, Roma

Contents

Preamble

During the three years of my Ph.D. I had the fruitful opportunity to take part in the activities of two independent research groups. These two collaborations are interconnected even if they deal with different research topics. In particular, at the beginning of my Ph.D. course I started to study a reversible parallel dynamics, called *shaken dynamics*, introduced in [3] jointly with R. D'Autilia, B. Scoppola, E. Scoppola and A. Troiani. This dynamics is inspired by a collection of probabilistic cellular automata on spin systems, considered in previous papers [36, 37, 84, 65], characterized by the presence of an inertial term q preventing the simultaneous update of a too large set of spins. In particular, the shaken dynamics is the composition of two consecutive parallel updating defined through a pair Hamiltonian $H(\sigma, \tau)$ which contains an asymmetric interaction with the neighboring spins associated to an interaction weight J plus a self-interaction controlled by the inertial parameter q and, possibly, an external magnetic field λ.

The shaken dynamics allows to extend the results obtained in [36, 84]. Indeed, we control explicitly its invariant measure π on general graphs and with non zero external field. Moreover, in the case of the square lattice we identify the invariant measure for different boundary conditions.

Besides the robust control of the stationary measure, the shaken dynamics is characterized also by a peculiar interplay among different geometries. Indeed, the introduction of a pair Hamiltonian in the definition of the dynamics has interesting effects on the geometry of the system. First, the configuration space is doubled and it is possible to define a new interaction graph, called *doubling graph* which has a different geometry with respect to the one of the original graph and is bipartite by construction. In particular, the shaken dynamics turns out to be the marginal of a parallel alternate dynamics on the Ising model defined on the doubling graph.

The geometry of the system can be tuned also by changing the self-interaction parameter q.

This approach is completely new. Namely, considering the limits $q \to 0$ and $q \to \infty$ we are able to interpolate between different geometries of the doubling graph. More precisely, when q tends to zero the corresponding edge in the doubling graph is cutted, whereas when q tends to infinity the two extremal vertices of the corresponding edge collapse. In both cases a new doubling graph is obtained. Finally, taking the self-interaction parameter q to be equal to the interaction parameter J, the doubling graph becomes homogeneous.

The geometric interpolation induced by the shaken dynamics inspired a second research project with V. Jacquier, F. R. Nardi and A. Troiani concerning the study of the metastability for the 2d Ising model on the homogeneous hexagonal lattice. Indeed, when the original graph is the regular square lattice, the shaken dynamics turns out to be the marginal of an alternate dynamics on the Ising model defined on the non homogeneous hexagonal lattice. Thus, the analysis of the metastability for the 2d Ising model on the homogeneous hexagonal lattice wants to be a first step towards the study of the convergence to equilibrium of the parallel alternate dynamics associated to the shaken dynamics in the low temperature regime and at fixed volume, when the original graph is the regular square lattice.

The organization of the thesis reflects the journey of my Ph.D. course. Indeed, it is divided into two independent parts:

I) **The Shaken dynamics**
Chapter 1 provides an introduction to the shaken dynamics. In particular, the motivations that inspired this research project are introduced. In addition, a formal definition of the dynamics and the main results obtained jointly with R. D'Autilia, B. Scoppola, E. Scoppola and A. Troiani in the paper [2] and in the preprint [3] are provided. Chapter 2 is devoted to proofs and discussions.

II) **Metastability for the Ising model on the homogeneous hexagonal lattice**
Chapter 3 provides an introduction to the problem of metastability for the 2d Ising model. In particular, the motivations that inspired the study of metastability are introduced. In addition, a formal definition of the model and the main results of the preprint [4], which is a joint work with V. Jacquier, F. R. Nardi and A. Troiani are provided.
Chapter 4 contains the proof of those theorems related to metastability, while in Chapter 5 the results concerning *polyiamonds* are given with the intent of providing a self contained set of tools that may be of use whenever the volume-surface competition plays a role in determining the properties of a statistical mechanics system living on the hexagonal lattice.

1 The Shaken dynamics

1.1 Motivations

According to plate tectonics, Earth's litosphere is broken into many pieces, called *plates*. These fragments lie on Earth's mantle, moving relative to one another and relative to the underlying mantle. In particular plates move at different velocities and these velocity gradients are responsible for earthquakes occurrence at plate boundaries. The relative movement of fault planes and the associated energy release show a characteristic pattern when considered as a function of time. Indeed, fault planes move relative one to another, not smoothly, but their motion exhibits a peculiar trend characterized by a loading phase followed by a sudden (with respect to the loading time scale) displacement with consequent energy release (see Fig. 1.1). This pattern, in jerks known as *stick-slip*, is quite universal and it appears in a variety of natural phenomena ranging from the sound produced by a bowed violin string to the one coming from a creaking door, from screeching brakes to the sound of tearing and grinding teeth.

All the previous systems, and in particular earthquake events, concern two mechanical objects sliding one relative to another, affected by friction at the contact interface. Therefore, understanding friction mechanism turns out to be a key step to get an insight into those phenomena governed by stick-slip dynamics.
A wide range of sliding friction models may be found in the literature. Mainly, most of them are based on Newtonian and classical dynamics and differ in the theoretical approach they apply. Here we provide a short review on the current models in tribological theory and refer to the rich Colloquium [91] for a further discussion on friction modeling.
In *minimalistic* models the studies are restricted to describe microscopic dynamics in terms of a very small number of degrees of freedom and the resulting equations of motion are those

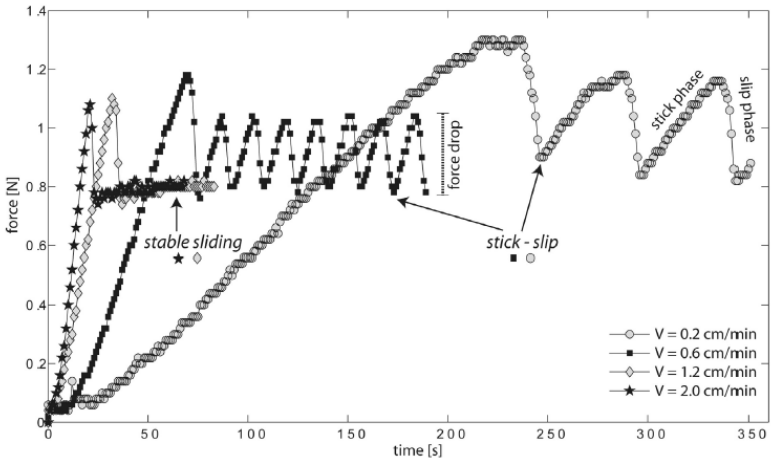

Figure 1.1 Typical time series of shear force values recorded by a digital force sensor for a gelatin–sand paper system considered in [35].

characterizing one or two dimensional systems. Among these models, the most successful are certainly the Prandl-Tomlinson (PT) [83, 90] and the Frenkel-Kontorova (FK) [49] models. PT model assumes that a point mass m is dragged over a one-dimensional periodic potential by means of a spring of effective elastic constant k with a constant velocity v_0 (see Fig 1.2a). Thermal effects can be taken into account by adding a viscous damping term $\eta\dot{x}$ and a random force $\Gamma(t)$. The associated equation of motion is

$$m\ddot{x} = k(v_0 t - x) - \eta\dot{x} - U_0 \sin(2\pi x/a) + \Gamma(t)$$

where x is the coordinate of the particle, U_0 the amplitude of the periodic force and a the spatial period of the potential. This model is, probably, the most widely used in the interpretation of tribological experiments due to its simplicity and ability of accounting for the main physical features of atomic-scale friction.
FK model describes a one dimensional chain of N harmonically coupled particles placed into a periodic potential (see Fig. 1.2b). The Hamiltonian of the model is

$$H = \sum_i \left[\frac{p_i^2}{2m} + \frac{k}{2}(x_{i+1} - x_i - a_c)^2 + \frac{U_0}{2}\cos\frac{2\pi x_i}{a_b} \right].$$

The parameters k and a_c identify respectively the elastic constant and the equilibrium distance of the harmonic interaction among the nearest neighbors in the chain, whereas the parameters U_0 and a_b represent the amplitude and the spatial period of the external potential. One of the main interesting features characterizing the static and dynamic properties of the FK model is the competition between the harmonic interaction among the particles and the substrate

periodic potential. Indeed, if the former favors a uniform separation a_c between particles, the latter tends to pin the atom positions to the bottom of the wells, evenly spaced by the period a_b. This competition is often referred to as frustration.
Even though both PT and FK models can account for many physical properties of atomic-scale friction, their simple mechanical descriptions can provide only qualitative interpretations of the underlying tribological processes.

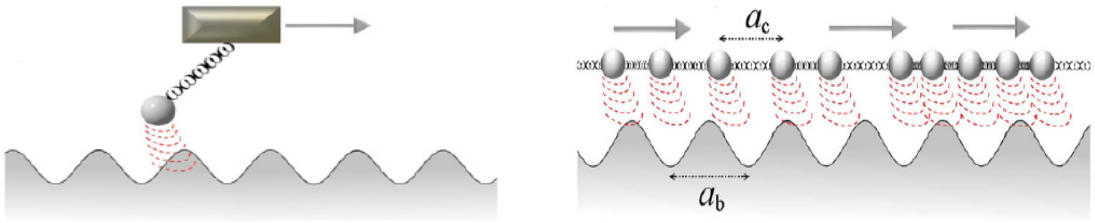

(a) **(b)**

Figure 1.2 The Prandl-Tomlinson model (a) and the Frenkel-Kontorova model (b).

Recent experimental studies of dynamics of cold welds [17] and adhesive boundary lubrication [40] have suggested that macroscopic friction might be the result of the formation and rupture of a huge number of microscopic bonds that form between surfaces in close vicinity. Furthermore, these findings indicate that stick-slip motion is connected to a collective behavior of the bonds [17]. A class of models, known as *multicontact* models, leverage on these experimental results and provide an alternative approach to the study of friction. Indeed, the description of sliding motion is given in terms of dynamical formation and rupture of elastically coupled contacts. Usually, each contact is modeled as an elastic spring connecting a slider and the underlying surface. Intact contacts go on stretching with a speed equal to the velocity of the slider and motion is inhibited until a critical threshold of rupture is reached. Once the contact is broken, it relaxes rapidly to its unstretched equilibrium state.
As a representative for this class we mention the Burridge-Knopoff (BK) model [18] for earthquakes. In BK model a set of frictional blocks of mass M coupled by springs is driven over a substrate (see Fig 1.3). In one dimension, the equation of motion for the displacement u_i of block i is given by

$$M\ddot{u}_i = k_0(u_{i+1} + u_{i-1} - 2u_i) + k_d(u_i - ia - vt) + f(\dot{u}_i)$$

where k_0 and k_d are the stiffnesses of the springs connecting the blocks between themselves and with the loading plate that moves at constant velocity v. Here a is the rest length of the springs connecting the blocks and $f(v)$ is a phenomenological friction force that weakens as the velocity of the block increases. The Burridge-Knopoff model shows a very rich dynamical

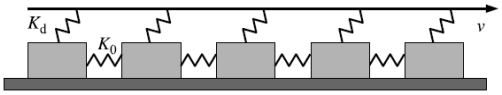

Figure 1.3 The Burridge-Knopoff model.

behavior with widely distributed slip events. Even though multicontact models allow to extend the results obtained in minimalistic models, one main problem of their approach is the multiplicity of empirical parameters they involve. Moreover the microscopic mechanism underlying the collective behavior of the bonds is an open problem.
Despite the growing efforts in understanding friction behavior and the advanced technologies (such as molecular dynamics simulations), most of the present models rely on phenomenological laws and a microscopic theory of friction is still lacking.
One of the main difficulties in understanding and predicting frictional response is the complexity of highly nonequilibrium processes going on in any tribological contact and the associated difficulty to treat nonequilibrium problems within traditional mechanics theory.
We propose an alternative approach to understand friction mechanism via a statistical mechanics model.

A mechanical system consisting of two sliding surfaces may be considered as a macroscopic system composed by a large number of interacting microscopic constituents representing its contact bonds. In particular, the macroscopic features observed in this system, indicating a collective behavior of the bonds, may be related to the properties of its microscopic constituents via the powerful probabilistic approach of Statistical Mechanics, providing a microscopic justification for stick-slip motion.
In this spirit, we represent the contact interface between two sliding surfaces via a finite simple graph $G = (V, E)$. A spin variable $\sigma(x) = \{-1, +1\}$ may be associated to each element $x \in V$. The spins at the vertices of V correspond to the microscopic bonds joining together the two sliding surfaces and they are responsible for sliding properties and inertia. If $\sigma(x) = -1$ we say that the bond at x is *intact* and the surfaces are locally locked at x, whereas if $\sigma(x) = +1$ we say that the bond is *broken* and the surfaces may locally move from x.
We are interested in constructing a Markovian dynamics for this spin system on arbitrary graphs $G = (V, E)$. The spin updating rule may be defined in terms of an Ising-like Hamiltonian. The value of the parameters in the Hamiltonian can be tuned to take into account different physical aspects:

1. one may consider a nearest neighbor interaction where the interaction parameter J may be constant or it may depend on the spin position. It is reasonable to choose $J > 0$. A positive J accounts for the tendency of the spins to be aligned with each other;

2. one can also consider the action of an external field, which may be constant or may depend on time and position. This parameter takes into account the strain produced by the relative sliding of the two surfaces acting either as a stress component which contributes to the bonds rupture or as an ordering component which restores the broken bonds.

The dynamics should be *parallel*, *i.e.* the spins must be synchronously updated in discrete time steps. This seems to be a quite natural choice from a physical point of view. Indeed, it is reasonable to think that the bonds along the contact interface can either break or fix themselves simultaneously depending only on the current state of their neighborhood. On the other hand, parallel Markovian dynamics on finite volume are a challenging topic in MCMC methods and Statistical Mechanics and the relative literature is quite vast. These algorithms may be naturally implemented both on distributed architectures (*e.g.*, computing clusters) and on massively parallel architectures (*e.g.*, GPUs) and the efficiency of parallel computing can be exploited in their simulation.
Motivated by these broad perspective, we define a parallel dynamics, the *shaken dynamics*, for a class of spin systems on general interaction graphs, we investigate its properties in the context of Equilibrium Statistical Mechanics and extend some results obtained in previous works (see [36, 37, 84]).

1.2 Parallel dynamics and pair Hamiltonians: a short review on the literature

From a theoretical point of view, studies on parallel dynamics imply two natural questions:

- Is it possible to control their invariant measure?
- How fast is their convergence to equilibrium?

Indeed, parallelization can drastically change the relaxation time. In some particular cases of dynamics updating all the spins at every step, rigorous results are available. We mention here two examples where the efficiency of parallel dynamics has been proved to be clearly higher than the efficiency of single-spin-flip dynamics. The first relevant example is given by the Swendsen-Wang (SW) cluster dynamics where a polynomial relaxation time in the size of the problem is proven [55]. Another particular example is given in [37] where an irreversible parallel dynamics related to the 2d Ising model is introduced in terms of a Probabilistic Cellular Automaton (PCA) (see definition(1.2.1) below). In this second example, the control of the mixing time is given in a particular regime of low-temperature in a finite box of

side L with periodic boundary conditions and the mixing time turns out to be polynomial in L.

The control of the invariant measure for parallel dynamics is a difficult task too. Hereafter we refer to the case of parallel Markovian dynamics introduced in terms of *Probabilistic Cellular Automata* (PCA), *i.e.* homogeneous discrete time Markov chains on a product space S^V with transition probabilities:

$$P(\sigma,\tau) := \prod_{i\in V} p_i(\tau_i|\sigma) \tag{1.2.1}$$

where $p_i(\tau_i|\sigma)$ is a probability on S for all $i \in V$ and $\sigma \in S$. Given a probability measure μ on S^V, the question is whether it is possible to construct a PCA whose stationary measure is μ. Usually we are interested in the case in which μ is a Gibbs measure. While Markov Chains with sequential dynamics having these features can always be constructed, the existence of a PCA with the given invariant measure μ is not granted. We shortly recall some related results. In [44] examples of infinite volume PCA whose invariant measures are not Gibbsian are provided. In [28] it has been proved that, in general, the stationary measure defined by a local PCA may be rather different from the Gibbs measure, giving rise to stable chessboard configurations.
In [64] explicit conditions on the measure μ for the existence of a reversible, with respect to μ, and ergodic PCA are provided and it is shown that no PCA can be designed in such a way to be reversible with respect to the stationary distribution of a 2d Ising model. In [67, 28] a PCA with a heat bath updating rule for the standard Ising interaction is defined as follows: spins on the even (odd) sublattice, *i.e.* those $(i,j) \in \mathbb{Z}^2$ with $i+j$ even (odd), are simultaneously updated at even (odd) times. The invariant measure of this Markov chain is proved to be a Gibbs measure, however it turns out to be completely different with respect to the Gibbs measure defined with the standard Ising Hamiltonian.
Following the ideas introduced in [58], a simple way to modify and extend the PCA in [28], is presented in [36]. The invariant measure of this PCA is proved to converge, in the thermodynamic limit, to the Gibbs measure of the Ising model at high temperature. In [84] a similar result is obtained in the low-temperature regime.

Both in [36] and [84] pair Hamiltonians turn out to be a necessary ingredient to define the dynamics. This is still true in the shaken dynamics.
In [36], the Hamiltonian of the 2d Ising model defined on a finite volume $V \subset \mathbb{Z}^2$ with symmetric ferromagnetic interaction $J_{ij} = J_{ji}\ \forall\ i,j \in V$, zero external field and empty

boundary conditions

$$H(\sigma) = -\sum_{\substack{i,j\in V:\\ i\neq j}} J_{ij}\sigma_i\sigma_j \tag{1.2.2}$$

is *lifted* to the pair Hamiltonian

$$H(\sigma,\sigma') = -\sum_{\substack{i,j\in V:\\ i\neq j}} J_{ij}\sigma_i\sigma'_j + q\sum_{i\in V}(1-\sigma_i\sigma'_i) \tag{1.2.3}$$

where $q > 0$. Clearly, the Hamiltonian (1.2.3) is symmetric, *i.e.* $H(\sigma,\tau) = H(\tau,\sigma)$, by definition. The PCA dynamics, introduced via the following transition probability

$$P^{\text{PCA}}(\sigma,\tau) := \frac{e^{-H(\sigma,\tau)}}{Z_\sigma} \qquad \text{with} \qquad Z_\sigma := \sum_{\sigma'} e^{-H(\sigma,\sigma')} = w^{\text{PCA}}(\sigma) \tag{1.2.4}$$

is reversible with respect to the measure

$$\pi^{\text{PCA}}(\sigma) = \frac{\sum_\tau e^{-H(\sigma,\tau)}}{\sum_{\tau,\tau'} e^{-H(\tau,\tau')}} \equiv \frac{w^{\text{PCA}}(\sigma)}{\sum_\tau w^{\text{PCA}}(\tau)} = \frac{w^{\text{PCA}}(\sigma)}{Z^{\text{PCA}}} \tag{1.2.5}$$

which turns out to be the marginal of the Gibbs measure on the space of pairs of configurations

$$\mu_2(\sigma,\tau) = \frac{e^{-H(\sigma,\tau)}}{Z^{\text{PCA}}}. \tag{1.2.6}$$

Moreover, it is shown that when the volume goes to infinity, $|V| \to \infty$, the total variation distance between π^{PCA} and the usual Gibbs measure π^G, associated to the Ising Hamiltonian (1.2.2) at high temperature, goes to zero when q is such that the mean density of flipped spins, $\delta := e^{-2q}$, satisfies $\lim_{|V|\to\infty} \delta^2|V| = 0$. The main tool used in the proof for the convergence is the Dobrushin uniqueness Theorem.
In [84] a similar result in the low-temperature regime is proved via a polymer expansion based on suitably defined Peierls-type contours in the following cases, always assuming a zero external field:

- with plus boundary conditions in the reversible case (*ie.* with symmetric pair Hamiltonian);
- with periodic boundary conditions in the reversible case;
- with periodic boundary conditions in the irreversible case.

In the irreversible case, when $H(\sigma,\tau) \neq H(\tau,\sigma)$, the identification of the stationary measure of the dynamics follows immediately from the following *weak symmetry condition*

$$\sum_{\tau\in\mathcal{X}} e^{-H(\sigma,\tau)} = \sum_{\tau\in\mathcal{X}} e^{-H(\tau,\sigma)}. \tag{1.2.7}$$

The arguments in the proof of identity (1.2.7) are based on Peierls-type contours suitably defined and they strongly rely on the translational invariance of the system (*i.e.*, periodic boundary conditions). This is the reason why the case of plus boundary conditions turns out to be not feasible.
The shaken dynamics extend the results of [36, 84]. First, the dynamics can be defined on general graphs, other than the square lattice considered in the previous works. Moreover, the control of the invariant measure is much more robust including the case of non-zero external field and different boundary conditions.

1.3 Definition of the dynamics

In this Section we give the formal definition of the shaken dynamics both on the square lattice $\mathbb{Z}^2$ and on arbitrary graphs and we present the results obtained in [3, 2].

1.3.1 The dynamics on $\mathbb{Z}^2$

Let Λ be a two-dimensional $L \times L$ square lattice in $\mathbb{Z}^2$ and let $\mathcal{B}_\Lambda$ denote the set of all nearest neighbors in Λ with periodic boundary conditions. We denote by $\mathcal{X}_\Lambda$ the set of spin configurations in Λ, *i.e.*, $\mathcal{X}_\Lambda = \{-1,+1\}^\Lambda$.
We identify a subset $B \in \Lambda$ where the spins are frozen throughout the evolution, providing the boundary conditions. This means that we will consider the state space $\mathcal{X}_{\Lambda,B} = \{\sigma \in \mathcal{X}_\Lambda : \sigma_x = +1 \quad \forall x \in B\}$.

To introduce the Markov chain defining the dynamics, following the same ideas used in [36, 65, 84], we consider the pair (doubled) Hamiltonian with asymmetric interaction

$$\begin{aligned} H(\sigma,\tau) &= -\sum_{x\in\Lambda} \left[J\sigma_x(\tau_{x^\uparrow} + \tau_{x^\rightarrow}) + q\sigma_x\tau_x + \lambda(\sigma_x+\tau_x)\right] \\ &= -\sum_{x\in\Lambda} \left[J\tau_x(\sigma_{x^\downarrow} + \sigma_{x^\leftarrow}) + q\tau_x\sigma_x + \lambda(\sigma_x+\tau_x)\right] \end{aligned} \tag{1.3.1}$$

where $x^\uparrow, x^\rightarrow, x^\downarrow, x^\leftarrow$ are, respectively, the up, right, down, left neighbors of the site x on the torus $(\Lambda, \mathcal{B}_\Lambda)$, $J > 0$ is the ferromagnetic interaction, $q > 0$ is an inertial constant and λ

represents an external field. We can write

$$H(\sigma,\tau) = -\sum_{x\in\Lambda}\sigma_x h^{ur}(\tau) - \lambda\sum_{x\in\Lambda}\tau_x = -\sum_{x\in\Lambda}\tau_x h^{dl}(\sigma) - \lambda\sum_{x\in\Lambda}\sigma_x \tag{1.3.2}$$

where the local up-right field $h^{ur}_x(\tau)$ due to the configuration τ is given by

$$h^{ur}_x(\tau) = \Big[J(\tau_{x^\uparrow} + \tau_{x^\rightarrow}) + q\tau_x + \lambda\Big] \tag{1.3.3}$$

and the local down-left field $h^{dl}_x(\sigma)$ due to the configuration σ is given by

$$h^{dl}_x(\sigma) = \Big[J(\sigma_{x^\downarrow} + \sigma_{x^\leftarrow}) + q\sigma_x + \lambda\Big] \tag{1.3.4}$$

Define the asymmetric updating rule

$$P^{dl}(\sigma,\tau) := \frac{e^{-H(\sigma,\tau)}}{\overrightarrow{Z}_\sigma} \quad \text{with} \quad \overrightarrow{Z}_\sigma = \sum_{\sigma'\in\mathcal{X}_{\Lambda,B}} e^{-H(\sigma,\sigma')} \tag{1.3.5}$$

Due to the definition of the pair Hamiltonian, the updating performed by the transition probability $P^{dl}(\sigma,\tau)$ is parallel, *i.e.* it can be written in the form (1.2.1). Indeed, given a configuration σ, at each site $x\in\Lambda$ the spin τ_x of the new configuration τ is chosen with a probability proportional to $e^{h^{dl}_x(\sigma)\tau_x}$ so that

$$P^{dl}(\sigma,\tau) := \frac{e^{-H(\sigma,\tau)}}{\overrightarrow{Z}_\sigma} = \prod_{x\in\Lambda}\frac{e^{h^{dl}_x(\sigma)\tau_x}}{2\cosh h^{dl}_x(\sigma)}$$

Note that $H(\sigma,\tau)\neq H(\tau,\sigma)$ and actually, by (1.3.2), $H(\tau,\sigma)$ corresponds to the opposite direction of the interaction for the transition from σ to τ. We define

$$P^{ur}(\sigma,\tau) := \frac{e^{-H(\tau,\sigma)}}{\overleftarrow{Z}_\sigma} \quad \text{with} \quad \overleftarrow{Z}_\sigma = \sum_{\sigma'\in\mathcal{X}_{\Lambda,B}} e^{-H(\sigma',\sigma)} \tag{1.3.6}$$

Similarly for $P^{ur}(\sigma,\tau)$ with the up-right field $h^{ur}_x(\sigma)$ we get

$$P^{ur}(\sigma,\tau) := \frac{e^{-H(\tau,\sigma)}}{\overleftarrow{Z}_\sigma} = \prod_{x\in\Lambda}\frac{e^{h^{ur}_x(\sigma)\tau_x}}{2\cosh h^{ur}_x(\sigma)}$$

Note that in the definition (1.3.2) of $H(\sigma,\tau)$ the term proportional to λ could be canceled obtaining the same value for the transition probabilities $P^{dl}(\sigma,\tau)$ and $P^{ur}(\sigma,\tau)$. We included it in the pair Hamiltonian for symmetry reasons. In particular, the fact that $H(\tau,\sigma)$ is the

correct pair Hamiltonian to define $P^{ur}(\sigma,\tau)$ is due to this symmetry. Note also that

$$H(\sigma,\sigma) = H(\sigma) - q|\Lambda|$$

where we define $H(\sigma)$ to be the usual Ising Hamiltonian with magnetic field 2λ

$$H(\sigma) = -J \sum_{\langle x,y\rangle \in \mathcal{B}_\Lambda} \sigma_x\sigma_y - 2\lambda \sum_{x\in\Lambda} \sigma_x \tag{1.3.7}$$

With these asymmetric transition probabilities we define on $\mathcal{X}_{\Lambda,B}$ the *shaken dynamics* as the Markov chain with transition probabilities

$$P^{sh}(\sigma,\tau) = \sum_{\sigma'\in\mathcal{X}_{\Lambda,B}} P^{dl}(\sigma,\sigma')P^{ur}(\sigma',\tau) = \sum_{\sigma'\in\mathcal{X}_{\Lambda,B}} \frac{e^{-H(\sigma,\sigma')}}{\overrightarrow{Z}_\sigma} \frac{e^{-H(\tau,\sigma')}}{\overleftarrow{Z}_{\sigma'}} \tag{1.3.8}$$

The shaken dynamics is, hence, the composition of two asymmetric steps, with interactions in opposite directions. Strictly speaking it can not be considered a PCA: it is a composition of PCAs since both the asymmetric steps have factorized transition probabilities.
Note that reversing the order of the "down–left" and the "up–right" updating rules one would obtain the chain with transition probabilities

$$P^{sh'}(\sigma,\tau) = \sum_{\sigma'\in\mathcal{X}_{\Lambda,B}} P^{ur}(\sigma,\sigma')P^{dl}(\sigma',\tau).$$

1.3.2 The dynamics on a general graph

Let $G=(V,E)$ be a finite weighted graph and $\mathcal{X}_V = \{-1,+1\}^V$ be the set of spin configurations on V. We consider the nearest neighbor interaction between spins given by the Ising Hamiltonian in the general form:

$$\begin{aligned} H(\sigma) &= -\sum_{e=\{x,y\}\in E} J_{xy}\sigma_x\sigma_y - 2\sum_{x\in V}\lambda_x\sigma_x \\ &= -\sum_x\sum_y \frac{1}{2} J_{xy}\mathbb{1}_{\{x,y\}\in E}\sigma_x\sigma_y - 2\sum_{x\in V}\lambda_x\sigma_x = -\langle \frac{1}{2}\mathcal{J}\sigma + 2\lambda, \sigma\rangle \end{aligned} \tag{1.3.9}$$

where the weight $J_{xy}\in\mathbb{R}$ associated to the edge $\{x,y\}$, represents the interaction, and can be written in compact form as a symmetric matrix $\mathcal{J}$ and we denote by $\langle\cdot,\cdot\rangle$ the scalar product. The vector $\lambda = \{\lambda_x\}_{x\in V}$ is an external field, possibly non uniform.

We introduce a class of bipartite weighted graphs $G^b = (V^b, E^b)$ *doubling the interaction graph* G. The idea is to duplicate the vertex set into two identical copies, $V^{(1)}$ and $V^{(2)}$, representing the two parts of the vertex set of the bipartite graph. For each $x \in V$ we denote by $x^{(1)}, x^{(2)}$ the vertices corresponding to $x \in V$ in $V^{(1)}$ and in $V^{(2)}$ respectively. The edges between $x^{(1)}$ and $x^{(2)}$ are all present, for any $x \in V$. On the other hand the edges between $x^{(1)}$ and $y^{(2)}$, with $x \neq y$, or between $y^{(1)}$ and $x^{(2)}$, can be present only if $\{x, y\} \in E$. Exactly one edge among the two possibilities $(x^{(1)}, y^{(2)})$ and $(y^{(1)}, x^{(2)})$ is in E^b if $\{x, y\} \in E$. This means that for any graph G there are many *doubling graphs* G^b. Note that doubling graphs are already present in the literature (see [64]). However the characteristic feature of our construction is that one and only one among $(x^{(1)}, y^{(2)})$ and $(y^{(1)}, x^{(2)})$ is present. More precisely:

Definition 1.3.1. *A bipartite weighted graph $G^b = (V^b, E^b)$ is the **doubling graph** of $G = (V, E)$ if*

- *the vertex set $V^b = V^{(1)} \cup V^{(2)}$ where the two parts $V^{(1)}$ and $V^{(2)}$ are two identical copies of V;*
- *for any $x \in V$ the edge $(x^{(1)}, x^{(2)}) \in E^b$ with weight q and we call it a **self-interaction edge**;*
- *if $\{x, y\} \in E$ then one, and only one, between the two edges $\{x^{(1)}, y^{(2)}\}$ and $\{y^{(1)}, x^{(2)}\}$ is in E^b. We call this kind of edge an **interaction edge**.*

To construct a doubling graph starting from the interaction graph $G = (V, E)$, choose an arbitrary orientation on the edge set and define a new oriented graph $G^o = (V, E^o)$. Using the oriented edges the set E^b is constructed as follows. For any $x \in V$ we have the self-interaction edge $(x^{(1)}, x^{(2)}) \in E^b$ with weight $w(x^{(1)}, x^{(2)}) = q$ and for $x \neq y \in V$ we have $(x^{(1)}, y^{(2)}) \in E^b$ if and only if $(x, y) \in E^o$ with weight $w(x^{(1)}, y^{(2)}) = J_{xy}$.

Note that the edges in E^b are not oriented. However, by construction, the graph is bipartite, so that for any $e = \{x, y\} \in E^b$ we have $x \in V^{(1)}, y \in V^{(2)}$ or viceversa and so we consider in the definition the natural order in the edges in E^b by setting $e = (e^{(1)}, e^{(2)})$ with $e^{(1)} \in V^{(1)}$, $e^{(2)} \in V^{(2)}$. For this reason we can use the oriented edges in E^o in order to define E^b.

We will sometimes omit the superscripts $^{(1)}$ and $^{(2)}$ and we will always consider (x, y) the ordered pair with $x \in V^{(1)}$, $y \in V^{(2)}$, and $\{x, y\}$ the unordered pair with $x, y \in V^b$.

In the case of $\Lambda \in \mathbb{Z}^2$, presented in Section 1.3.1, the graph G^b is the hexagonal graph, *i.e.*, the space of pairs of configurations with interaction given by $H(\sigma, \tau)$ can be represented as the configuration space $\mathcal{X}_{\mathbb{H}}$ for the Ising model on a hexagonal lattice $\mathbb{H}$.

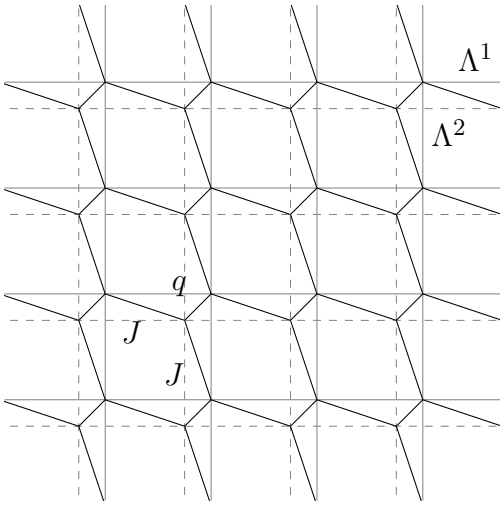

Figure 1.4 The doubling graph of $\mathbb{Z}^2$ represented in the figure turns out to be a hexagonal lattice.

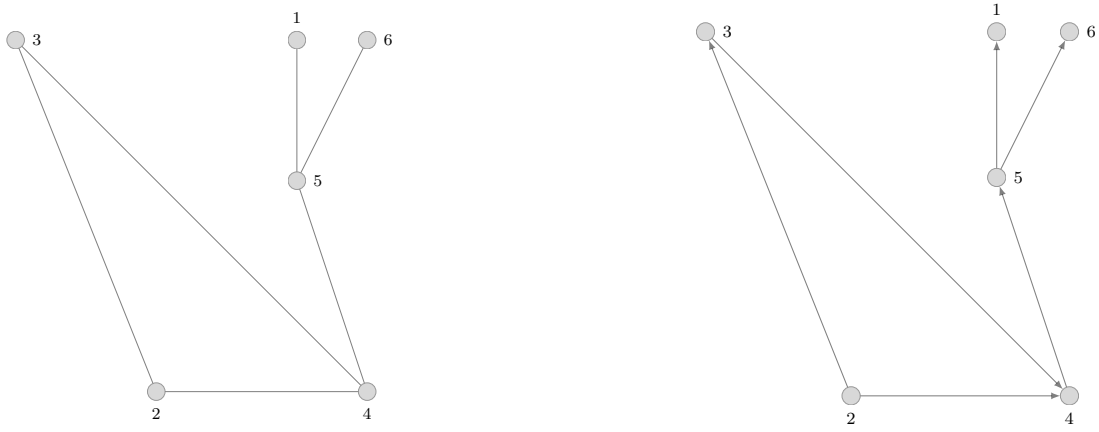

(a) **(b)**

Figure 1.5 An undirected graph (a) and a possible choice for the related directed graph (b)

Definition 1.3.2. *The pair Hamiltonian $H(\sigma^{(1)}, \sigma^{(2)})$ is the **doubling** of the Hamiltonian* (1.3.9) *with interaction graph G if there exists a doubling graph $G^b = (V^b, E^b)$ of G such that $H(\boldsymbol{\sigma})$, defined on the spin configurations $\boldsymbol{\sigma} \equiv (\sigma^{(1)}, \sigma^{(2)}) \in \mathcal{X}_{V^b} = \{-1, 1\}^{V^b}$, can be written as*

$$H(\boldsymbol{\sigma}) = -\sum_{\{x,y\} \in E^b} w(x,y) \boldsymbol{\sigma}_x \boldsymbol{\sigma}_y - \sum_{x \in V^b} \lambda_x \boldsymbol{\sigma}_x \tag{1.3.10}$$

with $w(x,y) = q$ if $\{x,y\}$ is a self-interaction edge and $w(x,y) = J_{xy}$ otherwise and with $\lambda_{x^{(1)}} = \lambda_{x^{(2)}} = \lambda_x$.

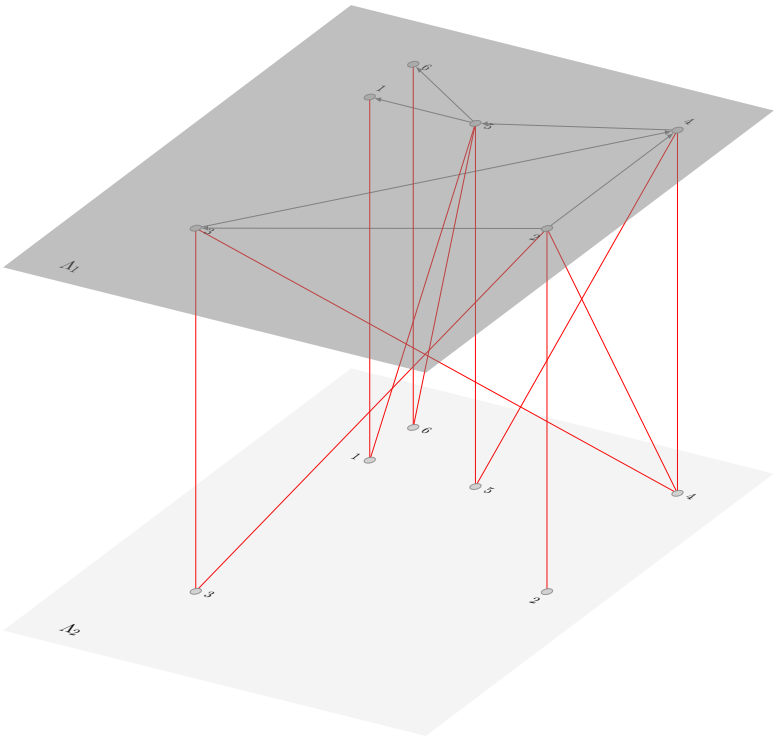

Figure 1.6 The doubling of the graph of Fig. 1.5a obtained from the directed graph of Fig. 1.5b

More explicitly we can write

$$\begin{aligned} H(\boldsymbol{\sigma}) &\equiv H(\sigma^{(1)},\sigma^{(2)}) \\ &= -\sum_{\{x^{(1)},y^{(2)}\}\in E^b} J_{xy}\sigma_x^{(1)}\sigma_y^{(2)} - \sum_{x\in V}\left(q\sigma_x^{(1)}\cdot\sigma_x^{(2)} + \lambda_x(\sigma_x^{(1)}+\sigma_x^{(2)})\right) \\ &= -\sum_{x\in V}\left(\sigma_x^{(1)}h_x^{2\to 1}(\sigma^{(2)}) + \lambda_x\sigma_x^{(2)}\right) \\ &= -\sum_{x\in V}\left(\sigma_x^{(2)}h_x^{1\to 2}(\sigma^{(1)}) + \lambda_x\sigma_x^{(1)}\right) \end{aligned} \tag{1.3.11}$$

with

$$h_x^{2\to 1}(\sigma^{(2)}) = \sum_{y\in V:\{x^{(1)},y^{(2)}\}\in E^b}\left(J_{xy}\sigma_y^{(2)}\right) + q\sigma_x^{(2)} + \lambda_x$$

and

$$h_x^{1\to 2}(\sigma^{(1)}) = \sum_{y\in V:\{y^{(1)},x^{(2)}\}\in E^b}\left(J_{xy}\sigma_y^{(1)}\right) + q\sigma_x^{(1)} + \lambda_x$$

By defining $\mathcal{J}^o$ the matrix of oriented interaction, *i.e.*, ${\mathcal{J}^o}_{xy} = J_{xy}\mathbb{1}_{(x,y)\in E^o}$, and its transposed $\mathcal{J}^{oT}$ corresponding to the opposite orientation, we can write

$$h_x^{2\to 1}(\sigma^{(2)}) = (\mathcal{J}^o\sigma^{(2)})_x + q\sigma_x^{(2)} + \lambda_x$$

$$h_x^{1\to 2}(\sigma^{(1)}) = (\mathcal{J}^{oT}\sigma^{(1)})_x + q\sigma_x^{(1)} + \lambda_x$$

and

$$\begin{aligned} H(\sigma^{(1)},\sigma^{(2)}) &= -\langle\sigma^{(1)},\mathcal{J}^o\sigma^{(2)}\rangle + q\langle\sigma^{(1)},\sigma^{(2)}\rangle + \langle\lambda,\sigma^{(1)}\rangle + \langle\lambda,\sigma^{(2)}\rangle \\ &= -\langle\mathcal{J}^{oT}\sigma^{(1)},\sigma^{(2)}\rangle + q\langle\sigma^{(1)},\sigma^{(2)}\rangle + \langle\lambda,\sigma^{(1)}\rangle + \langle\lambda,\sigma^{(2)}\rangle \end{aligned}$$

If we consider the case $\sigma^{(1)} = \sigma^{(2)} = \sigma$, *i.e.*, $\sigma_x^{(1)} = \sigma_x^{(2)}$ for any $x \in V$, then we have $H(\boldsymbol{\sigma}) \equiv H(\sigma,\sigma) = H(\sigma) - q|V|$. Indeed we have immediately $\mathcal{J} = \mathcal{J}^o + \mathcal{J}^{oT}$.
We construct now the *shaken dynamics* on the state space $\mathcal{X}_V$ by considering two subsequent updating defined as follows:

$$P^{1\to 2}(\sigma,\sigma') := \frac{e^{-H(\sigma,\sigma')}}{\overrightarrow{Z}_\sigma} = \prod_{x\in V}\frac{e^{h_x^{1\to 2}(\sigma)\sigma'}}{2\cosh h_x^{1\to 2}(\sigma)} \quad \text{with} \quad \overrightarrow{Z}_\sigma = \sum_{\zeta\in\mathcal{X}_V} e^{-H(\sigma,\zeta)} \tag{1.3.12}$$

$$P^{2\to 1}(\sigma',\tau) := \frac{e^{-H(\tau,\sigma')}}{\overleftarrow{Z}_{\sigma'}} = \prod_{x\in V}\frac{e^{h_x^{2\to 1}(\tau)\sigma'}}{2\cosh h_x^{2\to 1}(\tau)} \quad \text{with} \quad \overleftarrow{Z}_{\sigma'} = \sum_{\zeta\in\mathcal{X}_V} e^{-H(\zeta,\sigma')} \tag{1.3.13}$$

$$P^{sh}(\sigma,\tau) = \sum_{\sigma'\in\mathcal{X}_V} P^{1\to 2}(\sigma,\sigma')P^{2\to 1}(\sigma',\tau) = \sum_{\sigma'\in\mathcal{X}_V}\frac{e^{-H(\sigma,\sigma')}}{\overrightarrow{Z}_\sigma}\frac{e^{-H(\tau,\sigma')}}{\overleftarrow{Z}_{\sigma'}} \tag{1.3.14}$$

We conclude this section with the following observation concerning the choice of the pair Hamiltonian for the interaction and the doubling construction.
On one hand the introduction of a pair Hamiltonian in the dynamics defined on G suggests to represent the configuration space $\mathcal{X}_V$ as a *doubled* configuration space $\mathcal{X}_{V^b}$ for the Ising model on the graph G^b.
On the other hand the dynamics in (1.3.14) turns out to be an *alternate dynamics* on the doubling graph G^b, *i.e.*

$$P^{alt}(\boldsymbol{\sigma},\boldsymbol{\tau}) := P^{1\to 2}(\sigma^{(1)},\tau^{(2)})P^{2\to 1}(\tau^{(2)},\tau^{(1)}) \tag{1.3.15}$$

Therefore the construction of the doubling graph makes always possible to get a bipartite graph from the original one, whatever it is, and to exploit an alternate dynamics on the new graph.

1.4 Main results

Our first result concerns the identification of the stationary measure of the shaken dynamics defined in the general context of Section 1.3.2, *i.e.*

$$P^{sh}(\sigma,\tau) = \sum_{\sigma' \in \mathcal{X}_V} \frac{e^{-H(\sigma,\sigma')}}{\overrightarrow{Z}_\sigma} \frac{e^{-H(\tau,\sigma')}}{\overleftarrow{Z}_{\sigma'}} \tag{1.4.1}$$

with the pair Hamiltonian given in (1.3.10) which can be written as follows

$$H(\sigma,\tau) = - \sum_{\substack{x \neq y \in V: \\ \{x^{(1)},y^{(2)}\} \in E^b}} J_{xy}\sigma_x\tau_y - \sum_{x \in V} q\sigma_x\tau_x + \lambda_x(\sigma_x + \tau_x) \tag{1.4.2}$$

where $G^b = (V^b, E^b)$ is the doubling graph of the original graph $G = (V, E)$ and $(\sigma, \tau) \in \mathcal{X}_{V^b}$.

Theorem 1.4.1. *The stationary measure of the shaken dynamics is*

$$\pi(\sigma) = \frac{\overrightarrow{Z}_\sigma}{Z} \quad \textit{with} \quad \overrightarrow{Z}_\sigma := \sum_\tau e^{-H(\sigma,\tau)} \ \textit{and} \ Z := \sum_{\sigma,\tau} e^{-H(\sigma,\tau)} \tag{1.4.3}$$

and reversibility holds. This stationary measure is the marginal of the Gibbs measure on the space $\mathcal{X}_{V^b}$ of pairs of configurations $\boldsymbol{\sigma} := (\sigma^{(1)}, \sigma^{(2)})$ defined by:

$$\pi^b(\boldsymbol{\sigma}) := \frac{1}{Z} e^{-H(\boldsymbol{\sigma})}. \tag{1.4.4}$$

The shaken dynamics on $\mathcal{X}_V$ corresponds to an alternate dynamics on G^b in the following sense

$$P^{sh}(\sigma^{(1)}, \tau^{(1)}) = \sum_{\tau^{(2)} \in \{-1,+1\}^{V^{(2)}}} P^{alt}(\boldsymbol{\sigma}, \boldsymbol{\tau}) \tag{1.4.5}$$

with

$$P^{alt}(\boldsymbol{\sigma}, \boldsymbol{\tau}) = \frac{e^{-H(\sigma^{(1)},\tau^{(2)})}}{\overrightarrow{Z}_{\sigma^{(1)}}} \frac{e^{-H(\tau^{(1)},\tau^{(2)})}}{\overleftarrow{Z}_{\tau^{(2)}}} \tag{1.4.6}$$

the stationary measure of P^{alt} is $\pi^b(\boldsymbol{\sigma})$. This dynamics is in general non reversible.

On general graphs and under suitable choice of the parameters, the measure $\pi(\sigma)$ concentrates on the configurations minimizing the Hamiltonian $H(\sigma)$ defined in (1.3.9). Thus the shaken dynamics provides a parallel algorithm to solve discrete optimization problems. This is the statement of the next corollary, which immediately follows from Theorem 1.4.1.

Corollary 1.4.2. *Given a Hamiltonian $H(\sigma)$ of the form given in (1.3.9) on $\{-1,+1\}^V$, for any Hamiltonian $H(\sigma,\tau)$ which is the doubling of $H(\sigma)$, corresponding to a bipartite graph $G^b=(V^b,E^b)$, if*

$$q > \max_{x\in V}\Big\{\Big[\sum_{y:\{x,y\}\in E^b} |J_{xy}|+|\lambda_x|\Big]\Big\} \tag{1.4.7}$$

then the alternate dynamics defined with $H(\sigma,\tau)$ is a parallel algorithm to find configurations σ minimizing $H(\sigma)$. Indeed for q satisfying (1.4.7) we have

$$\min_{\sigma,\tau} H(\sigma,\tau) = \min_{\sigma} H(\sigma,\sigma) = \min_{\sigma} H(\sigma) - q|V|$$

Consider now the two-dimensional square lattice $\Lambda\in\mathbb{Z}^2$ with $J>0$ and $B=\emptyset$, *i.e.* with the standard periodic boundary conditions. Denote by $\pi_\Lambda = \frac{\overrightarrow{Z}_\sigma}{Z}$ the invariant measure of the shaken dynamics defined on Λ and note that under periodic boundary conditions we have $\overrightarrow{Z}_\sigma = \overleftarrow{Z}_\sigma = Z_\sigma$ (see [37, 65]).
We denote by π^G_Λ the Gibbs measure

$$\pi^G_\Lambda(\sigma) = \frac{e^{-H(\sigma)}}{Z^G} \qquad \text{with} \qquad Z^G = \sum_{\sigma\in\mathcal{X}_\Lambda} e^{-H(\sigma)}$$

with $H(\sigma)$ defined in (1.3.7) and we define the total variation distance, or L_1 distance, between two arbitrary probability measures μ and ν on $\mathcal{X}_{\Lambda,B}$ as

$$\|\mu-\nu\|_{TV} = \frac{1}{2}\sum_{\sigma\in\mathcal{X}_{\Lambda,B}} |\mu(\sigma)-\nu(\sigma)| \tag{1.4.8}$$

In the following Theorem 1.4.3 we control the distance between the invariant measure of the shaken dynamics and the Gibbs measure at low temperature and for q positive and large. We notice that this theorem is an extension of Theorem 1.2 in [84] to the case of Hamiltonians

with non zero external field. This result could be extended to the case $B \neq \emptyset$.

Theorem 1.4.3. *Set $\delta = e^{-2q}$, and let δ be such that*

$$\lim_{|\Lambda|\to\infty} \delta^2 |\Lambda| = 0 \tag{1.4.9}$$

Under the assumption (1.4.9), there exists $\bar{J}$ such that for any $J > \bar{J}$

$$\lim_{|\Lambda|\to\infty} \|\pi_\Lambda - \pi_\Lambda^G\|_{TV} = 0 \tag{1.4.10}$$

This result suggests that the shaken dynamics may provide a parallel algorithm for approximate sampling from the Gibbs measure.

The following theorem characterizes the measure $\pi(\sigma)$ from a static point of view. More precisely, we explicitly compute the average magnetization and the correlation functions with respect to $\pi(\sigma)$. In the remainder we will simply refer to these quantities as *thermodynamical relations* of $\pi(\sigma)$.

Consider the hexagonal lattice $\mathbb{H} = (V^b, E^b)$, *i.e.* the doubling graph of the square lattice $\Lambda \in \mathbb{Z}^2$ and recall that any doubling graph is bipartite by construction. According to Definition 1.3.1 we distinguish two types of edges, $E^b = E_J \cup E_q$ (see Fig. 1.4), where E_J is the set of the interaction edges and E_q is the set of the self-interaction edges and we denote the corresponding edge-weights by

$$\mathrm{J}_e = \begin{cases} J & \text{if } e \in E_J \\ q & \text{if } e \in E_q. \end{cases}$$

Assume periodic boundary conditions and consider the Gibbs measure on the space $\mathcal{X}_{V^b} := \mathcal{X}_\Lambda^2 = \mathcal{X}_\Lambda \times \mathcal{X}_\Lambda$ of pairs of configurations $\boldsymbol{\sigma} = (\sigma^{(1)}, \sigma^{(2)})$ on the hexagonal lattice

$$\pi_2(\boldsymbol{\sigma}) = \pi_2(\sigma^{(1)}, \sigma^{(2)}) = \frac{e^{-H(\sigma^{(1)}, \sigma^{(2)})}}{Z} \tag{1.4.11}$$

associated to the pair Hamiltonian (1.3.10) in the case of zero external field (*i.e.* $\lambda = 0$)

$$H(\sigma^{(1)}, \sigma^{(2)}) = -\sum_{e=\{x,y\}\in E^b} w(x,y)\boldsymbol{\sigma}_x\boldsymbol{\sigma}_y = -\sum_{e\in E^b} \mathrm{J}_e \sigma^{(1)}_{e^{(1)}} \sigma^{(2)}_{e^{(2)}} \tag{1.4.12}$$

where $x = e^{(1)}, y = e^{(2)}$ are the two sites in $\mathbb{H}$ connected by the edge e.

The analysis of the thermodynamical relations is based on the connection between $\pi(\sigma)$ and the Gibbs measure of the Ising model on the hexagonal lattice $\pi_2(\boldsymbol{\sigma})$ defined in (1.4.11). Leveraging on the standard coupling between the Ising model and the random-cluster model (RCM) we can extend the thermodynamical relations and the control of the critical behavior obtained for the measure $\pi_2(\boldsymbol{\sigma})$ to the marginal measure $\pi(\sigma)$.
Before stating our results concerning the thermodynamical relations we shortly recall some fundamental definitions of the RCM. A more detailed discussion on the random-cluster model and its powerful coupling with the Ising model is deferred to Section 2.4.1.
Let $\Omega = \{0,1\}^{E^b}$ and denote by ω the elements of this set. We say that the edge $e \in E^b$ is *open* (in $\omega \in \Omega$) if $\omega(e) = 1$, and it is *closed* if $\omega(e) = 0$. For $\omega \in \Omega$ let $\eta(\omega) = \{e \in E : \omega(e) = 1\} \subseteq E$ be the set of open edge and denote by $k(\omega)$ the number of connected components (or *open clusters*) of the graph $(V^b, \eta(\omega))$.
We consider the random-cluster measure defined on Ω

$$\Phi_{p_e}(\omega) = \frac{1}{Z_{RC}} \Big\{ \prod_{e \in E^b} p_e^{\omega(e)} (1-p_e)^{1-\omega(e)} \Big\} 2^{k(\omega)} \tag{1.4.13}$$

with partition function

$$Z_{RC} = \sum_{\omega \in \Omega} \Big\{ \prod_{e \in E^b} p_e^{\omega(e)} (1-p_e)^{1-\omega(e)} \Big\} 2^{k(\omega)}$$

where for any $e \in E^b$ the edge-weight $p_e \in [0,1]$ is defined as follows

$$p_e = \begin{cases} p_J = 1 - e^{-2J} & \text{if } e \in E_J \\ p_q = 1 - e^{-2q} & \text{if } e \in E_q \end{cases}$$

In what follows for any $x, y \in V^b$ we will denote by $\{x \leftrightarrow y\}$ the set of $\omega \in \Omega = \{0,1\}^{E^b}$ for which there exists a path, composed of edges with $\omega = 1$ only, joining the vertex x with the vertex y. We call such a path an *open path*.

Theorem 1.4.4. *Consider the measure π_2 defined in* (1.4.11) *and its marginal measure π defined in* (1.4.3)*. The following relations hold:*

1) The average magnetization with respect to the measure π and π_2 is the same, that is

$$m := \pi\Big(\frac{\sum_{x \in \Lambda} \sigma}{|\Lambda|}\Big) = m_2 := \pi_2\Big(\frac{\sum_{x \in \Lambda^{(1)} \cup \Lambda^{(2)}} \boldsymbol{\sigma}}{2|\Lambda|}\Big)$$

2) Let π^+ (π^-) be the previous measure with plus (minus) boundary conditions, then for any $x \in \Lambda$

$$\pi^{\pm}(\sigma_x) = \pm\Phi_{p_e}(x^{(1)} \leftrightarrow \partial\Lambda^{(1)})$$

3) For any x, $y \in \Lambda$

$$\pi(\sigma_x\sigma_y) = \Phi_{p_e}(x^{(1)} \leftrightarrow y^{(1)})$$

with the obvious notation $x^{(1)}, y^{(1)} \in \Lambda^{(1)}$ for the sites in the part $V^{(1)}$ corresponding to vertices x and y in Λ, respectively.

4) If the parameter q is sufficiently small, for any integer $\ell \in (0, L)$ there exist two constants $c_1 < c_2$ such that

$$\pi(\sigma_{(0,0)}\sigma_{(\ell,\ell)}) \leq c_1 < c_2 \leq \pi(\sigma_{(0,\ell)}\sigma_{(\ell,0)}).$$

The powerful connection with the random-cluster model makes possible to prove that our model exhibits phase transition. In the following theorem we identify the critical equation relating the parameters J and q of the Ising Hamiltonian

$$H(\boldsymbol{\sigma}) = -\sum_{\{x,y\}\in E} w(x,y)\boldsymbol{\sigma}_x\boldsymbol{\sigma}_y. \tag{1.4.14}$$

defined on the space of pairs of configurations $\boldsymbol{\sigma} = (\sigma^{(1)}, \sigma^{(2)})$ in the case of the hexagonal lattice $\mathbb{H}$.

Theorem 1.4.5. *The critical equation relating the parameters J and q in the measure π associated to the Hamiltonian* (1.4.14) *is given by the equation:*

$$J_c(q) = \tanh^{-1}\Big(-\tanh q + \sqrt{\tanh^2 q + 1}\Big) \tag{1.4.15}$$

Remark 1.4.6. *It is well know that the Gibbs measure π^G on the square lattice exhibits a phase transition at*

$$J_c^G = \tanh^{-1}\big(\sqrt{2}-1\big) = 0.441...$$

Note that

$$\lim_{q\to\infty} J_c(q) = J_c^G$$

Furthermore, the curve $J_c(q)$ intersects the line $J = q$ for $J = \tanh^{-1}\left(\frac{\sqrt{3}}{3}\right)$,corresponding to the critical value of J in the homogeneous hexagonal lattice (see Fig. 1.7) .

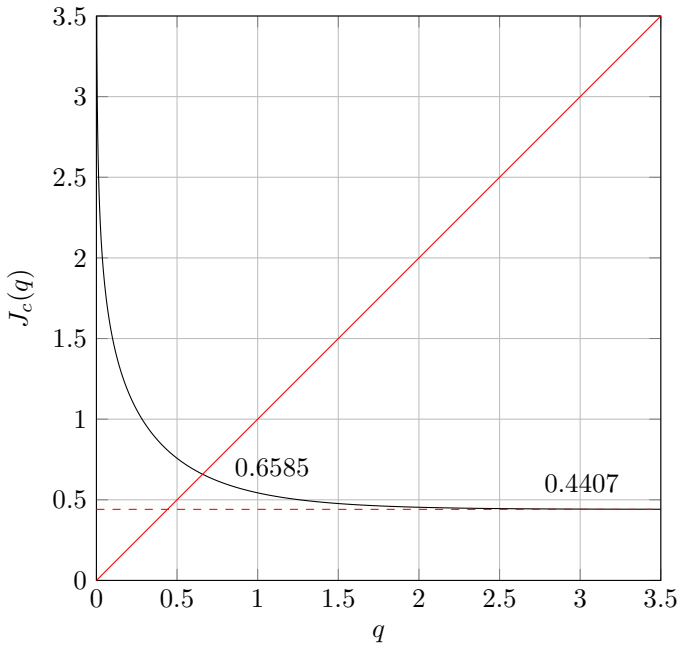

Figure 1.7 The function $J_c(q)$.

The inertial parameter q tunes the geometry of the system. In fact the limit $q \to 0$ corresponds to erasing the q-edges obtaining, from the hexagonal lattice, independent copies of 1-d Ising model. Indeed for $q \to 0$ we find $J_c \to \infty$ showing the absence of phase transition for the one-dimensional Ising model. The opposite limit, $q \to \infty$, corresponds to the collapse of the hexagonal lattice into the square one, by identifying the sites connected by the q-edges. The case $J = q$ corresponds to the homogeneous hexagonal graph.
The interpolation between lattices induced by the shaken dynamics may be applied to derive results on the critical behavior in the case of planar graphs different from the hexagonal lattice.
Consider for instance the Ising model on the triangular lattice. On this lattice we divide the 6 nearest neighbors of each vertex x into two sets, e.g. $\ell(x)$ left and $r(x)$ right nearest neighbors of x, and define a shaken dynamics with self interaction q. Hence the doubled Hamiltonian is

$$H^{\triangle}(\sigma,\tau) = -\sum_x \Big[\sum_{y\in\ell(x)} \Big(J\sigma_y\tau_x\Big) + q\sigma_x\tau_x \Big] = -\sum_x \Big[\sum_{y\in r(x)} \Big(J\tau_y\sigma_x\Big) + q\sigma_x\tau_x \Big] \quad (1.4.16)$$

The corresponding alternate dynamics turns out to be defined on the square lattice (see Fig. 1.8) with invariant measure the Gibbs one. In particular the square lattice is regular when we set $J = q$. The parameter q can be used to move through different geometries. The triangular lattice ($q \to \infty$) and the hexagonal lattice ($q = 0$) can be derived from the original

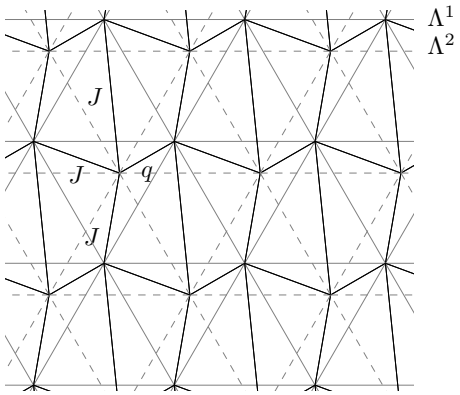

Figure 1.8 Interaction in the pair Hamiltonian for the shaken dynamics on the triangular lattice. Each spin of configuration σ (living on the solid lattice) interacts with the spin at the same location and the three spins on its left in τ (living on the dashed lattice). The red lines show that the pair interaction lives on a square lattice. For $q = J$ this lattice is homogeneous. As $q \to \infty$ the square lattice collapses onto the triangular lattice. If $q = 0$ the interaction graph becomes the homogeneous hexagonal lattice.

square lattice just tuning the value of q.
A more precise statement of this interpolation is given by the following

Theorem 1.4.7. *The critical equation relating the parameters J and q in the measure π associated to the Hamiltonian* (1.4.16) *is given by the equation:*

$$1 + \tanh^3(J)\tanh(q) = 3\tanh(J)\tanh(q) + 3\tanh^2(J) \tag{1.4.17}$$

In the case $q = J$ we obtain the Onsager critical temperature for the square lattice, for $q = 0$ we obtain the critical temperature for the hexagonal lattice and in the limit $q \to \infty$ we obtain the critical temperature for the triangular lattice.

1.5 The generalized shaken dynamics

We can generalize the construction of the shaken dynamics. Starting from a symmetric interaction $\mathcal{J}$ defining the Hamiltonian $H(\sigma)$, as in (1.3.9), we can define an arbitrary decomposition of the interaction matrix $\mathcal{J}$ in a sum of two matrices with non negative entries

$$\mathcal{J} = \mathcal{J}^o + \mathcal{J}^{oT}. \tag{1.5.1}$$

This means that every non oriented edge $\{x, y\}$ with weight J_{xy} is decomposed in a pair of oriented edges (x, y) and (y, x) with weight respectively $\mathcal{J}^o_{xy}$ and $\mathcal{J}^o_{yx}$. Call E^o the set of all

these oriented edges and apply the construction presented in Section 1.3.2 to construct the doubling graph by using this set E^o of oriented edges.

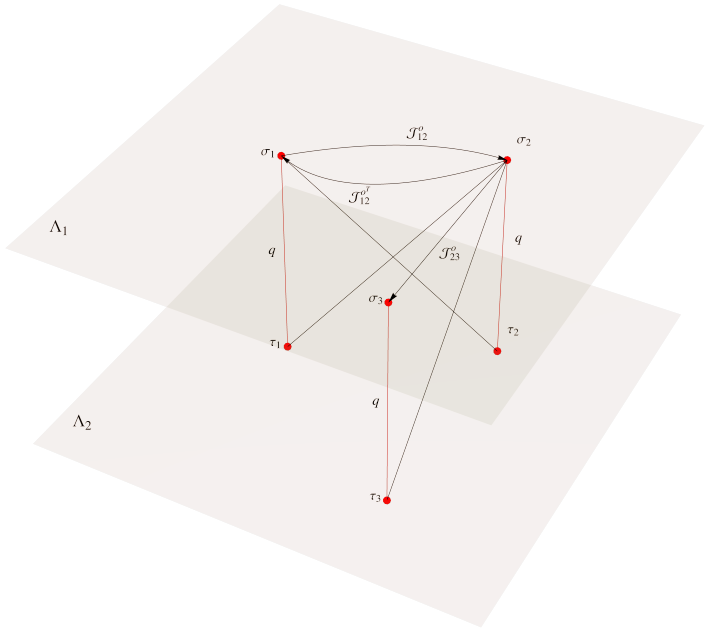

Figure 1.9 The construction of the doubling graph in the case of the generalized shaken dynamics.

We proceed as before defining the doubling Hamiltonian

$$\begin{aligned} H(\sigma^{(1)},\sigma^{(2)}) &= -\langle\sigma^{(1)},\mathcal{J}^o\sigma^{(2)}\rangle + q\langle\sigma^{(1)},\sigma^{(2)}\rangle + \langle\lambda,\sigma^{(1)}\rangle + \langle\lambda,\sigma^{(2)}\rangle \\ &= -\langle\mathcal{J}^{oT}\sigma^{(1)},\sigma^{(2)}\rangle + q\langle\sigma^{(1)},\sigma^{(2)}\rangle + \langle\lambda,\sigma^{(1)}\rangle + \langle\lambda,\sigma^{(2)}\rangle. \end{aligned}$$

In the case $\sigma^{(1)} = \sigma^{(2)} = \sigma$ by equation (1.5.1) we have again $H(\sigma,\sigma) = H(\sigma) - q|V|$.

The corresponding alternate dynamics on the state space $\mathcal{X}_V$ is defined with two subsequent updating as follows:

$$P^{1\to 2}(\sigma,\sigma') := \frac{e^{-H(\sigma,\sigma')}}{\overrightarrow{Z}_\sigma}, \qquad P^{2\to 1}(\sigma',\tau) := \frac{e^{-H(\tau,\sigma')}}{\overleftarrow{Z}_{\sigma'}} \tag{1.5.2}$$

and

$$P^{sh}(\sigma,\tau) = \sum_{\sigma' \in \mathcal{X}_V} P^{1\to 2}(\sigma,\sigma') P^{2\to 1}(\sigma',\tau) = \sum_{\sigma' \in \mathcal{X}_V} \frac{e^{-H(\sigma,\sigma')}}{\overrightarrow{Z}_{\sigma}} \frac{e^{-H(\tau,\sigma')}}{\overleftarrow{Z}_{\sigma'}} \tag{1.5.3}$$

The results obtained in Theorem 1.4.1 can be immediately extended to this more general case.

The choice of the shaken dynamics discussed in Section 1.3.2 is a particular case of generalized shaken dynamics in which $\mathcal{J}^o_{xy}\mathcal{J}^o_{yx} = 0$ for any pair x, y. In the general case the geometrical discussion of the doubling graph of interaction is much more complicated. Also the interpolation between different geometries obtained for different values of the parameter q, as discussed in Section 1.4, is more involved in this generalized case.

Another particular choice in this class of generalized shaken dynamics is $\mathcal{J}^o = \frac{1}{2}\mathcal{J}$ corresponding to the PCA discussed in [36].

2 The invariant measure: a dynamical and a static point of view

The present chapter contains the proofs of the results presented in Chapter 1. In Section 2.1 we briefly recall the main features of two classical statistical mechanics models that turn out to be necessary to prove our results in the remaining sections.

2.1 Preparatory tools

2.1.1 The random-cluster model and Edwards-Sokal coupling

The random-cluster model was introduced by Cees Fortuin and Piet Kasteleyn in the seventies [47] as an extrapolation of electrical networks and as common ground between percolation, Ising and Potts models. We provide here a short introduction to this model and we refer to the clear review by Grimmett [53] of the Fortuin–Kasteleyn construction for a more rigorous discussion and to the rich papers [1] and [41] for further developments.

Let $G = (V, E)$ be a finite graph and consider the elements ω of the set $\Omega = \{0,1\}^E$. We say that the edge $e \in E$ is *open* (in ω) if $\omega(e) = 1$, and it is *closed* if $\omega(e) = 0$. For $\omega \in \Omega$ let $\eta(\omega) = \{e \in E : \omega(e) = 1\} \subseteq E$ be the set of open edges. Note that the correspondence between the elements $\omega \in \Omega$ and the sets $\eta(\omega)$ is one to one. We denote by $k(\omega)$ the number of connected components (or *open clusters*) of the graph $(V, \eta(\omega))$. Isolated vertices, that is vertices incident to no open edge, are included in this definition.

A random-cluster measure on G is a member of a class of probability measures on Ω identified by two parameters, an 'edge-weight' $p \in [0,1]$ and a 'cluster-weight' $q \in (0,\infty)$

$$\phi_{p,q}(\omega) = \frac{1}{Z_{RC}} \Big\{ \prod_{e\in E} p^{\omega(e)}(1-p)^{1-\omega(e)} \Big\} q^{k(\omega)} \tag{2.1.1}$$

where Z_{RC} is the partition function and it is given by

$$Z_{RC} = Z_{RC}(p,q) = \sum_{\omega\in\Omega} \Big\{ \prod_{e\in E} p^{\omega(e)}(1-p)^{1-\omega(e)} \Big\} q^{k(\omega)}. \tag{2.1.2}$$

Remark 2.1.1. *Note that the parameter q in* (2.1.1)*, commonly used in the literature, is different from the inertial parameter q in the pair Hamiltonian of the shaken dynamics. We will warn the reader whenever there could be a case of ambiguity.*

Note that when $q = 1$ this measure is a product measure, that is edges are open or closed independently of one another and we recover the Bernoulli percolation model.
On the other hand, when $q < 1$ (respectively $q > 1$) configurations ω with fewer (respectively larger) clusters are favoured.

More precisely, it can be shown that for $q \in \mathbb{Z}$ and such that $q > 1$, the random-cluster model is strictly linked to the Potts model with q local states. Namely, there exists an extremely powerful coupling, introduced by Edwards and Sokal in 1988 [41] which allows to express magnetization properties in the Potts model (on a general graph G) as percolation properties in the random-cluster model. In particular this successful relationship between the two systems may be used to study phase transitions in Potts models leveraging on known results for the random-cluster model. Let us recall the Edwards and Sokal coupling and some important related results.
Let $G = (V,E)$ be a finite graph, $p \in [0,1]$ and $q \in \{2,3,...\}$. We define a probability mass function μ on the product space $\Sigma \times \Omega$, where $\Sigma = \{1,2,...,q\}^V$ and $\Omega = \{0,1\}^E$

$$\mu(\sigma,\omega) = \frac{1}{Z} \prod_{e\in E} \{(1-p)\delta_{\omega(e),0} + p\delta_{\omega(e),1}\delta_e(\sigma)\}, \qquad (\sigma,\omega) \in \Sigma\times\Omega \tag{2.1.3}$$

where $\delta_e(\sigma) = \delta_{\sigma_x,\sigma_y}$ for $e = \{x,y\} \in E$ and the constant of normalization Z is defined such that $\sum_{(\sigma,\omega)\in\Sigma\times\Omega} \mu(\sigma,\omega) = 1$. By construction, μ can be expressed in terms of the following product measure

$$\mu \propto \psi(\sigma)\phi_p(\omega)\mathbb{1}_F(\sigma,\omega), \qquad (\sigma,\omega) \in \Sigma\times\Omega \tag{2.1.4}$$

where ψ is the uniform probability measure on Σ, ϕ_p is the product measure on Ω with density p and $\mathbb{1}_F$ is the indicator function of the event

$$F = \{(\sigma,\omega) : \delta_e(\sigma) = 1 \text{ for any } e \text{ satisfying } \omega(e) = 1\} \subseteq \Sigma \times \Omega$$

This is equivalent to say that μ is equal (up to a renormalization constant) to the product measure $\psi \times \phi_p$ conditioned on the event F.

The following theorems clarify how the measure μ is a coupling of a Potts measure on V, together with the random-cluster measure on Ω.

Theorem 2.1.2 (Marginal measures of μ)**.** *Let $q \in \{2,3,...\}$, $p = 1 - e^{-\beta} \in [0,1)$.*

1. *The marginal measure $\mu_1(\sigma) = \sum_{\omega\in\Omega} \mu(\sigma,\omega)$ on Σ is the Potts measure*

$$\mu_1(\sigma) = \frac{1}{Z_P} \exp\left[\beta \sum_{e\in E} \delta_e(\sigma)\right] \qquad \sigma \in \Sigma$$

2. *The marginal measure $\mu_2(\omega) = \sum_{\sigma\in\Sigma} \mu(\sigma,\omega)$ on Ω is the random-cluster measure*

$$\mu_2(\omega) = \frac{1}{Z_{RC}} \Big\{ \prod_{e\in E} p^{\omega(e)}(1-p)^{1-\omega(e)} \Big\} q^{k(\omega)} \qquad \omega \in \Omega$$

3. *We have that*

$$\sum_{\omega\in\Omega} \Big\{ \prod_{e\in E} p^{\omega(e)}(1-p)^{1-\omega(e)} \Big\} q^{k(\omega)} = \sum_{\sigma\in\Sigma} \prod_{e\in E} \exp\left[\beta(\delta_e(\sigma) - 1)\right]$$

which is equivalent to say

$$Z_{RC}(p,q) = e^{-\beta|E|} Z_P(\beta,q)$$

Theorem 2.1.3 (Conditional measures of μ)**.** *Let $q \in \{2,3,...\}$, $p = 1 - e^{-\beta} \in [0,1)$.*

1. *For $\omega \in \Omega$ the conditional measure $\mu(\cdot|\omega)$ on Σ is obtained by putting random spins on entire clusters of ω. These spins are constant on given clusters, are independent between clusters, and each is uniformly distributed on the set $\{1,2,...,q\}$.*
2. *For $\sigma \in \Sigma$ the conditional measure $\mu(\cdot|\sigma)$ on Ω is obtained by setting $\omega(e) = 0$ if $\delta_e(\sigma) = 0$ and otherwise $\omega(e) = 1$ with probability p.*

Edwards and Sokal coupling may be used to show that correlations in Potts models correspond to open connections in random-cluster models: this is one of the most powerful features of

this coupling. In particular, in the case of infinite graphs, this correspondence implies that the phase transition of a Potts model corresponds to the creation of an infinite open cluster in the random-cluster model. Thus, arguments and results developed for the random-cluster model may be exploited in order to understand the correlation structure of the Potts system.

2.1.2 The dimer model and the critical temperature for the 2d Ising model

The dimer model is a two-dimensional statistical mechanics model introduced for the first time in a paper by Fowler and Rushbrooke [48] in 1937 with the aim to describe the adsorption of diatomic molecules (here the name *dimer*) on the surface of a crystal. It has been applied to model several other physical systems and to study combinatorics problems too. As discovered by Kasteleyn and Temperley-Fisher in the '60s it is exactly solvable in the sense that in finite volume, there exist explicit close formulas for its partition function and correlations that can be written in terms of determinants or Pfaffians. Moreover, the dimer model turns out to be strictly linked to the Ising model. The main result on the critical temperature for the 2d Ising model in [25], that we recall in this section, leverage on this successfull connection.

The dimer partition function: explicit computation

Let $G = (V, E)$ be a finite graph. We will assume that G is simple, that is *self-loops* (edges having two coinciding endpoints) and multiple edges between two vertices are not allowed. Anyway all the results presented hereafter can be extended to the case of non-simple graphs.

Definition 2.1.4. *A **dimer configuration**, or equivalently a perfect matching, on a graph G is a set $M \subset E$ whose elements are vertex-disjoint and cover all the vertices of the graph. Edges in M are called **dimers**.*

We denote by $\mathcal{M}(G)$ the set of dimer configurations on the graph G. Let $\nu : E \to (0, +\infty)$ be an edge weight system on G. We can define the corresponding measure on the set of all dimer coverings as follows

$$\mu(M) := \frac{\nu(M)}{Z} \tag{2.1.5}$$

where

$$\nu(M) := \prod_{e \in M} \nu(e) \qquad Z_D = Z_D(G, \nu) := \sum_{M \in \mathcal{M}(\mathcal{G})} \nu(M). \tag{2.1.6}$$

The dimer model concerns the study of the measure μ and particularly of the dimer partition function Z_D.

The first exact results about the dimer partition function on either $\mathbb{Z}^2$ or the hexagonal lattice, date back to the 1960's and are due to Kasteleyn [61] and independetly to Temperley and Fisher [89]. Using the so called *Pfaffian method* Kasteleyn extended these results to the case of any planar graph, where *planar* means that the graph can be embedded in the plane. This method has been extended later by Cimasoni-Reshetikhin to graphs embedded in orientable surfaces [26] and to graphs embedded in non-orientable surfaces [22].
In this section we provide a short description of the Pfaffian method which allows to write the partition function of dimers on planar graphs as the Pfaffian of a suitable adjacency matrix. We refer to the lecture notes given by David Cimasoni on the subject [24] for a further discussion.
Let A be a skew-symmetric matrix (*i.e.* $A^T = -A$) and let S_{2n} be the set of permutations of $2n$ objects.

Definition 2.1.5. *The **Pfaffian** of A is*

$$Pf(A) := \frac{1}{2^n n!} \sum_{\sigma \in S_{2n}} sign(\sigma) a_{\sigma(1)\sigma(2)} a_{\sigma(3)\sigma(4)} ... a_{\sigma(2n-1)\sigma(2n)} \tag{2.1.7}$$

if A has size $2n$ (i.e. even size) otherwise $Pf(A) = 0$.

A well-known fact is that the square of the Pfaffian of any skew-symmetric matrix A is equal to the determinant of A. Moreover, if the matrix A is a block matrix of the form

$$A = \left(\begin{array}{c|c} 0 & K \\ \hline -K^T & 0 \end{array} \right)$$

where K is a matrix of size n, then the following property holds

$$Pf(A) = (-1)^{\frac{n(n-1)}{2}} \det(K). \tag{2.1.8}$$

Consider now a finite weighted graph (G, ν) with $2n$ vertices and let ω be an arbitrary orientation on its edges.

Definition 2.1.6. *The **adjacency matrix** A^ω of the graph G is a $2n \times 2n$ skew-symmetric matrix whose entries are given by*

$$a^\omega_{i,j} = \begin{cases} \varepsilon^\omega_{i,j} \nu(e) & \text{if } e = \{i,j\} \in E \\ 0 & \text{otherwise} \end{cases} \tag{2.1.9}$$

where

$$\varepsilon^{\omega}_{i,j} = \begin{cases} +1 & e \text{ oriented by } \omega \text{ from } i \text{ to } j \\ -1 & e \text{ oriented by } \omega \text{ from } j \text{ to } i \end{cases}$$

We are interested in relating the Pfaffian of adjacency matrices of the graph G to the dimer partition function of G.
Let us compute the Pfaffian of A^{ω}. It can be shown that the only nonzero contributions to the sum (2.1.7) are those coming from matchings of the vertices of G realised by a dimer configuration of G. This observation implies that the sum in (2.1.7) is equivalent to a sum on the set $\mathcal{M}(G)$

$$Pf(A^{\omega}) = \sum_{M \in \mathcal{M}(G)} \varepsilon^{\omega}(M) \prod_{e \in M} \nu(e) \tag{2.1.10}$$

where

$$\varepsilon^{\omega}(M) := \text{sign}(\sigma)\varepsilon^{\omega}_{\sigma(1)\sigma(2)}\varepsilon^{\omega}_{\sigma(3)\sigma(4)}\cdots\varepsilon^{\omega}_{\sigma(2n-1)\sigma(2n)}$$

and σ is a permutation identifying the perfect matching $M \in \mathcal{M}(G)$.
By equation (2.1.10) we can conclude that $|Pf(A^{\omega})| = Z(G,\nu)$ if and only if the orientation ω is such that $\varepsilon^{\omega}(M) = \varepsilon^{\omega}(M')\ \forall M, M' \in \mathcal{M}(G)$. In other words, if one can find an orientation ω on G such that the signs in the sum (2.1.10) are constant for all dimer configurations then it is possible to write an explicit formula relating the dimer partition function of the weighted graph (G,ν) to the Pfaffian of the adjacency matrix of G with respect to the orientation ω. To this end, first observe that if $M, M' \in \mathcal{M}(G)$, then their symmetric difference $M\Delta M' := (M \cup M') \setminus (M \cap M')$ is given by the disjoint union of cycles of even lenght with edges alterned between M and M'. We denote by $\bigcup_i C_i$ the disjoint union of the cycles C_i, that are called *superposition cycles*. The following lemma holds.

Lemma 2.1.7. *Given $M, M' \in \mathcal{M}(G)$, consider their symmetric difference $M\Delta M' = \bigcup_i C_i$ and let $n^{\omega}(C_i)$ be the number of edges in C_i oriented backwards by ω when running along C_i, then*

$$\varepsilon^{\omega}(M)\varepsilon^{\omega}(M') = \prod_i (-1)^{n^{\omega}(C_i)+1} \tag{2.1.11}$$

Note that, since C_i has even lenght, the parity of $n^{\omega}(C_i)$ does not depend on the way one runs along C_i.

Note that if C is a superposition cycle then $\mathcal{M}(G \setminus C) \neq \emptyset$, *i.e.* the graph obtained removing C from G still admits a perfect matching.

Definition 2.1.8. *The orientation ω is a **pfaffian orientation** if for any cycle C of even lenght such that $\mathcal{M}(G \setminus C) \neq \emptyset$, $n^{\omega}(C)$ is odd.*

A graph is said to be *Pfaffian* if it admits a pfaffian orientation. By lemma (2.1.7) it follows that if one can find a pfaffian orientation ω on G, then it is possible to write the partition function for the dimer model on G in terms of the Paffian of the adjacency matrix A^ω.
More precisely, if the graph G is planar the following theorem holds.

Theorem 2.1.9 (Kasteleyn's Theorem)**.** *Given any planar graph G, there exists an orientation ω such that $n^\omega(\partial f)$ is odd for each face f, where ∂f is the boundary of f oriented counterclockwise. Furthermore such an orientation can be constructed in polynomial time and it is pfaffian.*

An orientation satisfiyng the conditions of Theorem 2.1.9 is said to be a *Kasteleyn orientation* and the corresponding adjacency matrix is called *Kasteleyn matrix*.
Given a Kasteleyn orientation, the dimer partition function of the graph G is equal to the absolute value of the Pfaffian of the corresponding Kasteleyn matrix. More precisely we have the following

Corollary 2.1.10. *If G is planar, one can compute $Z(G,\nu) = |Pf(A^\omega)|$ in polynomial time.*

In particular, if G is bipartite, from property (2.1.8) it follows that $Z(G,\nu) = |\det K|$.
The proof of Kasteleyn's Theorem is based on the crucial assumption that the graph is planar. In [26] Cimasoni and Reshetikhin extended the Kasteleyn method for the computation of the dimer partition function of any planar graph to graphs embedded in orientable surfaces [26]. In particular, if the graph G can be embedded in an orientable surface of genus g, its dimer partition function can be computed as an alternated sum of the Pfaffians of 2^{2g} well-chosen skew-adjacency matrices. The same authors extended Kasteleyn's result to graphs embedded in non-orientable surfaces [22].

The critical Ising temperature via the dimer model

One of the main features of the dimer model is that its partition function may be related to the partition function of the Ising model. There exist two equivalent approaches.
The first one concerns the so called *Fisher correspondence*. Following the ideas of Hurst-Green [57], Kasteleyn [61] and Fisher [45, 46], it can be established a correspondence between a given graph G and an auxiliary graph G' such that the dimer partition function on G' is equal to the Ising partition function on G. Once this correspondence, has been defined, one can apply the dimer model technology to solve the Ising model on G.
There is another combinatorial method to solve the 2d Ising model. It was originally introduced for planar graphs by Kac-Ward [60] and after extended to any finite graph in [68, 23]. With this method, no auxiliary graph is needed: the Ising partition function on a finite

graph G is computed as an alternated sum of the square roots of the determinants of 2^{2g} Kac-Ward matrices associated to the graph G.

Kac-Ward matrices and dimer model are the main tools used in the rich paper [25] where a simple characterization of the critical temperature for the Ising model on an arbitrary planar doubly periodic weighted graph is provided. More precisely, the authors show that the Kac-Ward determinants of a planar doubly periodic graph are proportional to the Kasteleyn determinants of a suitable associated bipartite graph and they leverage on this result to express the free energy of the 2d Ising model in terms of the Kac-Ward determinants, see Lemma 2.1.2 below. This Lemma turns out to be a key ingredient to show that the free energy is twice differentiable except possibly at criticality and to state the result on the critical temperature. Here, we recall the statement of [25, Theorem 1.1] and we provide a sketch of the proof. Interested readers are referred to [25] for more details.

The statement of [25, Theorem 1.1] is given in terms of the high-temperature expansion of the Ising partition function

$$Z_I^{\text{high}}(G) = \sum_{\gamma \in \mathcal{E}(G)} x(\gamma) \tag{2.1.12}$$

where $G = (V, E)$ is a finite graph, $\mathcal{E}(G)$ is the set of even subgraphs of G, that is, the set of subgraphs γ of G such that every vertex of G is adjacent to an even number of edges of γ and $x(\gamma) := \prod_{e \in \gamma} x_e$ with $x_e := \tanh(\beta J_e)$.

Denote by $(\mathcal{G}, J)$ a planar non-degenerate locally-finite doubly periodic weighted graph, and call G the embedding of $\mathcal{G}$ in the torus $\mathbb{T}^2$.

Theorem (Theorem 1.1 in [25])**.** *The critical inverse temperature β_c for the Ising model on the weighted graph $(\mathcal{G}, J)$ is the unique solution $0 < \beta < \infty$ to the equation*

$$\sum_{\gamma \in \mathcal{E}_0(G)} x(\gamma) = \sum_{\gamma \in \mathcal{E}_1(G)} x(\gamma) \tag{2.1.13}$$

where $\mathcal{E}_0(G)$ denotes the set of even subgraphs of G that wind around each of the two directions of the torus an even number of times and $\mathcal{E}_1(G) = \mathcal{E}(G) \setminus \mathcal{E}_0(G)$.

The proof relies on the following arguments. We denote by $x \in (0,1)^E$ an edge weight system on the graph G, with $x_e := \tanh(\beta J_e)$. The free energy $\log Z_x$ can be expressed in terms of Kac-Ward determinants $P^{z,w}(G, x)$, each identified by a pair of non-vanishing complex numbers (z, w). This is the object of the following

Lemma (Lemma 4.3 in [25])**.** *For any $x \in (0,1)^E$,*

$$\log Z_x = \frac{1}{2(2\pi i)^2} \int_{\mathbb{T}^2} \log P^{z,w}(G, x) \frac{dz}{z} \frac{dw}{w} \tag{2.1.14}$$

For any x such that $P^{z,w}(G,x)$ has a zero on $\mathbb{T}^2 := \{(z,w) : |z| = 1, |w| = 1\}$, the free energy is shown not to be twice differentiable at x. [25, Lemma 4.1] shows that the only zeros of $P^{z,w}(G,x)$ are localized at $(1,1)$. The statement of this lemma is the main technical difficulty. The result is achieved by showing that the Kac-Ward determinants are proportional to the Kasteleyn determinants of an associated bipartite graph (see [25, Theorem 3.1]).
By standard arguments on the Ising model $\log Z_x$ is proved to be twice differentiable at any J_e except at criticality $\beta = \beta_c$. The proof is completed by observing that Equation (2.1.13) is equivalent to the vanishing of the Kac-Ward determinant at $(z,w) = (1,1)$, which translates into the free energy not being twice differentiable in some variable J_e at $\beta = \beta_c$.

2.2 The invariant measure

In this section we first provide the proof of Theorem 1.4.1. We then discuss an interesting feature induced by the doubling construction, *i.e.* the relation between the shaken dynamics and the corresponding alternate dynamics.

Proof of Theorem 1.4.1. We have immediately the detailed balance condition w.r.t. the measure $\pi(\sigma)$ indeed

$$\sum_{\sigma' \in \mathcal{X}_V} \frac{e^{-(H(\sigma,\sigma')+H(\tau,\sigma'))}}{\overleftarrow{Z}_{\sigma'}} = \overrightarrow{Z}_{\sigma} P^{sh}(\sigma,\tau) = \overrightarrow{Z}_{\tau} P^{sh}(\tau,\sigma) = \sum_{\sigma' \in \mathcal{X}_V} \frac{e^{-(H(\tau,\sigma')+H(\sigma,\sigma'))}}{\overleftarrow{Z}_{\sigma'}} \tag{2.2.1}$$

It is straightforward to prove that $\pi^b(\sigma^{(1)},\sigma^{(2)})$ is the stationary measure of P^{alt}

$$\begin{aligned}\sum_{\sigma^{(1)},\sigma^{(2)}} \pi^b(\sigma^{(1)},\sigma^{(2)}) P^{alt}(\boldsymbol{\sigma},\boldsymbol{\tau}) &= \sum_{\sigma^{(1)},\sigma^{(2)}} \frac{e^{-H(\sigma^{(1)},\sigma^{(2)})}}{Z} \frac{e^{-H(\sigma^{(1)},\tau^2)}}{\overrightarrow{Z}_{\sigma^{(1)}}} \frac{e^{-H(\tau^{(1)},\tau^{(2)})}}{\overleftarrow{Z}_{\tau^{(2)}}} \\ &= \frac{e^{-H(\tau^{(1)},\tau^{(2)})}}{Z} = \pi^b(\tau^{(1)},\tau^{(2)})\end{aligned} \tag{2.2.2}$$

□

Note that, in general

$$\pi^b(\sigma^{(1)},\sigma^{(2)}) P^{alt}(\boldsymbol{\sigma},\boldsymbol{\tau}) \neq \pi^b(\tau^{(1)},\tau^{(2)}) P^{alt}(\boldsymbol{\tau},\boldsymbol{\sigma}).$$

For instance consider the bipartite complete graph $K_{n,n}$ with equal weights on all edges and where, for all i, $(\sigma_i^{(1)},\sigma_i^{(2)}) = (+1,+1)$ and $(\tau_i^{(1)},\tau_i^{(2)}) = (+1,-1)$.

In the case $\Lambda \in \mathbb{Z}^2$ the shaken dynamics defined in Section 1.3.1 is the marginal of the alternate dynamics on the hexagonal lattice.
In this square case we could have directly used the alternate dynamics, since $\mathbb{Z}^2$ is already a bipartite graph. Indeed we can consider the chessboard splitting of the sites in $\Lambda = V^{(1)} \cup V^{(2)}$, in black and white sites, with $|V^{(1)}| = |V^{(2)}| = |V| = |\Lambda|/2$. Black sites interact only with white sites and viceversa with the usual Ising Hamiltonian

$$\begin{aligned} H(\boldsymbol{\sigma}) &\equiv H(\sigma^{(1)}, \sigma^{(2)}) \\ &= - \sum_{x \in V^{(1)}} \left(\sigma_x^{(1)} h_x^{2\to 1}(\sigma^{(2)}) + \lambda_x \sigma_x^{(2)} \right) \\ &= - \sum_{x \in V^{(2)}} \left(\sigma_x^{(2)} h_x^{1\to 2}(\sigma^{(1)}) + \lambda_x \sigma_x^{(1)} \right). \end{aligned}$$

By Theorem 1.4.1 we immediately obtain that the invariant measure of the alternate dynamics is the Gibbs measure $\pi^G(\boldsymbol{\sigma}) = e^{-H(\boldsymbol{\sigma})}/Z$.
Anyway, one of the main interesting features of the doubling construction is that it makes always possible to perform an alternate dynamics since it allows to pass from the original graph to a new one which is bipartite by construction. In particular, the geometry of the doubling graph is strictly linked to the explicit form of the interaction given in the doubling Hamiltonian. Consider the case of the two dimensional square lattice $\mathbb{Z}^2$ and let $\Lambda \subset \mathbb{Z}^2$ be a finite box. Starting from this interaction graph we can define the graph $\Lambda^o = (V, E^o)$ orienting the edges down-left. The associated doubling graph turns out to be the hexagonal lattice and the corresponding doubling Hamiltonian coincides with the Hamiltonian (1.3.1) of the shaken dynamics. The same doubling graph would have been obtained by choosing the orientation up-right, with a pair Hamiltonian of the same form but with opposite direction for the interaction. Clearly, by choosing a different orientation instead of down-left and up-right in $\Lambda \in \mathbb{Z}^2$, a different doubling graph for the interaction can be derived with a resulting different pair Hamiltonian.
The shaken dynamics, as already said, turns out to be the marginal of the alternate dynamics defined on the doubling graph. Alternate dynamics on even and odd sites are already present in the literature (see [27]). Actually, in the shaken dynamics, the idea of alternate dynamics is combined with that of the doubling Hamiltonian and this interconnection enables to explore different geometries in the system moving from the original graph to its doubling, usually very different from the first.

2.3 Dynamical point of view

In the past, several approaches have been proposed to use the capabilities of parallel architecture to simulate statistical mechanics lattice models in an effective way and to apply Monte Carlo methods to solve discrete Optimization Problems. However, these methods are strongly tied to the particular architecture used for the simulation and make use of the similarities between the structure of the graph and the structure of the hardware in use. The literature on the topic is quite vast, especially in the computer engineering and applied physics communities. Some attention, though, should be paid to the theoretical foundation of these methods. Indeed, the control of the stochastic dynamics, or at least of its stationary measure, seems to be a minimal requirement in order to develop random algorithms in combinatorial optimization.
One of the main achievements of the shaken dynamics is that we are able to control explicitly its invariant measure in a more robust way with respect to the dynamics introduced in [36, 84]. First, we identify the stationary measure of the shaken dynamics defined on arbitrary graphs and not only on the regular square lattice. Moreover, this result holds when the dynamics is defined in the presence of an external field. Finally, in the case of $\mathbb{Z}^2$ we control the invariant measure also for different boundary conditions.
Another relevant feature of our dynamics is that its algorithm is natively parallel and it is not bound to any particular architecture or graph structure. Therefore its performances are likely to benefit from the development of parallel computing.
Even if the efficiency and the convergence to equilibrium of the shaken dynamics are not analyzed in this thesis, some preliminary numerical tests suggest that, comparing the single spin flip (SSF) dynamics, the PCA dynamics and the shaken (Sh) dynamics, their efficiency depends on the particular considered regime. A comparison between these dynamics defined on $\mathbb{Z}^2$ is discussed in Section 2.3.1. In Section 2.3.2 a possible application of the shaken dynamics to discrete optimization problems is described. Finally, Section 2.3.3 is devoted to the proof of Theorem 1.4.3.

2.3.1 Convergence to equilibrium: a comparison

We present here, as a remark, a comparison among the single spin flip (SSF) dynamics, the PCA dynamics and the shaken (Sh) dynamics in a simple case of "metastable regime": finite volume $\Lambda \in \mathbb{Z}^2$ with periodic boundary conditions and low temperature. More precisely let

$0 < q < \lambda < J$ and consider, for each $x \in \Lambda$, the local fields

$$h_x^{SSF}(\sigma) = \left[\frac{J}{2}(\sigma_{x^\uparrow} + \sigma_{x^\rightarrow} + \sigma_{x^\downarrow} + \sigma_{x^\leftarrow}) + 2\lambda\right]$$

$$h_x^{PCA}(\sigma) = \left[\frac{J}{2}(\sigma_{x^\uparrow} + \sigma_{x^\rightarrow} + \sigma_{x^\downarrow} + \sigma_{x^\leftarrow}) + q\sigma_x + \lambda\right]$$

$h_x^{ur}(\sigma)$ and $h_x^{dl}(\sigma)$ defined in (1.3.3) and (1.3.4), and the local transition probabilities

$$p_x^*(\sigma,\tau) := \frac{e^{\beta h_x^*(\sigma)\tau_x}}{2\cosh \beta h_x^*(\sigma)}, \qquad * = SSF, PCA, ur, dl$$

we have

$$\begin{aligned} P^{SSF}(\sigma,\tau) &= \frac{1}{|\Lambda|} p_x^{SSF}(\sigma,\tau) \qquad \text{with } \tau_y = \sigma_y \quad \forall y \neq x \\ P^{PCA}(\sigma,\tau) &= \prod_{x\in\Lambda} p_x^{PCA}(\sigma,\tau) \\ P^{Sh}(\sigma,\tau) &= \sum_{\sigma'\in\mathcal{X}_\Lambda} \prod_{x\in\Lambda} p_x^{dl}(\sigma,\sigma') \prod_{x\in\Lambda} p_x^{ur}(\sigma',\tau). \end{aligned}$$

For large inverse temperature β we have $p_x^*(\sigma,\tau) \sim 1$ if τ_x is parallel to the local field $h_x^*(\sigma)$. We call such a local move "along the drift". On the other hand $p_x^*(\sigma,\tau) \sim e^{-2\beta|h_x^*(\sigma)|}$ if τ_x is anti-parallel to the local field $h_x^*(\sigma)$. We call such a local move "against the drift".

The SSF dynamics is reversible with Gibbs invariant measure

$$\pi_\Lambda^G(\sigma) = \frac{e^{\beta\sum_x h_x^{SSF}(\sigma)\sigma_x}}{Z}$$

and the invariant measure of PCA and shaken dynamics is $\pi(\sigma)$ given in (1.4.3). All these measures, in the regime of large β, concentrate on the configuration with all positive spins $\underline{+1}$ representing the stable state. The configuration $\underline{-1}$ with all spins -1 represents, in this regime of low temperature, a metastable state. Indeed, by considering the first hitting time $\tau_{\underline{+1}}$ to $\underline{+1}$ starting from $\underline{-1}$, for the SSF dynamics we have for any $\delta > 0$ (see for instance [82], [12]):

$$\lim_{\beta\to\infty} P_{\underline{-1}}^{SSF}(\tau_{\underline{+1}} > e^{\beta(\Gamma-\delta)}) = 1 \tag{2.3.1}$$

with

$$\Gamma = 4J\ell_c - 2\lambda\ell_c^2 + 2\lambda(\ell_c - 1)$$

and critical size $\ell_c = \left[\frac{J}{\lambda}\right] + 1$, where $\left[\,\cdot\,\right]$ denotes the integer part. The typical exit paths from the metastable state $\underline{-1}$ follow a sequence of growing squares and rectangles (quasi squares) of plus spins up to the critical size ℓ_c. Starting from a rectangular droplet of plus spins a move against the drift is necessary to create a new line, and the line is completed with subsequent moves along the drift. A similar result holds for the PCA dynamics following the same arguments since again moves along the drift lead to rectangular droplets of plus spins and parallel updating against the drift has small probability for large β.

A different growth takes place in the case of shaken dynamics. Indeed using a similar argument as in [37] it is simple to prove that configurations with complete diagonals of plus spins can be used to construct a competitive way to go from the metastable to the stable state. Starting from the metastable state we have $h_x^{dl}(\underline{-1}) = -2J - q + \lambda$ for any x and so with a probability of order $e^{-2\beta(2J+q-\lambda)}$ a spin is flipped in a site x_0. In the subsequent semi-step (up–right interaction) of the dynamics with probability of order one we have plus spins in the sites $x_0^{\leftarrow}$ and $x_0^{\downarrow}$. The diagonal containing these sites grows with probability of order one in the subsequent moves of the shaken dynamics and it is complete after $L/2$ steps, with L the side of the volume Λ. To destroy a complete diagonal of plus spins a first move of probability

$$e^{-2\beta(2J-q+\lambda)}$$

is necessary and every successive erosion has a probability $e^{-2\beta(\lambda-q)}$. On the other hand, the probability to construct a new plus diagonal near the first one has a probability

$$e^{-2\beta(2J-q-\lambda)}.$$

Comparing these probabilities, we can obtain the estimate

$$P_\sigma^{Sh}(\tau_{\underline{+1}} < T_0) > a$$

with $T_0 = e^{2\beta[(2J+q-\lambda)]}$ and a not exponentially small in β, for any starting configuration σ. Indeed, it is sufficient to require that no move of probability asymptotically smaller than $e^{-2\beta(2J+q-\lambda)}$ takes place within T_0, a first complete diagonal is formed in the time interval $[0, T_0/2]$ and $L-1$ other complete diagonals are formed in the remaining time. We can conclude that for any $\delta > 0$

$$\lim_{\beta\to\infty} P_{\underline{-1}}^{Sh}(\tau_{\underline{+1}} < e^{2\beta[(2J+q-\lambda)+\delta]}) = 1.$$

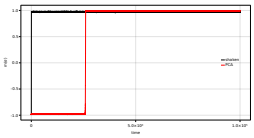

(a) $\beta = 1.3, q = 0.1, \lambda = 0.15$

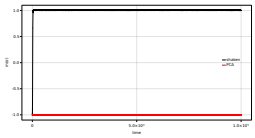

(b) $\beta = 2.3, q = 0.1, \lambda = 0.15$

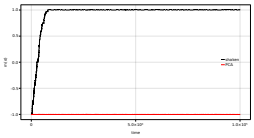

(c) $\beta = 3.3, q = 0.1, \lambda = 0.15$

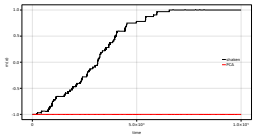

(d) $\beta = 4.0, q = 0.1, \lambda = 0.15$

Figure 2.1 Comparison of the magnetization over time for PCA and shaken dynamics for several values of the inverse temperature β.

This means that the crossover takes place for the shaken dynamics, typically, within a time corresponding to the time it takes, for the SSF and PCA, to flip the first spin to $+1$. In other words, the metastable behavior is no more present in the shaken dynamics (see Figure 2.1 for a numerical simulation). The asymmetric nature of the interaction gives the shaken dynamics a higher mobility with respect to its symmetric counterpart ("standard" PCA). This is the reason of shorter tunneling times. Note also that this higher mobility causes a slightly smaller magnetization at equilibrium.

This fact has been highlighted in [65, 66] where a comparison between the symmetric PCA and an irreversible PCA with totally asymmetric interaction has been performed in the case $\lambda = 0$. In Figure 2.2 a comparison between the evolution of the magnetization for a system subject to a symmetric PCA evolution and to shaken dynamics is shown for the same values of the parameters of [66]. It is clear that, with respect to the tunneling behavior, the shaken dynamics retains the same features of the irreversible PCA. However, in the case of the shaken dynamics the control of the invariant measure is more manageable thanks to reversibility.

On the other hand, with the same choice of parameters, if we compare the time necessary to reach the stable state $\underline{+1}$ starting from a configuration given by a supercritical square of plus spins in a see of minuses, the PCA dynamics is more rapid than the shaken dynamics if $J > 2q$.

This means that it is not possible to establish, *a priori*, whether the PCA or the shaken dynamics is faster, but it is necessary to take into account both the application and the starting configuration. This will be the subject of further investigations.

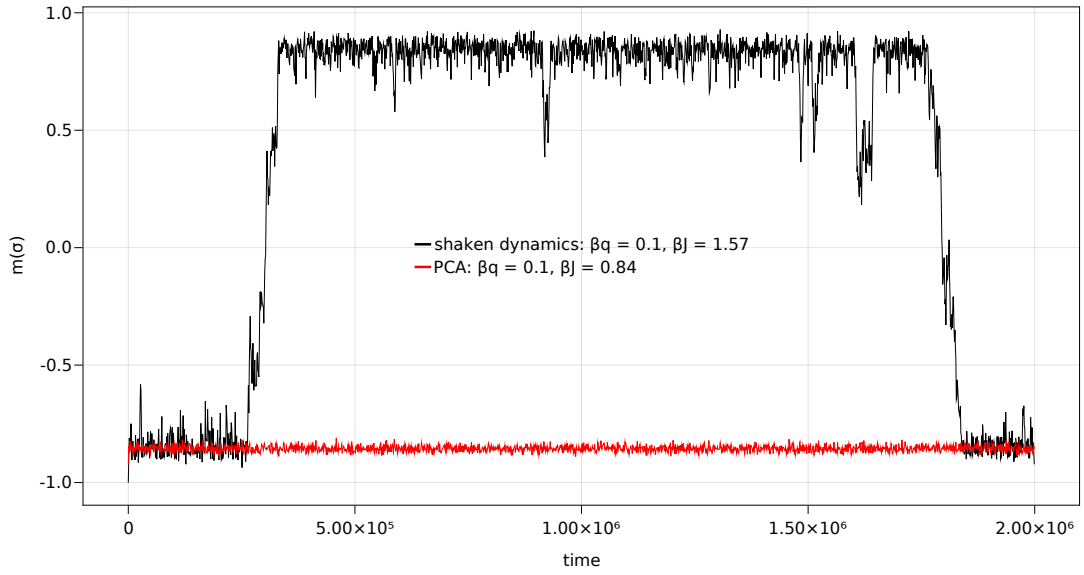

Figure 2.2 Comparison of the evolution of the magnetization for a spin system evolving according to a shaken dynamics (black) and according to a symmetric PCA (red). The values of the parameters are such that both dynamics exhibit the same spontaneous magnetization and are consistent with those of [66].

2.3.2 A parallel algorithm for discrete optimization problems

Corollary 1.4.2 shows how the definition of the shaken dyanmics on a general graph and its relation with the alternate dynamics gets the possibility to look for the minimum of a general Hamiltonian

$$H(\sigma) = -\sum_{e=\{x,y\}\in E} J_{xy}\sigma_x\sigma_y - 2\sum_{x\in V}\lambda_x\sigma_x \tag{2.3.2}$$

defined on $\{-1,+1\}^V$, by means of a parallel dynamics. In combinatorial optimization this result can be used as a parallel approach to the Quadratic Unconstrained Binary Optimization (QUBO) *i.e.*, the problem of minimizing a quadratic polynomial of binary variables.

To assess the effectiveness of the strategy presented in Corollary 1.4.2, we put forward some preliminary numerical tests on a simplified version of the Edward-Anderson model where the weight of the edges connecting neighboring sites is set to $J = +1$ with probability $\frac{1}{2}$ and $J = -1$ with probability $\frac{1}{2}$ and where the external field is zero. In this case, setting $q > 2$ is sufficient to satisfy the hypotheses of the corollary. We compared the results with those obtained with single spin flip heat bath dynamics simulations and considered "grids" with side length 128 and 256. With this setting, the heuristic minima that we obtained with

the shaken dynamics are essentially equivalent to those obtained with the single spin flip dynamics. However the speed up with respect to the single spin flip dynamics was significant. To be as fair as possible in this comparison, we renormalized the time of the single spin flip dynamics with the number of vertices in the graph so to have the same number of "attempted spin flips". We observed a speed-up of about 10 times when considering, for both algorithms, a CPU implementation and up to 200 times when comparing the CPU implementation of the single spin flip dynamics with a GPU implementation of the shaken dynamics. We believe these preliminary numerical results to be rather encouraging and we plan to perform a more thorough investigation of the performances of the shaken dynamics to find the minimizers of $H(\sigma)$ in a future work.

2.3.3 A parallel algorithm for approximate sampling from the Gibbs measure

We provide the proof of Theorem 1.4.3 stating that on the regular square lattice $\mathbb{Z}^2$ and with homogeneous ferromagnetic interaction, the invariant measure of the shaken dynamics is close in total variation distance to the Gibbs measure with Hamiltonian (1.3.7)

$$H(\sigma) = -J \sum_{\langle x,y\rangle \in \mathcal{B}_\Lambda} \sigma_x \sigma_y - 2\lambda \sum_{x\in\Lambda} \sigma_x. \tag{2.3.3}$$

Proof of Theorem 1.4.3. To prove Theorem 1.4.3 it is possible to argue as in the proof of Theorem 1.2 in [84].
In our notation π_Λ and π_Λ^G have the role, respectively, of π_{PCA} and π_G used in [84]. Further let $g_x(\sigma) := J(\sigma_{x^\downarrow} + \sigma_{x^\leftarrow})$ be the analogue of $h_i(\sigma)$ in [84]. Here we assume $\lambda < 0$. The case $\lambda > 0$ can be treated likewise.
Recalling that $\delta = e^{-2q}$, it is possible to write Z_σ in the following way:

$$\begin{aligned} Z_\sigma &= \sum_\tau e^{-H(\sigma,\tau)} = \sum_\tau e^{-H(\sigma,\sigma)} e^{-[H(\sigma,\tau)-H(\sigma,\sigma)]} \\ &= e^{q|\Lambda|} e^{-H(\sigma)} \sum_\tau e^{\sum_{x:\sigma_x\neq\tau_x} -2g_x(\sigma)\sigma_x - 2q - 2\lambda\sigma_x} \\ &= e^{q|\Lambda|} e^{-H(\sigma)} \sum_{I\subset\Lambda} \delta^{|I|} \prod_{x\in I} e^{-2g_x(\sigma)\sigma_x - 2\lambda\sigma_x} \\ &= e^{q|\Lambda|} e^{-H(\sigma)} \prod_{x\in\Lambda} (1 + \delta e^{-2g_x(\sigma)\sigma_x - 2\lambda\sigma_x}) \end{aligned} \tag{2.3.4}$$

where the sum over τ has been rewritten as the sum over all subsets $I \subset \Lambda$ such that $\tau_x = -\sigma_x$ if $x \in I$ and $\tau_x = \sigma_x$ otherwise. The factor $e^{q|\Lambda|}$ does not depend on σ and cancels out in the ratio $\frac{Z_\sigma}{Z}$.
Call $f(\sigma) := \prod_{x\in\Lambda}(1 + \delta e^{-2g_x(\sigma)\sigma_x - 2\lambda\sigma_x})$, $w(\sigma) := e^{-H(\sigma)}f(\sigma) = w^G(\sigma)f(\sigma)$. Then (2.3.4) can be rewritten as

$$\pi_\Lambda(\sigma) = \frac{w(\sigma)}{\sum_\tau w(\tau)} = \frac{w^G(\sigma)f(\sigma)}{\sum_\tau w^G(\tau)f(\tau)} = \frac{\frac{w^G(\sigma)}{Z^G}f(\sigma)}{\sum_\tau \frac{w^G(\tau)}{Z^G}f(\tau)} = \frac{\pi^G_\Lambda(\sigma)f(\sigma)}{\pi^G_\Lambda(f)}$$

with $\pi^G_\Lambda(f) = \sum_\sigma \pi^G_\Lambda(\sigma)f(\sigma)$.
As in [84], using Jensen's inequality the total variation distance between π_Λ and π^G_Λ can be bounded as

$$\|\pi_\Lambda - \pi^G_\Lambda\|_{TV} \leq \sqrt{\frac{\pi^G_\Lambda(f^2)}{(\pi^G_\Lambda(f))^2} - 1} =: \sqrt{(\Delta(\delta))}.$$

To prove the theorem, it will be shown that $\Delta(\delta) = O(\delta^2|\Lambda|)$.
By writing $\Delta(\delta) = e^{\log(\pi^G_\Lambda(f^2)) - 2\log(\pi^G_\Lambda(f))} - 1$, the claim follows by showing that the argument of the exponential divided by $|\Lambda|$ is analytic in δ and that the first order term of its expansion in δ cancels out.
In other words the claim follows thanks to the following lemma.

Lemma 2.3.1. *There exists J_c such that, for all $J > J_c$*

1. $\frac{\log(\pi^G_\Lambda(f^2))}{|\Lambda|}$ *and* $\frac{\log(\pi^G_\Lambda(f))}{|\Lambda|}$ *are analytic in δ for $|\delta| < \delta_J$*
2. $\frac{\log(\pi^G_\Lambda(f^2))}{|\Lambda|} - 2\frac{\log(\pi^G_\Lambda(f))}{|\Lambda|} = O(\delta^2)$

Proof of Lemma 2.3.1. The analyticity of $\frac{\log(\pi^G_\Lambda(f^2))}{|\Lambda|}$ and $\frac{\log(\pi^G_\Lambda(f))}{|\Lambda|}$ is proven by showing that these quantities can be written as partition functions of an abstract polymer gas. The analyticity is obtained using standard cluster expansion.
To carry over this task, we will rewrite $\pi^G_\Lambda(f^k)$ in terms of standard Peierls contours. Divide the sites in Λ according to the value of the spins and number of edges of the Peierls contour left and below the site in the following way:

- $\Lambda_{\substack{--\\-}}$: $\{x \in \Lambda : \sigma_x = -1 \wedge (\sigma_{x^\leftarrow} = -1, \sigma_{x^\downarrow} = -1)\}$;
- $\Lambda_{\substack{+-\\-}}$: $\{x \in \Lambda : \sigma_x = -1 \wedge ((\sigma_{x^\leftarrow} = +1, \sigma_{x^\downarrow} = -1) \vee (\sigma_{x^\leftarrow} = -1, \sigma_{x^\downarrow} = +1))\}$;
- $\Lambda_{\substack{+-\\+}}$: $\{x \in \Lambda : \sigma_x = -1 \wedge \sigma_{x^\leftarrow} = +1, \sigma_{x^\downarrow} = +1\}$;

- $\Lambda_{\substack{++\\+}}$: $\{x \in \Lambda : \sigma_x = +1 \wedge (\sigma_{x^{\leftarrow}} = +1, \sigma_{x^{\downarrow}} = +1)\}$;
- $\Lambda_{\substack{-+\\+}}$: $\{x \in \Lambda : \sigma_x = +1 \wedge ((\sigma_{x^{\leftarrow}} = +1, \sigma_{x^{\downarrow}} = -1) \vee (\sigma_{x^{\leftarrow}} = -1, \sigma_{x^{\downarrow}} = +1))\}$;
- $\Lambda_{\substack{-+\\-}}$: $\{x \in \Lambda : \sigma_x = +1 \wedge (\sigma_{x^{\leftarrow}} = -1, \sigma_{x^{\downarrow}} = -1)\}$;

With this notation, $f(\sigma)$ can be written as

$$\begin{aligned} f(\sigma) &= (1+\delta e^{-4J+2\lambda})^{|\Lambda|} \prod_{x\in\Lambda_{\substack{+-\\-}}} \frac{(1+\delta e^{+2\lambda})}{(1+\delta e^{-4J+2\lambda})} \prod_{x\in\Lambda_{\substack{+-\\+}}} \frac{(1+\delta e^{+4J+2\lambda})}{(1+\delta e^{-4J+2\lambda})} \\ &\prod_{x\in\Lambda_{\substack{++\\+}}} \frac{(1+\delta e^{-4J-2\lambda})}{(1+\delta e^{-4J+2\lambda})} \prod_{x\in\Lambda_{\substack{-+\\+}}} \frac{(1+\delta e^{-2\lambda})}{(1+\delta e^{-4J+2\lambda})} \prod_{x\in\Lambda_{\substack{-+\\-}}} \frac{(1+\delta e^{+4J-2\lambda})}{(1+\delta e^{-4J+2\lambda})} \\ &= (1+\delta e^{-4J+2\lambda})^{|\Lambda|} \tilde{\xi}(\sigma,\lambda) \end{aligned} \tag{2.3.5}$$

with

$$\begin{aligned} \tilde{\xi}(\sigma,\lambda) = &\left[\frac{(1+\delta e^{+2\lambda})}{(1+\delta e^{-4J+2\lambda})}\right]^{\left|\Lambda_{\substack{+-\\-}}\right|} \left[\frac{(1+\delta e^{+4J+2\lambda})}{(1+\delta e^{-4J+2\lambda})}\right]^{\left|\Lambda_{\substack{+-\\+}}\right|} \\ &\left[\frac{(1+\delta e^{-4J-2\lambda})}{(1+\delta e^{-4J+2\lambda})}\right]^{\left|\Lambda_{\substack{++\\+}}\right|} \left[\frac{(1+\delta e^{-2\lambda})}{(1+\delta e^{-4J+2\lambda})}\right]^{\left|\Lambda_{\substack{-+\\+}}\right|} \left[\frac{(1+\delta e^{+4J-2\lambda})}{(1+\delta e^{-4J+2\lambda})}\right]^{\left|\Lambda_{\substack{-+\\-}}\right|} \end{aligned} \tag{2.3.6}$$

For a given a configuration $\sigma \in \mathcal{X}_\Lambda$, we denote by $\gamma(\sigma)$ its Peierls contour in the dual $\mathcal{B}^*_\Lambda = \cup_{(x,y)\in\mathcal{B}_\Lambda}(x,y)^*$

$$\gamma(\sigma) := \{(x,y)^* \in \mathcal{B}^*_\Lambda : \ \sigma_x\sigma_y = -1\} \tag{2.3.7}$$

Noting that $e^{-H(\sigma)} = e^{(2J-2\lambda)|\Lambda|} e^{-2J|\gamma(\sigma)|+4\lambda|V_+(\sigma)|}$, with $|V_+(\sigma)| = \sum_{x\in\Lambda} 1_{\{\sigma_x=+1\}}$ is the number of plus spins in Λ of configuration σ, we have

$$\pi^G_\Lambda(f^k) = \frac{1}{Z^G} e^{(2J-2\lambda)|\Lambda|} (1+\delta e^{-4J+2\lambda})^{k|\Lambda|} \sum_\sigma \left[e^{-2J|\gamma(\sigma)|+4\lambda|V_+(\sigma)|} \tilde{\xi}^k(\sigma,\lambda)\right] \tag{2.3.8}$$

Setting

$$\xi(\sigma,\lambda)=\left[\frac{(1+\delta e^{+2\lambda})}{(1+\delta e^{-4J+2\lambda})}\right]^{\left|\Lambda\,{}^{+-}_{-}\right|}\left[\frac{(1+\delta e^{+4J+2\lambda})}{(1+\delta e^{-4J+2\lambda})}\right]^{\left|\Lambda\,{}^{+-}_{+}\right|}$$
$$\left[\frac{e^{+2\lambda}(1+\delta e^{-4J-2\lambda})}{(1+\delta e^{-4J+2\lambda})}\right]^{\left|\Lambda\,{}^{++}_{+}\right|}\left[\frac{e^{+2\lambda}(1+\delta e^{-2\lambda})}{(1+\delta e^{-4J+2\lambda})}\right]^{\left|\Lambda\,{}^{-+}_{+}\right|}\left[\frac{e^{+2\lambda}(1+\delta e^{+4J-2\lambda})}{(1+\delta e^{-4J+2\lambda})}\right]^{\left|\Lambda\,{}^{-+}_{-}\right|} \tag{2.3.9}$$

allows us to write, for $k\in\{1,2\}$,

$$\sum_{\sigma}\left[e^{-2J|\gamma(\sigma)|+4\lambda|V_+(\sigma)|}\tilde{\xi}^k(\sigma,\lambda)\right]=\sum_{\sigma}\left[e^{-2J|\gamma(\sigma)|}\left(e^{+2\lambda|V_+(\sigma)|}\right)^{2-k}\xi^k(\sigma,\lambda)\right] \tag{2.3.10}$$

A straightforward computation yields $\xi^k(\sigma,\lambda)\le\xi^k(\sigma,0)$ and then

$$\sum_{\sigma}\left[e^{-2J|\gamma(\sigma)|}\left(e^{+2\lambda|V_+(\sigma)|}\right)^{2-k}\xi^k(\sigma,\lambda)\right]\le\sum_{\sigma}e^{-2J|\gamma(\sigma)|}\xi^k(\sigma,0)=2\sum_{\gamma}e^{-2J|\gamma|}\xi^k(\gamma,0)$$

where $\xi^k(\gamma,0)$ coincides with $\xi^I_k(\Gamma)$ in the proof of Lemma 2.3 in [84], with $\left|\Lambda\,{}^{+-}_{-}\right|+\left|\Lambda\,{}^{-+}_{+}\right|=|l_1(\Gamma)|$ and $\left|\Lambda\,{}^{+-}_{+}\right|+\left|\Lambda\,{}^{-+}_{-}\right|=|l_2(\Gamma)|$.

This implies that the proof can be concluded following the same steps as in [84]. □

2.4 Static point of view

The present section is devoted to the study of the thermodynamical relations (*i.e.* average magnetization and correlation functions) and the critical behavior of the measure π, defined in (1.4.3), in the case of the square and triangular lattices and with no external field.
In Section 2.4.1, we first illustrate how the powerful connection between the Ising model and the random-cluster model may be applied to our model by exploiting the representation of the doubling construction. Sections 2.4.2 and 2.4.3 are devoted to the proofs of those theorems concerning the analysis of the measure π from the static point of view.

2.4.1 The coupling

Consider the hexagonal lattice $\mathbb{H}=(V^b,E^b)$, *i.e.* the doubling graph of the square lattice $\Lambda\in\mathbb{Z}^2$. As already discussed in Section 1.4, we distinguish two types of edges, $E^b=E_J\cup E_q$

and we denote the corresponding edge-weights by

$$\mathrm{J}_e = \begin{cases} J & \text{if } e \in E_J \\ q & \text{if } e \in E_q. \end{cases}$$

Exploiting this representation, we can apply to our model the successful connection between the Ising model and the random-cluster model.
Assume periodic boundary conditions and for any $e \in E^b$ define the edge-weight $p_e \in [0,1]$ as follows

$$p_e = \begin{cases} p_J = 1 - e^{-2J} & \text{if } e \in E_J \\ p_q = 1 - e^{-2q} & \text{if } e \in E_q \end{cases}$$

Consider the measure on Ω

$$\Phi_{p_e}(\omega) = \frac{1}{Z_{RC}} \Big\{ \prod_{e \in E^b} p_e^{\omega(e)} (1-p_e)^{1-\omega(e)} \Big\} 2^{k(\omega)} \tag{2.4.1}$$

with partition function

$$Z_{RC} = \sum_{\omega \in \Omega} \Big\{ \prod_{e \in E^b} p_e^{\omega(e)} (1-p_e)^{1-\omega(e)} \Big\} 2^{k(\omega)}$$

and consider the Gibbs measure on the space $\mathcal{X}_{V^b} := \mathcal{X}_\Lambda^2 = \mathcal{X}_\Lambda \times \mathcal{X}_\Lambda$ of pairs of configurations $\boldsymbol{\sigma} = (\sigma^{(1)}, \sigma^{(2)})$ on the hexagonal lattice

$$\pi_2(\sigma^{(1)}, \sigma^{(2)}) = \frac{e^{-H(\sigma^{(1)}, \sigma^{(2)})}}{Z} \tag{2.4.2}$$

associated to the pair Hamiltonian (1.3.10) in the case of zero external field (*i.e.* $\lambda = 0$)

$$H(\sigma^{(1)}, \sigma^{(2)}) = - \sum_{e=\{x,y\} \in E^b} w(x,y) \boldsymbol{\sigma}_x \boldsymbol{\sigma}_y = - \sum_{e \in E^b} \mathrm{J}_e \sigma^{(1)}_{e^{(1)}} \sigma^{(2)}_{e^{(2)}} \tag{2.4.3}$$

where $x = e^{(1)}, y = e^{(2)}$ are the two sites in $\mathbb{H}$ connected by the edge e.

Following the general theory described in Section 2.1.1 we define now a coupling between our pairs of configurations $\boldsymbol{\sigma} = (\sigma^{(1)}, \sigma^{(2)}) \in \mathcal{X}_\Lambda^2$ and the random-cluster configuration $\omega \in \Omega$ by the following probability mass on $\mathcal{X}_\Lambda^2 \times \Omega$:

$$\mu(\boldsymbol{\sigma}, \omega) \propto \prod_{e \in E} \Big\{ (1-p_e)\delta_{\omega(e),0} + p_e \delta_{\omega(e),1} \delta_e(\boldsymbol{\sigma}) \Big\} \tag{2.4.4}$$

where

$$\delta_e(\boldsymbol{\sigma}) = \delta_{\sigma_x^{(1)},\sigma_y^{(2)}} \quad \text{for} \quad e=(x,y), \text{ with } x \in V^{(1)}, y \in V^{(2)}$$

The classical results of Theorems 2.1.2 and 2.1.3 may be stated now as follows:

Proposition 2.4.1. *If $p_J = 1 - e^{-2J}$ and $p_q = 1 - e^{-2q}$*

1) the marginal on $\mathcal{X}^2_\Lambda$ of $\mu(\boldsymbol{\sigma},\omega)$ is

$$\mu_1(\boldsymbol{\sigma}) = \sum_{\omega\in\Omega} \mu(\boldsymbol{\sigma},\omega) = \pi_2(\sigma^{(1)},\sigma^{(2)})$$

2) the marginal on Ω of $\mu(\boldsymbol{\sigma},\omega)$ is

$$\mu_2(\omega) = \sum_{\boldsymbol{\sigma}\in\mathcal{X}^2_{\Lambda,B}} \mu(\boldsymbol{\sigma},\omega) = \Phi_{p_e}(\omega)$$

3) the conditional measure on $\mathcal{X}^2_\Lambda$ given ω is obtained by putting uniformly random spins on entire clusters of ω. These spins are constant on given clusters, are independent between clusters and each is uniformly distributed on the set $\{-1,+1\}$.

4) the conditional measure on Ω given $\boldsymbol{\sigma}$ is obtained by setting $\omega(e)=0$ if $\delta_e(\boldsymbol{\sigma})=0$ and otherwise $\omega(e)=1$ with probability p_J (p_q) for $e \in E_J$ ($e \in E_q$).

With this construction we can easily prove that our model exhibits a phase transition and we can compute the strong anisotropy of the correlation functions.

2.4.2 Thermodynamical relations

We provide the proof of Theorem 1.4.4 concerning the thermodynamical relations of the measures π.

Proof of Theorem 1.4.4.

1) The statement immediately follows from direct computation, indeed:

$$m = \sum_\sigma \frac{\sum_{x\in\Lambda}\sigma_x}{|\Lambda|} \cdot \sum_\tau \frac{e^{-H(\sigma,\tau)}}{Z} = \frac{1}{2}\sum_{(\sigma,\tau)} \frac{\sum_{x\in\Lambda}(\sigma_x+\tau_x)}{|\Lambda|} \cdot \frac{e^{-H(\sigma,\tau)}}{Z} = m_2$$

where the second equality follows by a symmetry argument.

2) The standard coupling between Ising and the RCM on $\mathbb{H}$ yields

$$\begin{aligned}\pi^+(\sigma_x) &= \sum_{\sigma}\sum_{\tau}\sigma_x\pi^+(\sigma) = \sum_{\boldsymbol{\sigma}}\sigma^{(1)}_{x^{(1)}}\pi_2^+(\boldsymbol{\sigma}) = \pi_2^+(\sigma^{(1)}_{x^{(1)}})\\ &= \sum_{\omega\in\Omega}\sum_{\boldsymbol{\sigma}}\mu(\boldsymbol{\sigma},\omega)\sigma^{(1)}_{x^{(1)}}\left(\mathbb{1}_{x^{(1)}\leftrightarrow\partial\Lambda^{(1)}} + \mathbb{1}_{x^{(1)}\nleftrightarrow\partial\Lambda^{(1)}}\right)\\ &= \Phi_{p_e}(x^{(1)}\leftrightarrow\partial\Lambda^{(1)}) + \sum_{\omega\in\Omega}\sum_{\boldsymbol{\sigma}}\left[\mu(\boldsymbol{\sigma},\omega|\omega)\sigma^{(1)}_{x^{(1)}}\mathbb{1}_{x^{(1)}\nleftrightarrow\partial\Lambda^{(1)}}\right]\Phi_{p_e}(\omega)\\ &= \Phi_{p_e}(x^{(1)}\leftrightarrow\partial\Lambda^{(1)})\end{aligned}$$

since by Proposition 2.4.1 the square bracket vanishes. The minus boundary conditions can be treated in the same way.

3) The proof of point (3) can be obtained following the same argument.

4) Let $\gamma\subset E^b$ be a path of open edges connecting two vertices $x^{(1)}$, $y^{(1)}\in V^{(1)}$. We introduce the notation $\eta(\omega)\supset\gamma$ to identify all the configurations $\omega\in\Omega$ such that $\omega(e)=1, \forall e\in\gamma$. By definition

$$\begin{aligned}\Phi_{p_e}(x\leftrightarrow y) &= \sum_{\gamma:x\leftrightarrow y}\sum_{\substack{\omega\in\Omega:\\ \eta(\omega)\supset\gamma}}\Phi_{p_e}(\omega)\\ &= \frac{1}{Z_{RC}}\sum_{\gamma:x\leftrightarrow y}\left(\prod_{e\in\gamma}p_e\right)\sum_{\omega'\in\{0,1\}^{E^b\setminus\gamma}}\left(\prod_{e\in E^b\setminus\gamma}p_e^{\omega'(e)}(1-p_e)^{1-\omega'(e)}\right)2^{k(\eta(\omega')\cup\gamma)}\\ &= \frac{1}{Z_{RC}}\sum_{\gamma:x\leftrightarrow y}\left(\prod_{e\in\gamma}p_e\right)Z_\gamma\end{aligned}$$

where

$$Z_\gamma = \sum_{\omega'\in\{0,1\}^{E^b\setminus\gamma}}\left(\prod_{e\in E^b\setminus\gamma}p_e^{\omega'(e)}(1-p_e)^{1-\omega'(e)}\right)2^{k(\eta(\omega')\cup\gamma)}$$

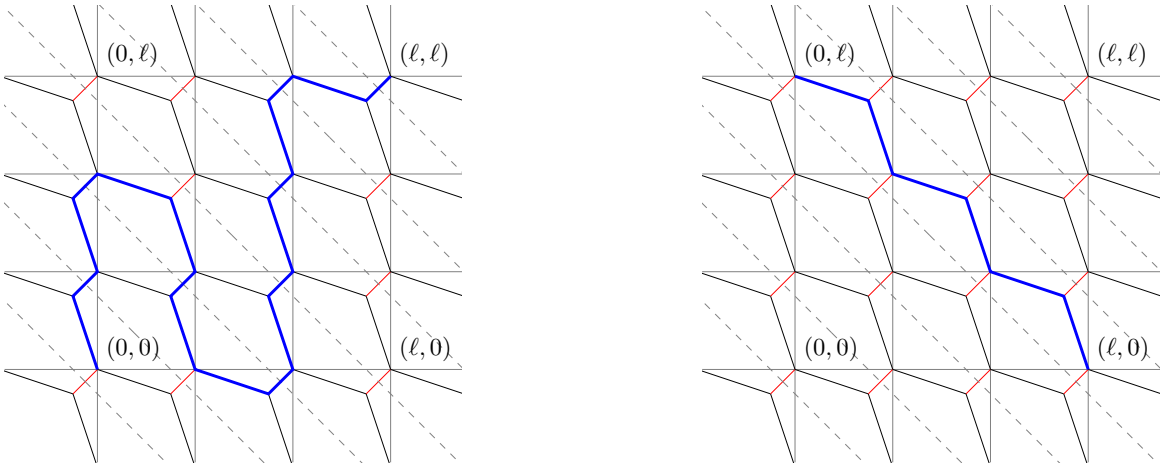

(a) **(b)**

Figure 2.3 The lattice $\mathbb{H}$ with the slices used for the estimation of the correlation functions. Picture (a) shows an example of path $\gamma : (0,0) \leftrightarrow (\ell,\ell)$. Picture (b) shows the diagonal path γ^*.

Upper bound

For any path γ and any configuration $\omega \in \Omega$ we denote by ω' the restriction of ω to the set of edges in $E^b \setminus \gamma$ and by ω'' its restriction to the set of edges in γ.

Since $k(\eta(\omega)) \geq k(\eta(\omega') \cup \gamma)$ we can state the following inequality for the partition function

$$\begin{aligned} Z_{RC} &\geq \sum_{\omega\in\Omega} \left(\prod_{e\in\gamma} p_e^{\omega(e)} (1-p_e)^{1-\omega(e)} \right) \left(\prod_{e\in E^b\setminus\gamma} p_e^{\omega(e)} (1-p_e)^{1-\omega(e)} \right) 2^{k(\eta(\omega')\cup\gamma)} \\ &= \left(\prod_{e\in\gamma} \sum_{\omega''\in\{0,1\}^{|\gamma|}} p_e^{\omega(e)} (1-p_e)^{1-\omega(e)} \right) Z_\gamma = Z_\gamma \end{aligned}$$

This observation implies

$$\Phi_{p_e}(x \leftrightarrow y) \leq \sum_{\gamma : x\leftrightarrow y} \left(\prod_{e\in\gamma} p_e \right) \tag{2.4.5}$$

Now let us suppose to slice the lattice $\mathbb{H}$ as in Fig. 2.3. It is easy to see that each path $\gamma : (0,0) \leftrightarrow (\ell,\ell)$ must visit all slices separating $(0,0)$ and (ℓ,ℓ) and therefore it crosses at least 2ℓ q-edges (see Fig. 2.3a). We give an upper bound for the sum in (2.4.5) in terms of possible crossing-paths that start in $(0,0)$ and stop in the slice which contains (ℓ,ℓ).

The transition from one slice to the other is determined by the crossing of a q-edge. After a q-edge has been crossed the path must traverse an arbitrary number of J-edges, either on the left or on the right, before crossing the next q-edge. Denoting by $\Gamma(n, 2\ell)$ the number of one dimensional random walks between slices of lenght n arriving at distance 2ℓ from the origin, we can write

$$\begin{aligned}\Phi_{p_e}((0,0) \leftrightarrow (\ell,\ell)) &\leq \sum_{n=2\ell}^{\infty} \Gamma(n,2\ell)(2p_q p_J)^n \left(\sum_{m=0}^{\infty} p_J^m\right)^n \\ &= \sum_{n=2\ell}^{\infty} \Gamma(n,2\ell)(2p_q p_J)^n \left(\frac{1}{1-p_J}\right)^n \\ &= \sum_{n=2\ell}^{\infty} \binom{n}{\frac{n+2\ell}{2}} \left(\frac{2p_q p_J}{1-p_J}\right)^n \leq \sum_{n=2\ell}^{\infty} \left(\frac{4p_q p_J}{1-p_J}\right)^n.\end{aligned}$$

The last sum converges if q is sufficiently small so that the parameters p_J and p_q satisfy the condition $\frac{4p_q p_J}{1-p_J} < 1$ and we get

$$c_1 = \frac{\left(\frac{4p_q p_J}{1-p_J}\right)^{2\ell}}{1-\left(\frac{4p_q p_J}{1-p_J}\right)}.$$

Lower bound

We introduce the diagonal path γ^* connecting $(0,\ell)$ and $(\ell,0)$ remaining in the same slice as in Fig. 2.3b and $\bar{\gamma} = \gamma^* \cup \partial\gamma^*$. Let $Z_{E^b\setminus\bar{\gamma}}$ be the partition function of the random-cluster model defined on the graph $\mathbb{H}_{\bar{\gamma}} = (V^b, E^b \setminus \bar{\gamma})$. By Theorem (3.60) in [53] we have that $Z_{E^b\setminus\bar{\gamma}} \geq Z_{E^b} = Z_{RC}$ and hence we can give a lower bound for the correlation function as follows

$$\begin{aligned}&\Phi_{p_e}((0,\ell) \leftrightarrow (\ell,0)) \geq \\ &\geq \frac{1}{Z_{RC}} \left(\prod_{e\in\gamma^*} p_e\right) \sum_{\omega''\in\{0,1\}^{E\setminus\bar{\gamma}}} \left[\prod_{e\in\partial\gamma^*} (1-p_e)\right] \left[\prod_{e\in E^b\setminus\bar{\gamma}} p_e^{\omega''(e)}(1-p_e)^{1-\omega''(e)}\right] 2^{k(\omega'')+1} \\ &= \frac{1}{Z_{RC}} \left(\prod_{e\in\gamma^*} p_e\right) \left[\prod_{e\in\partial\gamma^*} (1-p_e)\right] 2Z_{E\setminus\bar{\gamma}} \\ &\geq 2\left(\prod_{e\in\gamma^*} p_e\right) \left[\prod_{e\in\partial\gamma^*} (1-p_e)\right] \\ &= 2e^{-4J}(1-e^{-2J})^{2\ell} e^{-2q(2\ell+1)} = c_2.\end{aligned}$$

If q is sufficiently small such that, for instance,

$$\frac{4p_q}{(1-p_q)(1-p_J)} < \frac{1}{2}$$

and

$$\left(\frac{p_q}{1-p_q}\right)^2 < \frac{(1-p_J)^3(1-p_q)}{16},$$

we immediately get $c_1 < c_2$. Note that the first of these two conditions is stronger than $\frac{4p_q p_J}{1-p_J} < 1$ and, therefore, c_1 is well defined.

□

2.4.3 Critical behavior

We prove Theorem 1.4.5 concerning the critical behavior of the measure π on the hexagonal lattice. The proof of Theorem 1.4.7 which provides the critical curve for the shaken dynamics defined on the triangular lattice follows by similar arguments.

Proof of Theorem 1.4.5. This is an application of Theorem 1.1 in [25] holding for a planar non-degenerate locally-finite doubly periodic weighted graph $\mathcal{G}$. Here we consider the case where $\mathcal{G}$ is the hexagonal lattice $\mathbb{H}$. We denote by $G = (V, E)$ the embedding of the hexagonal lattice in the torus which can be obtained by periodically glueing on the torus the cell represented in Fig. 2.4. As shown in [25] the critical curve relating the parameters J and q of the Hamiltonian (1.4.14) is the unique solution of the equation (2.1.13), which assumes the following explicit form in the hexagonal case

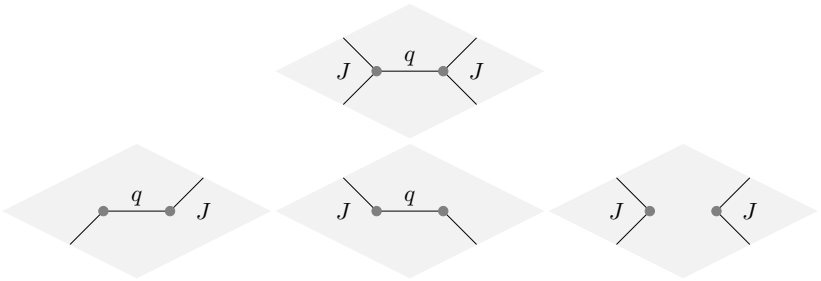

Figure 2.4 The periodic cell on the torus and the three corresponding even subgraphs $\gamma \in \mathcal{E}_1$.

$$1 = 2\tanh J \tanh q + \tanh^2 J \tag{2.4.6}$$

where on the r.h.s. we have the sum of the contributions from the three even subgraphs in $\mathcal{E}_1$ shown in Fig. 2.4 while on the l.h.s. 1 is the contribution of the unique graph in $\mathcal{E}_0$ without edges. We refer to Section 2.1.2 for the formal definition of $\mathcal{E}_0$ and $\mathcal{E}_1$.
Solving equation (2.4.6) w.r.t. J gives the curve

$$J(q) = \tanh^{-1}\left(\sqrt{\tanh^2 q + 1} - \tanh q\right) \tag{2.4.7}$$

represented in Fig. 1.7. □

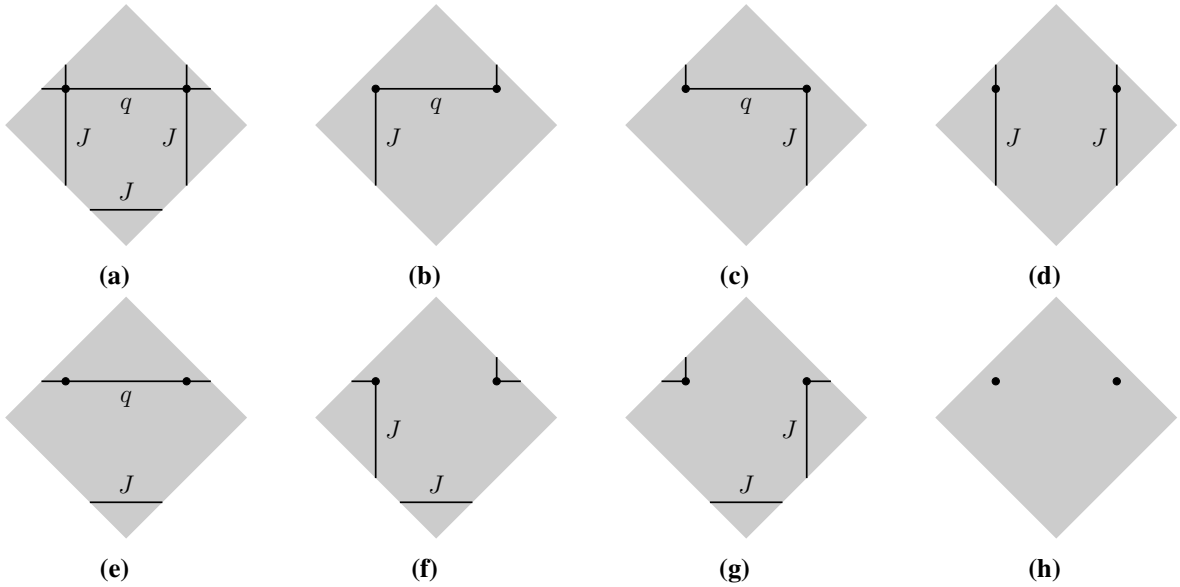

Figure 2.5 The elementary cell (a) for the shaken interaction on the triangular lattice and the corresponding even subgraphs. Subgraphs (a) and (h) wind around the torus an even number of times and are, therefore, in $\mathcal{E}_0$ whereas the remaining subgraphs are in $\mathcal{E}_1$.

Proof of Theorem 1.4.7. Again, this is an application of Theorem 1.1 in [25].
The square lattice induced by the shaken dynamics on the triangular lattice, with $J_e = q$ for the self–interaction edges and $J_e = J$ for the other edges, satisfies the hypotheses of the theorem and can be obtained by periodically repeating the elementary cell of Figure 2.5. A direct application of (2.1.13) yields the claim. □

3 Metastability for the Ising model on the hexagonal lattice

3.1 Motivations and overview on the literature

A thermodynamical system, subject to a *noisy dynamics*, exhibits metastable behavior when it remains for a long time in the vicinity of a state that is a local minimum of the energy before reaching a more stable state through a sudden transition. On a short time scale, the system behaves as if it were in equilibrium whereas, on a long time scale, it moves between regions of its state space. This motion, linked to first order phase transitions, is triggered by the appearance of a *critical* microscopic configuration of the system via a spontaneous fluctuation or some external perturbation.
Several termodynamical systems, ranging from magnets immersed into an external magnetic field to supercooled liquids to supersaturated gases, may show metastability. However this phenomenon is not exclusive of thermodynamical systems, but it appears in a plethora of diverse fields including biology, chemistry, computer science, economics.

Given the peculiar features of metastability outlined above, when studying the metastable behavior of a system one is typically interested in studying the properties of the *transition time* towards the stable state, the features of the critical configurations and the characterization of typical paths along which the transition takes place.
A first dynamical approach to the rigorous study of metastability, known as *pathwise approach*, was initiated in [19] and developed in [80, 81, 88], see also [82, 20]. This approach derives large deviation estimates of the first hitting time, of the critical configurations and of the tube of typical trajectories. It is based on the notions of cycles and cycle paths and it hinges on a detailed knowledge of the energy landscape. The pathwise approach was further developed in [69, 29, 31, 42, 43] to disentangle the study of transition time from the one of typical trajectories and to treat irreversible systems. This method has been applied to study

the metastable behavior for the Ising model with isotropic and anisotropic interaction, in different dimensions, with different external magnetic fields evolving according to Glauber dynamics in [8, 63, 62, 74, 78, 79, 82, 59]. Pathwise approach has been used also for a variety of models evolving according to Glauber dynamics: Blume Capel model in [34, 29], Potts model in [76] and hard-core model in [77, 92, 56].
Another approach is the *potential-theoretic approach*, initiated in [13]. We refer to [12] for an extensive discussion and applications to different models. The potential-theoretical approach is based on the study of the hitting time through the use of the Dirichlet form and spectral properties of the transition matrix. One of the advantages of this method is that it provides an estimate of the expected value of the transition time including the prefactor, by exploiting a detailed knowledge of the critical configurations, see [14, 12]. This method was applied for Ising-like models evolving according to Glauber dynamics [5, 16, 33].
Recently other approaches are described in [6, 7, 51] and in [11].
Metastability for the Ising model in different regimes: infinite volume limit, at low temperature or vanishing magnetic field, was studied for Glauber dynamics via pathwise approach in [21, 39, 71, 72, 86, 87] and via the potential-theoretical approach in [15, 52].
However, though several approaches to the study of metastability have been proposed, the understanding of how the transition from a mestastable state to the stable one takes place for a given system can not be completed without investigating the effects of the peculiar features of the statistical mechanics model under consideration. For instance, the shape of the critical configurations is heavily dependent on the temperature and on the geometry of the space where configurations live (*e.g.* the possible anisotropy of the space or the features of the interaction graph in the case of discrete models). Another fundamental aspect to take into account is the type of dynamics according to which the system evolves. It is indeed possible that, even if two models have the same Hamiltonian and the same state space, different dynamics may have a completely different set of metastable states. This is especially true when parallel dynamics are taken into account, see [32, 9].

3.2 Definition of the model

3.2.1 Ising model on hexagonal lattice

Consider the discrete hexagonal lattice $\mathbb{H}^2$ embedded in $\mathbb{R}^2$ and let $\mathbb{T}^2$ be its dual, *i.e.* the triangular lattice. Let Λ be the subset of $\mathbb{H}^2$ obtained by cutting a parallelogram of side length L along two of the coordinate axes of the triangular lattice so that $|\Lambda| = 2L^2$. On Λ we impose periodic boundary conditions. To each site $i \in \Lambda$ we associate a spin variable $\sigma(i) \in \{-1, +1\}$

and, on the configuration space $\mathcal{X} := \{-1, +1\}^{\Lambda}$, we consider the Hamiltonian function $H : \mathcal{X} \longrightarrow \mathbb{R}$ defined as

$$H(\sigma) := -\frac{J}{2} \sum_{\substack{i,j \in \Lambda \\ d(i,j)=1}} \sigma(i)\sigma(j) - \frac{h}{2} \sum_{i \in \Lambda} \sigma(i), \tag{3.2.1}$$

where $J > 0$ represents the ferromagnetic interaction between two spins, $h > 0$ is the external magnetic field and $d(\cdot, \cdot)$ is the lattice distance on $\mathbb{H}^2$.
We consider a Markov chain $(X_t)_{t \in \mathbb{N}}$ on $\mathcal{X}$ defined via the so called *Metropolis Algorithm*. The transition probabilities of this dynamics are given by

$$P_\beta(\sigma, \eta) = q(\sigma, \eta) e^{-\beta [H(\eta) - H(\sigma)]_+}, \qquad \text{for all } \sigma \neq \eta, \tag{3.2.2}$$

where $[\cdot]_+$ denotes the positive part and $q(\sigma, \eta)$ is a connectivity matrix independent of β, defined, for all $\sigma \neq \eta$, as

$$q(\sigma, \eta) = \begin{cases} \frac{1}{|\Lambda|} & \text{if } \exists\, x \in \Lambda : \sigma^{(x)} = \eta \\ 0 & \text{otherwise} \end{cases} \tag{3.2.3}$$

where

$$\sigma^{(x)}(z) = \begin{cases} \sigma(z) & \text{if } z \neq x \\ -\sigma(x) & \text{if } z = x \end{cases} \tag{3.2.4}$$

In the remainder we will omit the symbol β in $P_\beta(\sigma, \eta)$ and we will write the transition probability between the states σ and η simply as $P(\sigma, \eta)$.
Table 3.1 shows all possible single spin flip probabilities.
It is possible to check that $(X_t)_{t \in \mathbb{N}}$ is an ergodic aperiodic Markov chain on $\mathcal{X}$ satisfying the detailed balance condition

$$\mu(\sigma) P(\sigma, \eta) = \mu(\eta) P(\eta, \sigma), \tag{3.2.5}$$

with respect to the Gibbs measure

$$\mu(\sigma) = \frac{e^{-\beta H(\sigma)}}{\sum_{\eta \in \mathcal{X}} e^{-\beta H(\eta)}}, \tag{3.2.6}$$

where $\beta := \frac{1}{T} > 0$ is the inverse temperature.
Let $\underline{+1}$, $\underline{-1}$ be respectively the configurations in which all the spins have value $+1$, -1.
It is straightforward to check that $\underline{+1}$ maximizes both sums in (3.2.1) and, consequently, we have the following

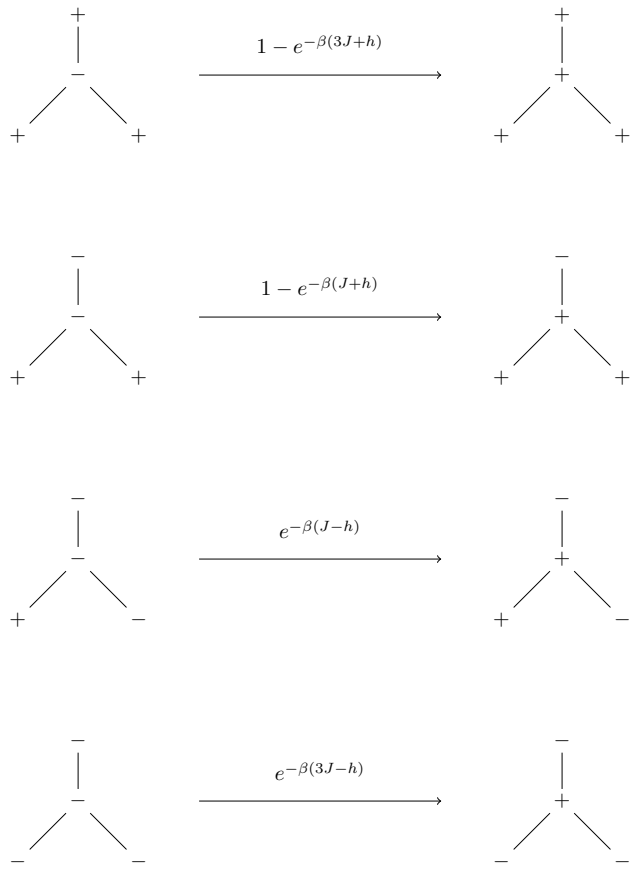

Table 3.1 Transition probabilities when the local configuration on the right is obtained from the local configuration on the left by changing the value of the central spin for all possible values of the neighboring spins. The probability that the change happens at the site at the center is uniform over all sites of Λ.

Lemma 3.2.1. $\underline{+1}$ *is the global minimum (or ground state) of the Hamiltonian* (3.2.1).

In the remainder we will show that $\underline{-1}$ is the unique *metastable* state, that is the *deepest local minimum* of the Hamiltonian (see Theorem 3.3.3).

3.2.2 Definitions and notation

The problem of metastability is the study of the first arrival of the process $(X_t)_{t\in\mathbb{N}}$ to the set of the stable states, corresponding to the set of absolute minima of H, when starting from an initial local minimum. Local minima can be ordered in terms of their increasing stability level, *i.e.*, the height of the barrier separating them from lower energy states. More precisely, for any $\sigma \in \mathcal{X}$, let $\mathcal{I}_\sigma$ be the set of configurations with energy strictly lower than $H(\sigma)$, *i.e.*,

$$\mathcal{I}_\sigma := \{\eta \in \mathcal{X} \,|\, H(\eta) < H(\sigma)\}. \tag{3.2.7}$$

Let $\omega = \{\omega_1, \dots, \omega_n\}$ be a finite sequence of configurations in $\mathcal{X}$. We call ω a *path* from ω_1 to ω_n and we denote by $\Theta(\omega_1, \omega_n)$ the set of all these paths. We say that n is the length of the path ω and we write $|\omega| = n$. The *communication height* between two configurations σ and η is the maximal height along the minimal path in $\Theta(\sigma, \eta)$, *i.e.*,

$$\Phi(\sigma, \eta) := \min_{\omega \in \Theta(\sigma,\eta)} \max_{\zeta \in \omega} H(\zeta). \tag{3.2.8}$$

By $\Phi(\omega)$ we denote the communication height along the path $\omega = \{\omega_1, \dots, \omega_n\}$, i.e. $\Phi(\omega) = \max_{i=1,\dots,n} H(\omega_i)$. Similarly, we also define the *communication height* between two sets $A, B \subset \mathcal{X}$ as

$$\Phi(A, B) := \min_{\sigma \in A, \eta \in B} \Phi(\sigma, \eta). \tag{3.2.9}$$

Now we are able to formally define the *stability level* of a state σ as

$$V_\sigma := \Phi(\sigma, \mathcal{I}_\sigma) - H(\sigma). \tag{3.2.10}$$

If $\mathcal{I}_\sigma$ is empty, we set $V_\sigma = \infty$. Note that the stability level V_σ of σ is the minimal cost that, starting from σ, has to be payed in order to reach states at energy lower than $H(\sigma)$. We denote by $\mathcal{X}^s$ the set of global minima of the energy, and we refer to these as ground states. To define the set of metastable states, we introduce the *maximal stability level*

$$\Gamma_m := \max_{\sigma \in \mathcal{X} \setminus \mathcal{X}^s} V_\sigma. \tag{3.2.11}$$

The metastable states are those attaining the maximal stability level $\Gamma_m < \infty$, that is

$$\mathcal{X}^m := \{y \in \mathcal{X} \,|\, V_y = \Gamma_m\}. \tag{3.2.12}$$

Since the metastable states are defined in terms of their stability level, a crucial role in our proofs is played by the set of all configurations with stability level strictly greater than V, that is

$$\mathcal{X}_V := \{\sigma \in \mathcal{X} \mid V_\sigma > V\}. \tag{3.2.13}$$

To study the transition between $\mathcal{X}^m$ and $\mathcal{X}^s$, we define the *first hitting time* to $A \subset \mathcal{X}$ for the process X_t^σ starting from $\sigma \in \mathcal{X}$

$$\tau_A^\sigma := \inf\{t > 0 \,|\, X_t^\sigma \in A\}. \tag{3.2.14}$$

Whenever possible we shall drop the superscript denoting the starting point σ from the notation and we denote by $\mathbb{P}_\sigma(\cdot)$ and $\mathbb{E}_\sigma[\cdot]$ respectively the probability and the average along the trajectories of the process started at σ. Now we define formally the *energy barrier* Γ as

$$\Gamma := \Phi(m,s) - H(m) \qquad \text{with } m \in \mathcal{X}^m,\, s \in \mathcal{X}^s. \tag{3.2.15}$$

In what follows we consider the set of paths realizing the minimal value of the maximal energy in the paths between any metastable state and the set of the stable states. To this end, we define the set of *optimal paths*.

Definition 3.2.2. *We write $(\mathcal{A} \to \mathcal{B})_{opt}$ to denote the set of* optimal paths*, i.e., the set of all paths from $\mathcal{A}$ to $\mathcal{B}$ realizing the min-max* (3.2.8) *in $\mathcal{X}$ between $\mathcal{A}$ and $\mathcal{B}$.*

Another basic notion is the set of *saddles* defined as the set of all maxima in the optimal paths between two configurations.

Definition 3.2.3. *The set of* minimal saddles *between $\sigma, \eta \in \mathcal{X}$ is defined as*

$$\mathscr{S}(\sigma,\eta) := \{\zeta \in \mathcal{X} \,|\, \exists \omega : \sigma \to \eta, \omega \ni \zeta \text{ such that } \max_{\xi\in\omega} H(\xi) = H(\zeta) = \Phi(\sigma,\eta)\}. \tag{3.2.16}$$

$$\mathscr{S}(\mathcal{A},\mathcal{B}) := \bigcup_{\substack{\sigma\in\mathcal{A},\,\eta\in\mathcal{B}:\\ \Phi(\sigma,\eta)=\Phi(\mathcal{A},\mathcal{B})}} \mathscr{S}(\sigma,\eta). \tag{3.2.17}$$

We focus on the subsets of saddles that are typically visited during the last excursion from a metastable state to the set of the stable states. To this end, we introduce the *gates* from metastability to stability, defined as the subsets of $\mathscr{S}$ visited by all the optimal paths. More precisely,

Definition 3.2.4. *Given a pair of configurations $\sigma, \eta \in \mathcal{X}$, we say that $\mathcal{W} \equiv \mathcal{W}(\sigma,\eta)$ is a* gate *for the transition from σ to η if $\mathcal{W}(\sigma,\eta) \subseteq \mathscr{S}(\sigma,\eta)$ and $\omega \cap \mathcal{W} \neq \emptyset$ for all $\omega \in (\sigma \to \eta)_{opt}$.*

Moreover,

Definition 3.2.5. *A gate $\mathcal{W}$ is a* minimal gate *for the transition from σ to η if for any $\mathcal{W}' \subset \mathcal{W}$ there exists $\omega' \in (\sigma \to \eta)_{opt}$ such that $\omega' \cap \mathcal{W}' = \emptyset$.*
For a given pair η, η', there may be several disjoint minimal gates. We denote by $\mathscr{G}(\eta,\eta')$ the union of all minimal gates:

$$\mathscr{G}(\eta,\eta') := \bigcup_{\mathcal{W}\, \text{minimal gate for } (\eta,\eta')} \mathcal{W} \tag{3.2.18}$$

Obviously, $\mathscr{G}(\sigma,\sigma') \subseteq \mathscr{S}(\sigma,\sigma')$ and $\mathscr{S}(\sigma,\sigma')$ is a gate (but in general it is not minimal). The configurations $\xi \in \mathscr{S}(\eta,\eta') \setminus \mathscr{G}(\eta,\eta')$ (if any) are called dead ends.

In words, a minimal gate is a minimal (by inclusion) subset of $\mathscr{S}(\sigma,\eta)$ that is visited by all optimal paths. The configurations in the *minimal gates* have the physical meaning of *critical configurations* and are central objects both from a probabilistic and from a physical point of view.

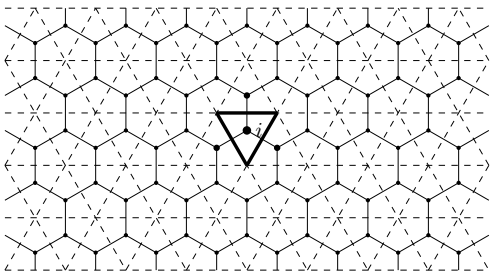

Figure 3.1 The solid lines show the hexagonal lattice, whereas the dashed lines show its dual, the triangular lattice. The solid triangle highlights the triangular face centered at site i. The thicker vertices are the nearest neighbors of site i on the hexagonal lattice.

To study the function $H(\sigma)$ it is convenient to associate to each configuration $\sigma \in \mathcal{X}$ certain geometrical objects and, then, to study their properties.
To this end, recall that $\mathbb{H}^2$ is the discrete hexagonal lattice embedded in $\mathbb{R}^2$ and its dual, $\mathbb{T}^2$, is the discrete triangular lattice embedded in $\mathbb{R}^2$. Given a configuration $\sigma \in \mathcal{X}$, consider the set $C(\sigma) \subseteq \Lambda$ defined as the union of the closed triangular faces centered at sites i with the boundary contained in $\mathbb{T}^2$ and such that $\sigma(i) = +1$ (see Figure 3.1) and look at the maximal connected components $C_1, \ldots, C_m, m \in \mathbb{N}$, of $C(\sigma)$. If a maximal connected component wraps around the torus it is called a *plus strip*, otherwise it is called a *cluster (of pluses)*. This construction leads to a bijection that associates to each configuration a collection of its clusters and plus strips. Likewise, other geometrical objects may be associated to a configuration σ by considering the connected components of triangular faces centered at the sites of the lattice with spin value minus one. Among these, there could be a connected component which contains two or three lines that wrap around the torus parallel to the coordinate axes of $\mathbb{T}^2$. If this is the case, the component is called a *sea of minuses*. Similarly, if there is only one line that wraps around the torus we call it a *minus strip*. The other connected components of triangular faces centered at minus spins are called *holes*.
Given a configuration $\sigma \in \mathcal{X}$ we denote by $\gamma(\sigma)$ its Peierls contour that is the boundary of the clusters. Note that Peierls contours live on the dual lattice $\mathbb{T}^2$ and are the union of piecewise linear curves separating spins with opposite sign in σ. In particular in each dual vertex there are 0, 2, 4, 6 dual bonds contained in $\gamma(\sigma)$.

In this setting, it is immediate to see that for each configuration σ we have

$$H(\sigma) - H(\underline{-1}) = J|\gamma(\sigma)| - hN^+(\sigma), \tag{3.2.19}$$

where

$$N^+(\sigma) = \sum_{x\in\Lambda} \frac{\sigma(x)+1}{2}, \tag{3.2.20}$$

represents the number of plus spins and $|\gamma(\sigma)|$ is the lenght of the Peierls contour $\gamma(\sigma)$. In this way the energy of each configuration is associated to the area and the length of the boundary of a suitable collection of triangular faces.
Call r^* the *critical radius*:

$$r^* := \Big\lfloor \frac{J}{2h} - \frac{1}{2} \Big\rfloor, \tag{3.2.21}$$

and let $\delta \in (0,1)$ be the fractional part of $\frac{J}{2h} - \frac{1}{2}$, that is

$$\delta = \frac{J}{2h} - \frac{1}{2} - r^*. \tag{3.2.22}$$

We will show that for our model the energy barrier Γ is equal to

$$\Gamma^{Hex} := \begin{cases} -6{r^*}^2 h + 6r^* J - 10r^* h + 7J - 5h & \text{if } 0 < \delta < \frac{1}{2} \\ -6(r^*+1)^2 h + 6(r^*+1)J - 2(r^*+1)h + 3J - h & \text{if } \frac{1}{2} < \delta < 1 \end{cases} \tag{3.2.23}$$

The value of Γ^{Hex} is obtained by computing the energy of the *critical configurations*. We will see that these configurations consist of a cluster having a shape that is close to a hexagon of radius r^* and, in particular, we will compute the *critical area* to be

$$\begin{aligned} A_1^* &= 6{r^*}^2 + 10r^* + 5 && \text{if } 0 < \delta < \frac{1}{2}, \\ A_2^* &= 6(r^*+1)^2 + 2(r^*+1) + 1 && \text{if } \frac{1}{2} < \delta < 1. \end{aligned} \tag{3.2.24}$$

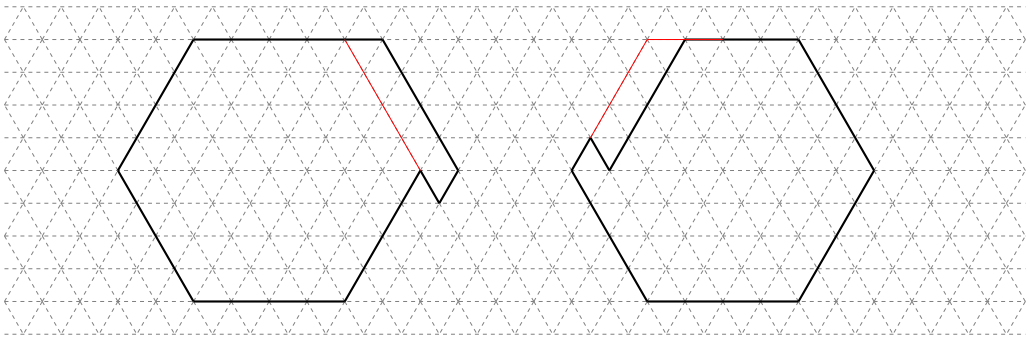

Figure 3.2 On the left, $S(A_2^*)$ with $A_2^* = 6(r^*+1)^2 + 2(r^*+1) + 1$ and $\frac{1}{2} < \delta < 1$. On the right, $S(A_1^*)$ with $A_1^* = 6r^{*2} + 10r^* + 5$ and $0 < \delta < \frac{1}{2}$.

3.3 Main results

Our results concerning the metastable behavior of the model are given under the assumption that the torus is large compared to the size of the critical clusters. More precisely, we assume the following

Condition 3.3.1. *The magnetic field h, the ferromagnetic interaction J and the torus Λ are such that $0 < h < 1$, $J \geq 2h$, $\frac{J}{2h} + \frac{1}{2}$ is not integer, and $|\Lambda| \geq (\frac{4J}{h})^2$ finite.*

Note that the assumption $\frac{J}{2h} + \frac{1}{2}$ not integer is common in literature and is made so to avoid strong degeneracy of the critical configurations.

We say that a function $\beta \mapsto f(\beta)$ is *super exponentially small* (SES) if

$$\lim_{\beta\to\infty} \frac{1}{\beta} \log f(\beta) = -\infty.$$

With this notation we can state our first theorem concerning the recurrence of the system to either the state $\underline{-1}$ or $\underline{+1}$.

Theorem 3.3.2 (Recurrence property)**.** *Let $V^* = 2J$, we have $\mathcal{X}_{V^*} = \{\underline{-1}, \underline{+1}\}$ and for any $\epsilon > 0$ and sufficiently large β, we have*

$$\sup_{\sigma\in\mathcal{X}} \mathbb{P}_\sigma(\tau_{\mathcal{X}_{V^*}} > e^{\beta(V^*+\epsilon)}) = SES. \tag{3.3.1}$$

Equation (3.3.1) implies that the system reaches with high probability either the state $\underline{-1}$ (which is a local minimum of the Hamiltonian) or the ground state in a time shorter than $e^{\beta(V^*+\epsilon)}$, uniformly in the starting configuration σ for any $\epsilon > 0$. In other words we can say that the dynamics speeded up by a time factor of order $e^{\beta V^*}$ reaches with high probability

$\{\underline{-1}, \underline{+1}\}$. In Corollary 4.2.6 we give a geometrical description of $\mathcal{X}_V$ for $V = J - h$ and we discuss the behavior of the speeded up dynamics by a time factor of order $e^{\beta(J-h)}$.
In the next theorem we identify the metastable state and we compute the maximal stability level. Recalling the Definition of Γ^{Hex} in Equation (3.2.23) we have

Theorem 3.3.3 (Identification of metastable state)**.** *$\mathcal{X}^m = \{\underline{-1}\}$ and $\Gamma_m = \Gamma^{Hex}$.*

In the next theorems, we give the asymptotic behavior (for $\beta \to \infty$) of the transition time for the system starting at the metastable state. In particular, in Theorem 3.3.4 we give an upper and lower bound for the transition time, in Theorem 3.3.5 we estimate the expected value of the transition time and in Theorem 3.3.6 we give its asymptotic distribution.

Theorem 3.3.4 (Asymptotic behavior of $\tau_{\underline{+1}}$ in probability)**.** *For any $\epsilon > 0$, we have*

$$\lim_{\beta\to\infty} \mathbb{P}_{\underline{-1}}(e^{\beta(\Gamma^{Hex}-\epsilon)} < \tau_{\underline{+1}} < e^{\beta(\Gamma^{Hex}+\epsilon)}) = 1. \tag{3.3.2}$$

Theorem 3.3.5 (Sharp estimates of $\tau_{\underline{+1}}$)**.** *For β large enough, we have*

$$\mathbb{E}_{\underline{-1}}[\tau_{\underline{+1}}] = \frac{1}{k} e^{\beta\Gamma^{Hex}}(1 + o(1)), \tag{3.3.3}$$

where

$$k = \begin{cases} 5(l-1) & \text{if } \delta \in (0, \frac{1}{2}), \\ 10(l-1) & \text{if } \delta \in (\frac{1}{2}, 1). \end{cases} \tag{3.3.4}$$

Theorem 3.3.6 (Asymptotic distribution of $\tau_{\underline{+1}}$)**.** *Let* $T_\beta := \inf\{n \geq 1 \,|\, \mathbb{P}_{\underline{-1}}(\tau_{\underline{+1}} \leq n) \geq 1 - e^{-1}\}$

$$\lim_{\beta\to\infty} \mathbb{P}_{\underline{-1}}(\tau_{\{\underline{+1}\}} > tT_\beta) = e^{-t} \tag{3.3.5}$$

and

$$\lim_{\beta\to\infty} \frac{\mathbb{E}_{\underline{-1}}(\tau_{\{\underline{+1}\}})}{T_\beta} = 1. \tag{3.3.6}$$

The following theorem concerns the long-run behavior of the Metropolis Markov chain $(X_t)_{t\in\mathbb{N}}$ of our model. In particular, we give an estimate of the mixing time of the chain and its spectral gap. Both these quantities are classical notions that may be used to examine the speed of convergence of Markov chains to their stationary distribution. Mixing time describes the time required for the distance to stationarity to become small and it is defined as

$$t_\beta^{mix}(\epsilon) := \min\{n \geq 0 \,|\, \max_{\sigma\in\mathcal{X}} \|P_\beta^n(\sigma, \cdot) - \mu_\beta(\cdot)\|_{TV} \leq \epsilon\} \tag{3.3.7}$$

where $P_\beta^n(\cdot,\cdot)$ is the transition probability defined in (3.2.2) at time n, $\mu_\beta(\cdot)$ is the stationary measure of the chain and $\|\cdot\|_{TV}$ denotes the total variation distance among two probability measures (see definition (1.4.8)).
Spectral gap is defined as

$$\rho_\beta := 1 - a_\beta^{(2)} \tag{3.3.8}$$

where $1 = a_\beta^{(2)} > a_\beta^{(2)} \geq ... \geq a_\beta^{(2)} \geq -1$ are the eigenvalues of the matrix $(P_\beta(\sigma,\tau))_{\sigma,\tau\in\mathcal{X}}$.

Theorem 3.3.7 (Mixing time and spectral gap)**.** *For any $0 < \epsilon < 1$ we have*

$$\lim_{\beta\to\infty} \frac{1}{\beta} \log t_\beta^{mix}(\epsilon) = \Gamma^{Hex}, \tag{3.3.9}$$

and if ρ_β is the spectral gap, there exist two constants $0 < c_1 < c_2 < \infty$ independent of β such that for every $\beta > 0$

$$c_1 e^{-\beta(\Gamma^{Hex}+\gamma_1)} \leq \rho_\beta \leq c_2 e^{-\beta(\Gamma^{Hex}-\gamma_2)}, \tag{3.3.10}$$

where γ_1, γ_2 are functions of β that vanish for $\beta \to \infty$.

In the theorem below, we characterize the gate for the transition from $\underline{-1}$ to $\underline{+1}$. To do this, we give an intuitive definition of the configurations denoted by $\tilde{\mathcal{S}}(A_i^*)$ and $\tilde{\mathcal{D}}(A_i^*)$ that play the role of *critical configurations*. $\tilde{\mathcal{S}}(A_i^*)$ is a configuration with a cluster such that its area is A_i^* and its shape is that in Figure 3.3 (a)-(c); $\tilde{\mathcal{D}}(A_i^*)$ is a configuration with a cluster such that its area is A_i^* and its shape is that in Figure 3.3 (b)-(d). We refer the reader to Notation 4.1.21 for a precise definition of $\tilde{\mathcal{S}}(A_i^*)$ and $\tilde{\mathcal{D}}(A_1^*)$ and to Corollary 4.3.6 for the values of A_i^* with $i \in \{1,2\}$. We observe that Γ^{Hex} is equal to $H(\tilde{\mathcal{S}}(A_i^*)) - H(\underline{-1})$. See Figure 3.2 to have the two pictures of standard clusters with area A_i^* according to the values of parameters.

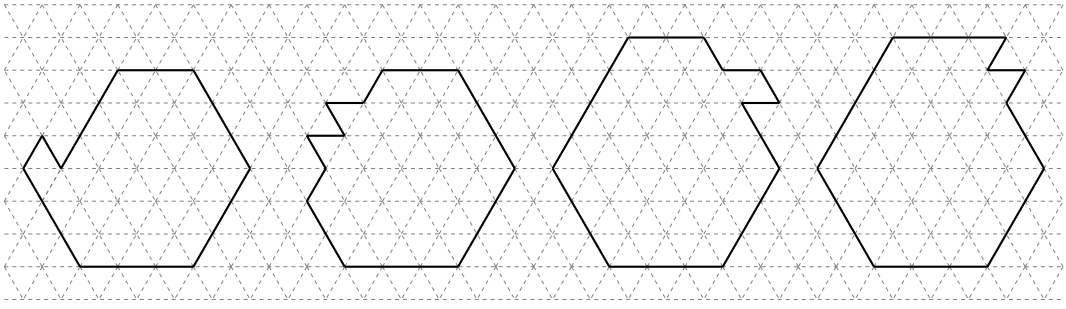

(a) **(b)** **(c)** **(d)**

Figure 3.3 On the left there are two examples of two configurations $\tilde{\mathcal{S}}(A_1^*)$, $\tilde{\mathcal{D}}(A_1^*)$ belonging to the gate for $\delta \in (0, 1/2)$. On the right there are other two examples $\tilde{\mathcal{S}}(A_2^*)$, $\tilde{\mathcal{D}}(A_2^*)$ for $\delta \in (1/2, 1)$.

Theorem 3.3.8 (Gate)**.** *Given* $\delta \in (0,1)$*,* $A_i^* \in \{A_1^*, A_2^*\}$ *in* (3.2.24)*. We have that any optimal path* $\omega \in (\underline{-1} \to \underline{+1})_{opt}$ *visits* $\tilde{\mathcal{S}}(A_i^*) \cup \tilde{\mathcal{D}}(A_i^*)$ *, i.e. there exists an integer* j *such that* $\omega \ni \omega_j \equiv \tilde{\mathcal{S}}(A_i^*)$ *or* $\omega \ni \omega_j \equiv \tilde{\mathcal{D}}(A_i^*)$*. In other words* $\tilde{\mathcal{S}}(A_i^*) \cup \tilde{\mathcal{D}}(A_i^*)$ *is the union of all minimal gates from* $\underline{-1}$ *to* $\underline{+1}$*.*

From a physical point of view, the configurations in the gate are those that must be visited, for a system at very low temperature, in order for the transition to the stable state to take place. Moreover, the characterization of the gate allows to compute the sharp estimates for the transition time in Theorem 3.3.5 using a potential theoretic approach. Using solely a pathwise approach, exponential asymptotics for the expected transition time could have been obtained as well without this detailed description of the gate. To this purpose, using the model dependent results of Theorem 3.3.3, one could apply [70, Theorem 4.9] (setting $\eta_0 = \{\underline{-1}\}$) to get

$$\lim_{\beta\to\infty} \frac{1}{\beta} \log \mathbb{E}_{\underline{-1}}[\tau_{\underline{+1}}] = \Gamma^{Hex}. \tag{3.3.11}$$

4 Transition time, critical configurations and typical paths

4.1 Preparatory tools

Since the faces of a cluster live naturally on the triangular lattice it is beneficial to associate clusters to plane polyforms obtained by joining equilateral triangles along their edges (*polyiamonds*). In this way it will be possible to characterize spin configurations that are relevant for the dynamics under consideration in terms of the area and the perimeter of the polyiamond associated to their clusters. Though we will consider polyiamonds to study the Ising model on the hexagonal lattice, the properties that will derive may be of use to study other statistical mechanics lattice models for which the notion of clusters may be linked to that of polyiamonds.

Definition 4.1.1. *A* polyiamond $P \subset \mathbb{R}^2$ *is a finite maximally edge-connected union of faces of the lattice* $\mathbb{T}^2$*. Each face belonging to the polyiamond is called* triangular unit *whereas the faces of* $\mathbb{T}^2$ *outside of* P *are called* empty triangular units.

We remark that two faces are not connected if they share a single point.
Note that with this construction there is a bijection between clusters of plus spins not wrapping around the torus and polyiamonds. Analogously, minus spins are associated to the empty triangular units of the lattice $\mathbb{T}^2$. Strictly speaking, this mapping is different from the one introduced before which is a bijection between the configuration space $\mathcal{X}$ and the set of sea of minuses, strips, clusters and holes. Both these bijections are relevant.

Definition 4.1.2. *An* elementary rhombus *is a set of two triangular units sharing an edge.*

In the remainder of the section we will give the definitions and the key results concerning polyiamonds that are used in Sections 4.2 and 4.3 whereas a more comprehensive and self-contained discussion on polyiamonds is deferred to Section 5.

Definition 4.1.3. *The* area A *of a polyiamond is the number of its triangular units. For any polyiamond P, we denote its area by $||P||$. Analogously for any cluster C, we denote by $||C||$ the number of plus spins in C.*

Definition 4.1.4. *The* boundary *of a polyiamond P is the collection of unit edges of the lattice $\mathbb{T}^2$ such that each edge separates a triangular unit belonging to P from an empty triangular unit. The* edge-perimeter $p(P)$ *of a polyamond P is the cardinality of its boundary.*

In other words the perimeter is given by the number of interfaces on the discrete triangular lattice between the sites inside the polyiamond and those outside. If not specified differently, we will refer to the edge-perimeter simply as perimeter.

Definition 4.1.5. *The* external boundary *of a polyiamond consists of the connected components of the boundary such that for each edge there exists a hexagonal-path in $\mathbb{H}^2$ which connects this edge with infinity. The* internal boundary *of a polyiamond consists of the connected components of the boundary that are not external. The* external perimeter*, respectively the* internal perimeter*, of a polyiamond is the cardinality of the external, respectively internal, boundary.*

Definition 4.1.6. *A* hole *of a polyiamond P is a finite maximally connected component of empty triangular units surrounded by the internal boundary of P.*

We refer to holes consisting of a single empty triangular unit as *elementary holes*.

Definition 4.1.7. *Orient the external boundary counter-clockwise and the internal boundary clockwise. For each pair of oriented edges, the angle defined rotating counter-clockwise the second edge on the first edge is called* internal angle*. See Figure 4.1.*

Definition 4.1.8. *A polyiamond is* regular *if it has only internal angles of π and $\frac{2}{3}\pi$ and it has no holes.*

We note that a regular polyiamond has the shape of a hexagon.

Definition 4.1.9. *A polyiamond is a* regular hexagon *if it is a regular polyiamond with all equal sides. We denote by $E(r)$ the regular hexagon, where r is its radius.*

Definition 4.1.10. *A* bar $B(l)$ *with larger base l is a set of $||B(l)|| = 2l-1$ triangular units obtained as the difference between an equilateral triangle with side length l and another equilateral triangle with side length $l-1$.*

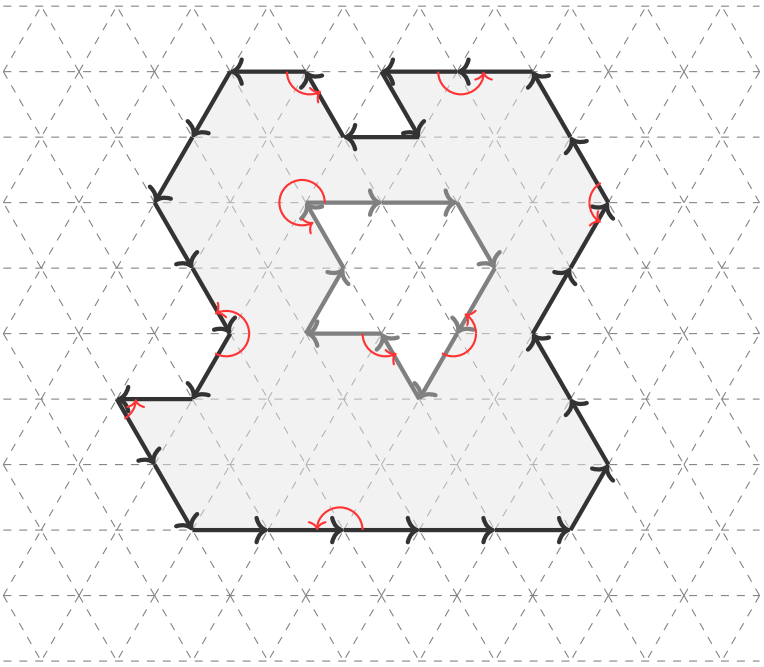

Figure 4.1 An example of polyiamond with in black the external boundary oriented counter-clockwise, and in gray the internal boundary oriented clockwise. In red, some internal angles of the polyiamond.

Definition 4.1.11. *We denote by $E_{B_1}(r)$ the polyiamond obtained attaching a bar $B(r)$ along its larger base to the a side of the regular hexagon, see Figure 4.2, so that $E_{B_1}(r)$ is contained in $E(r+1)$. Analogously, we denote by $E_{B_i}(r)$ for $i = 2,\dots,5$ the polyiamonds obtained attaching a bar $B(r+1)$ along its larger base to a suitable side of $E_{B_{i-1}}(r)$ so that, again, $E_{B_i}(r)$ is contained in $E(r+1)$. Finally, we denote by $E_{B_6}(r)$ the polyiamond obtained attaching a bar $B(r+2)$ along its larger base to $E_{B_5}(r)$ so to obtain $E(r+1)$. We call $E_{B_i}(r)$ a* quasi-regular hexagon*, where r is the radius of the regular hexagon $E(r)$ and $i \in \{1,\dots,6\}$ is the number of bars attached to it.*

Note that $E_{B_i}(r)$ is defined up to translations and rotations of $z\frac{\pi}{3}$ for $z \in \mathbb{Z}$. Moreover $E_{B_0}(r) := E(r)$ and $E(r+1) \equiv E_{B_6}(r)$.

Definition 4.1.12. *An* incomplete bar *of cardinality $k < 2l-1$ is an edge-connected subset of a bar $B(l)$ attached to a hexagon along its longest base, see Figure 4.3.*

Observe that an incomplete bar has either the shape of a trapeze or of a parallelogram with unitary height.

Definition 4.1.13. *For any $A \in \mathbb{N}$, the* minimal quasi-regular hexagon *R_A is the smallest quasi-regular hexagon containing at least A triangular units.*

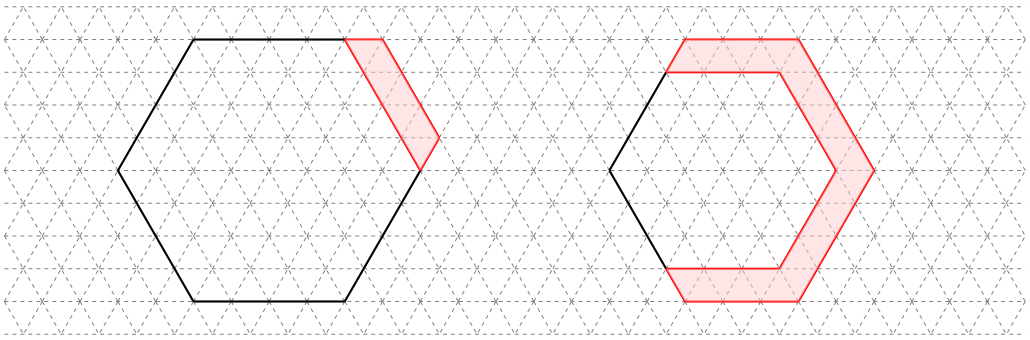

Figure 4.2 On the left the quasi-regular hexagon $E_{B_1}(4)$. On the right the quasi-regular hexagon $E_{B_4}(3)$.

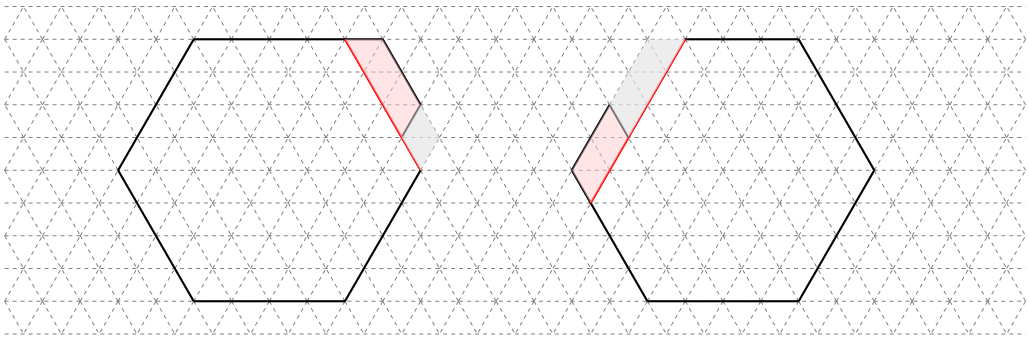

Figure 4.3 On the left an incomplete bar having the shape of a trapeze and of cardinality $k = 5$ attached to the regular hexagon $E(4)$. We observe that the cardinality of the bar containing the incomplete bar is $||B_1|| = 7 > k$. On the right an incomplete bar with the shape of a parallelogram of cardinality $k = 4$, attached to the quasi-regular hexagon $E_{B_5}(3)$. We observe that the cardinality of the bar containing the incomplete bar is $||B_6|| = 9 > k$. Both configurations are examples of *standard polyiamonds*.

Thus, R_A has area $A + k$, where k is the smallest number of triangular units added to P to build a quasi-regular hexagon.

Definition 4.1.14. *For any $A \in \mathbb{N}$, the* maximal quasi-regular hexagon R'_A *is the largest quasi-regular hexagon containing at most A triangular units.*

Thus, R'_A has area $A - q$, where q is the smallest number of triangular units that must be removed from P to build a quasi-regular hexagon.

Definition 4.1.15. *A* canonical polyiamond *of area A, denoted by $\tilde{S}(A)$, is a quasi-regular hexagon $E_{B_i}(r)$, for $i \in \{0, \ldots, 5\}$, with possibly an additional incomplete bar of cardinality k and such that it is contained in $E_{B_{i+1}}(r)$ (see Fig. 4.3).*

Definition 4.1.16. *Orient the external boundary clockwise and attach an incomplete bar to $E_{B_i}(r)$, for $i \in \{0, \ldots, 5\}$, following this orientation. We call this canonical polyiamond* standard polyiamond *and denote it by $S(A)$, where A is its area.*

Definition 4.1.17. *A polyiamond consisting of a quasi-regular hexagon with two triangular units attached to one of its longest sides at triangular lattice distance 2 one from the other is called* defective *and is denoted by $\tilde{D}(A)$, where A is its area.*

Note that a standard polyiamond $S(A)$ is determined solely by its area A. We characterize $S(A)$ in terms of its radius r, the number i of bars attached to the regular hexagon $E(r)$ to obtain $E_{B_i}(r)$ and the cardinality k of the possibly incomplete bar. The values of r, i and k for any value of A, together with the minimal and the maximal quasi-regular hexagons R_A and R'_A, can be obtained with the following:

Algorithm 4.1.18. *Construction of standard polyiamond with area A. Given A as input, the outputs r, k, i, R_A, R'_A are obtained as follows:*

1) Set $r = [\sqrt{\frac{A}{6}}]$.

2) Let l be the difference between A and $6r^2$, i.e., $l = A - 6r^2$:

a) If $l = 0$, then $R_A = R'_A = E(r)$; $i = 0$, $k = 0$.

b) If $l - (2r-1) < 0$, then $R_A = E_{B_1}(r)$ and $R'_A = E(r)$; $i = 0$, $k = A - \|R'_A\|$.

c) If $l - (2r-1) = 0$, then $R_A = R'_A = E_{B_1}(r)$; $i = 1$, $k = 0$.

d) If $l - ((2r-1) + (2r+1)) < 0$, then $R_A = E_{B_2}(r)$ and $R'_A = E_{B_1}(r)$; $i = 1$, $k = A - \|R'_A\|$.

e) If $l - ((2r-1) + (2r+1)) = 0$, then $R_A = R'_A = E_{B_2}(r)$; $i = 2$, $k = 0$.

f) If $l - ((2r-1) + 2(2r+1)) < 0$, then $R_A = E_{B_3}(r)$ and $R'_A = E_{B_2}(r)$; $i = 2$, $k = A - \|R'_A\|$.

g) If $l - ((2r-1) + 2(2r+1)) = 0$, then $R_A = R'_A = E_{B_3}(r)$; $i = 3$, $k = 0$.

h) If $l - ((2r-1) + 3(2r+1)) < 0$, then $R_A = E_{B_4}(r)$ and $R'_A = E_{B_3}(r)$; $i = 3$, $k = A - \|R'_A\|$.

i) If $l - ((2r-1) + 3(2r+1)) = 0$, then $R_A = R'_A = E_{B_4}(r)$; $i = 4$, $k = 0$.

j) If $l - ((2r-1) + 4(2r+1)) < 0$, then $R_A = E_{B_5}(r)$ and $R'_A = E_{B_4}(r)$; $i = 4$, $k = A - \|R'_A\|$.

k) If $l - ((2r-1) + 4(2r+1)) = 0$, then $R_A = R'_A = E_{B_5}(r)$; $i = 5$, $k = 0$.

l) If $l - ((2r-1) + 4(2r+1) + (2r+3)) < 0$, then $R_A = E_{B_6}(r)$ and $R'_A = E_{B_5}(r)$; $i = 5$, $k = A - \|R'_A\|$.

Once the standard polyiamonds of area A have been described in the previous terms, it is straightforward to write their perimeter as follows:

Remark 4.1.19. *The perimeter of $S(A)$ is $p(A) = 6r + i + \mathbb{1}_{\{k>0\}} + \mathbb{1}_{\{k>0 \text{ even}\}}$ with r, i and k given by the previous algorithm.*

Notation 4.1.20. *We denote by $\mathcal{E}(r)$ the configuration $\sigma \in \mathcal{X}$ such that σ has a unique cluster (of pluses) with shape $E(r)$. We denote by $\mathcal{E}_{B_i}(r)$ the configuration $\sigma \in \mathcal{X}$ such that σ has a unique cluster (of pluses) with shape $E_{B_i}(r)$.*

Notation 4.1.21. *We denote by $\tilde{\mathcal{S}}(A)$ (respectively $\mathcal{S}(A)$, $\tilde{\mathcal{D}}(A)$) the configuration $\sigma \in \mathcal{X}$ such that σ has a unique cluster (of pluses) with shape $\tilde{S}(A)$ (respectively $S(A)$, $\tilde{D}(A)$).*

Each of these geometrical definitions and properties can be extended from polyiamonds to clusters. So, for example, when we call a cluster *standard cluster*, our meaning is that the cluster has the shape and the properties of a standard polyiamond.
The next theorem states that the set of polyiamonds of minimal perimeter and area A contains the set of standard polyiamonds with area A. In other words, standard polyiamonds minimize the perimeter for any given number of triangular units.

Theorem 4.1.22. *For any $A \in \mathbb{N}$ the perimeter of a polyiamond P of area A is at least $p(S(A))$ where $p(S(A))$ is the perimeter of a standard polyiamond $S(A)$.*

The proof of Theorem 4.1.22 is deferred to Chapter 5.

Considering the construction of minimal R_A and maximal R'_A quasi-regular hexagons given in the Algorithm 4.1.18, we get immediately the following:

Corollary 4.1.23. *For any A positive integer there exist four positive integers r, k_1, k_2 and k_3 such that one of the following conditions applies:*

1. *$A = 6r^2 + k_1$ with $0 \leq k_1 < 2r - 1$. Then the set of polyiamonds of area A and minimal perimeter contains the polyiamond $S(6r^2 + k_1)$.*
2. *$A = 6r^2 + 2r - 1 + k_2$ with $0 \leq k_2 < 2r + 1$. Then the set of polyiamonds of area A and minimal perimeter contains the polyiamond $S(6r^2 + 2r - 1 + k_2)$.*
3. *$A = 6r^2 + 4r + k_2$ with $0 \leq k_2 < 2r + 1$. Then the set of polyiamonds of area A and minimal perimeter contains the polyiamond $S(6r^2 + 4r + k_2)$.*
4. *$A = 6r^2 + 6r + 1 + k_2$ with $0 \leq k_2 < 2r + 1$. Then the set of polyiamonds of area A and minimal perimeter contains the polyiamond $S(6r^2 + 6r + 1 + k_2)$.*
5. *$A = 6r^2 + 8r + 2 + k_2$ with $0 \leq k_2 < 2r + 1$. Then the set of polyiamonds of area A and minimal perimeter contains the polyiamond $S(6r^2 + 8r + 2 + k_2)$.*
6. *$A = 6r^2 + 10r + 3 + k_3$ with $0 \leq k_3 < 2r + 3$. Then the set of polyiamonds of area A and minimal perimeter contains the polyiamond $S(6r^2 + 10r + 3 + k_3)$.*

Moreover, the next lemma, proved in Section 5, states that for some specific values of the area A there exists a unique class of polyiamonds that minimize the perimeter, namely the class of quasi-regular hexagons with area A.

Lemma 4.1.24. *If the area A of a polyiamond is $6r^2+2mr+(m-2)\mathbb{1}_{\{m>0\}}$ for $m \in \{0,1,\dots,5\}$ the set of polyiamonds of area A and minimal perimeter contains only the quasi-regular hexagons.*

Proof of Lemma 4.1.24. Note that areas of the form $6r^2+2mr+(m-2)\mathbb{1}_{\{m>0\}}$ for $m \in \{0,1,\dots,5\}$ are compatible with the area of quasi-regular hexagons. Let A be the area of a quasi-regular hexagon and let $\bar{p}$ be its edge-perimeter. The Lemma is clearly implied by Lemma 5.2.3. □

4.2 Recurrence proposition

The goal of this section is to prove Theorem 3.3.2. To achieve it we give some preliminary definitions. Recalling Definitions (3.2.21) and (3.2.24), we divide the set of standard clusters into three classes: *supercritical*, *critical* and *subcritical* clusters.

Definition 4.2.1. *We call a standard cluster* supercritical *(respectively* subcritical*) if it has the shape of $S(A)$ with area $A > A_i^*$ (respectively $A < A_i^*$) for $i \in \{1,2\}$. A* critical *standard cluster is a standard cluster which has the shape of $S(A)$ with area $A = A_i^*$.*

We will see that supercritical standard clusters have the tendency to grow with high probability, whereas subcritical standard clusters have the tendency to shrink with high probability.
The following definition distinguishes if two or more regular clusters of a configuration do interact or they do not.

Definition 4.2.2. *Two regular clusters Q and $\tilde{Q}$ are* non-interacting *if $d(Q,\tilde{Q}) > 2$, where $d(\cdot,\cdot)$ is the lattice distance. Otherwise, the two regular clusters are called* interacting.

Definition 4.2.3. *We call a* corner of a standard cluster C *the pair of triangular faces of C contained in the internal angle of $\frac{2}{3}\pi$.*

4.2.1 Recurrence property to the set $\mathcal{X}_{J-h}$

In this section we identify the configurations in $\mathcal{X}_{J-h}$, that is those configurations having a "small" stability level, and partition this set into five subsets. This partition will turn out to be convenient in the next section.

Lemma 4.2.4. *A configuration σ that satisfies at least one of the following conditions is not in $\mathcal{X}_0$:*

1. *σ has either a cluster or a plus strip C with an internal angle of $\frac{5}{3}\pi$;*
2. *σ has either a cluster or a plus strip C with an internal angle of $\frac{1}{3}\pi$.*

Moreover, a configuration σ is not in $\mathcal{X}_{J-h}$ if the cluster or the plus strip C has an internal angle of $\frac{4}{3}\pi$.

Proof of Lemma 4.2.4. Suppose that C has an internal angle $\alpha = \frac{5}{3}\pi$. Let j be the site at distance one from a site in C such that $\sigma(j) = -1$ and that belongs to the closed triangular face intersecting the boundary of C in two or more edges, see Figure 4.4, case (a). Since by Table 3.1

$$H(\sigma^{(j)}) - H(\sigma) = -(J+h) < 0, \tag{4.2.1}$$

$\sigma^{(j)}$ belongs to $\mathcal{I}_\sigma$. Thus the stability level is equal to $V_\sigma = 0$ and it follows that $\sigma \notin \mathcal{X}_0$. Suppose now that C has an internal angle $\alpha = \frac{1}{3}\pi$. Let j be a site such that $\sigma(j) = +1$ and

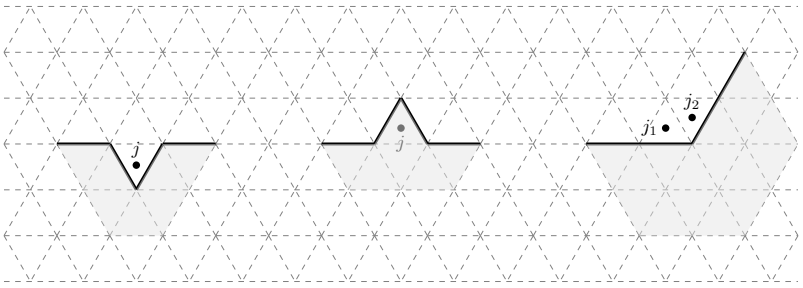

(a) **(b)** **(c)**

Figure 4.4 On the left hand side (respectively in the middle) we depict the site j as in case 1 (respectively case 2). On the right hand side we depict the two sites j_1, j_2 when σ has an internal angle of $\frac{4}{3}\pi$.

that belongs to the closed triangular face of C intersecting its boundary in two edges, see Figure 4.4, case (b). Since by Table 3.1

$$H(\sigma^{(j)}) - H(\sigma) = -(J-h) < 0, \tag{4.2.2}$$

$\sigma^{(j)}$ belongs to $\mathcal{I}_\sigma$. Thus the stability level is equal to $V_\sigma = 0$ and it follows that $\sigma \notin \mathcal{X}_0$.
Next we prove that if a configuration σ has a cluster or a plus strip C with an internal angle of $\frac{4}{3}\pi$, then $\sigma \notin \mathcal{X}_{J-h}$. Suppose that C has an internal angle $\alpha = \frac{4}{3}\pi$. We construct a path that starts from $\sigma \equiv \omega_0$ and we define ω_1 as follows. Let j_1, j_2 be two sites such that $\sigma(j_1) = \sigma(j_2) = -1$, $d(j_1, j_2) = 1$ and let each of them belong to one closed triangular face

intersecting the boundary of C in one edge, see Figure 4.4, case (c). Pick one of the two sites, for example j_1 and flips its spin, i.e., $\omega_1 := \omega_0^{(j_1)}$. Then flip the spin of j_2, i.e. $\omega_2 := \omega_1^{(j_2)}$. The stability level is bounded above by

$$V_\sigma \leq H(\omega_1) - H(\omega_0) = J - h, \tag{4.2.3}$$

indeed the configuration ω_2 is in $\mathcal{I}_\sigma$ since

$$\begin{aligned} H(\omega_2) - H(\omega_0) &= (H(\omega_2) - H(\omega_1)) + (H(\omega_1) - H(\omega_0)) \\ &= -(J+h) + (J-h) = -2h < 0. \end{aligned} \tag{4.2.4}$$

Thus $\sigma \notin \mathcal{X}_{J-h}$. □

Corollary 4.2.5. *A configuration $\sigma \in \mathcal{X}_{J-h}$ if it only has non-interacting clusters or plus strips with internal angles of $\frac{2}{3}\pi$ or π only.*

Proof of Corollary 4.2.5. Suppose $\sigma \in \mathcal{X}_{J-h}$. By Lemma 4.2.4, it follows that the clusters (or the plus strips) of σ do not have angles of $\frac{5}{3}\pi$, $\frac{1}{3}\pi$ and $\frac{4}{3}\pi$. So, either $\sigma \equiv \underline{+1}$ or the clusters (or the plus strips) of σ have only internal angles of π and $\frac{2}{3}\pi$.
We observe that if two clusters C_1 and C_2 are interacting, there exists a triangular face with minus spin that shares a side with the external boundary of C_1 and a side with the external boundary of C_2. This case can be treated as the case of clusters with an internal angle of $\frac{5}{3}\pi$, therefore by Lemma 4.2.4 these configurations do not belong to $\mathcal{X}_{J-h}$. □

Partition of $\mathcal{X}_{J-h}$. We partition the set $\mathcal{X}_{J-h} \setminus \{\underline{-1}, \underline{+1}\}$ into four subsets Z, R, U, Y. Let Z be the set of configurations consisting of a single quasi-regular hexagonal cluster, see Figure 4.5. More precisely, $Z = Z_1 \cup Z_2$, where:

- Z_1 is the collection of configurations such that there exists only one cluster with shape $E_{B_m}(r) \subset \Lambda$ with $r \leq r^*$ and $m \in \{0,1,2,3,4,5\}$;
- Z_2 is the collection of configurations such that there exists only one cluster with shape $E_{B_m}(r) \subset \Lambda$ with $r \geq r^* + 1$ and $m \in \{0,1,2,3,4,5\}$.

We define the set R to be the set of configurations consisting of a single regular cluster see Figure 4.5. Formally, $R = R_1 \cup R_2$, where:

- R_1 is the collection of configurations such that there exists only one cluster with hexagonal shape $E \subset \Lambda$ such that it contains the greatest quasi-regular hexagon with radius $r \leq r^*$;

- R_2 is the collection of configurations such that there exists only one cluster with hexagonal shape $E \subset \Lambda$ such that it contains the greatest quasi-regular hexagon with radius $r \geq r^* + 1$.

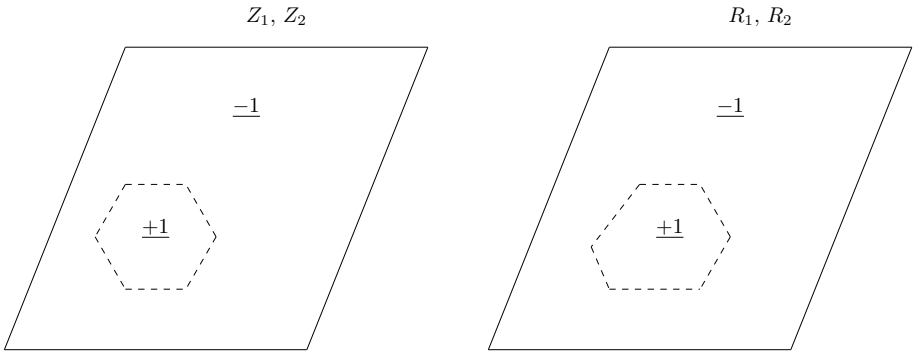

Figure 4.5 On the left an example of configuration in Z, on the right an example of configuration in R.

Let U be the set of configurations with more than one hexagonal cluster of the types in Z_1, Z_2, R_1, R_2, see Figure 4.6. More precisely, we have $U = U_1 \cup U_2$, where:

- U_1 is the collection of configurations such that there exists a family of non-interacting clusters with hexagonal shape such that it contains the greatest quasi-regular hexagon with radius $r \leq r^*$;
- U_2 is the collection of configurations such that there exists a family of clusters with at least one having hexagonal shape containing the greatest quasi-regular hexagon with radius $r \geq r^* + 1$.

In other words U_1 contains a collection of clusters of the same type of those in Z_1 or R_1, and U_2 contains a collection of clusters where at least one is of the same type of those in Z_2 or R_2.
Let Y be the set of all possible (plus or minus) strips with only π internal angles on their boundary and, possibly, some hexagonal clusters, see Figure 4.6.

Corollary 4.2.6. *We have $\mathcal{X}_{J-h} = Z \cup R \cup U \cup Y \cup \{\underline{+1}, \underline{-1}\}$ and for any $\epsilon > 0$ and sufficiently large β,*

$$\sup_{\sigma \in \mathcal{X}} \mathbb{P}_\sigma(\tau_{\mathcal{X}_{J-h}} > e^{\beta(J-h+\epsilon)}) = SES. \tag{4.2.5}$$

Equation (4.2.5) implies that the system visits with high probability a state with a stability level greater than $J - h$ in a time shorter than $e^{\beta(J-h+\epsilon)}$. In other words, the states in $\mathcal{X}_{J-h}$ are the relevant ones for a dynamics speeded up by a factor $e^{\beta(J-h)}$.

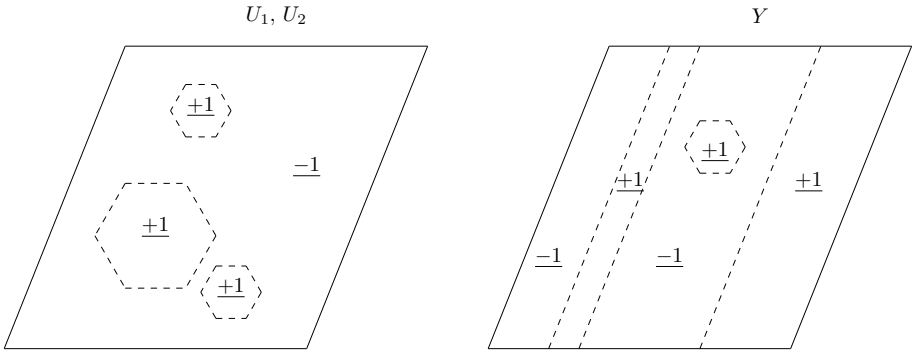

Figure 4.6 On the left an example of configuration in U, on the right an example of configuration in Y.

Proof of Corollary 4.2.6. By the partition described above, Definition (3.2.13) and Corollary 4.2.5 it follows that $\mathcal{X}_{J-h} = Z \cup R \cup U \cup Y \cup \{\underline{+1}, \underline{-1}\}$. By [70, Theorem 3.1] for $V = J - h$ and by the partition of $\mathcal{X}_{J-h}$, we get (4.2.5). □

4.2.2 Proof of Theorem 3.3.2

Lemma 4.2.7 (Estimate of stability levels)**.** *For every $\eta \in \mathcal{X}_{J-h} \setminus \{\underline{-1}, \underline{+1}\}$, there exists $V^* = 2J$ such that $V_\eta \leq V^*$.*

Proof of Lemma 4.2.7. We begin by considering the set Z.

Case Z_1**.** For any configuration $\sigma \in Z_1$ we construct a path $\overline{\omega} \in \Theta(\sigma, I_\sigma \cap (Z_1 \cup \{\underline{-1}\}))$ that dismantles the bar on one of the shortest sides of the quasi-regular hexagon starting from one of its corners. Starting from $\sigma \equiv \omega_0 \in Z_1$, we define ω_1 as follows. Consider a corner in one of the shortest sides of the cluster in $\mathcal{E}_{B_m}(r)$ and let j be a site belonging to this corner. Flip the spin in j, *i.e.*, $\omega_1 := \omega_0^{(j)}$. Define $\omega_2 := \omega_1^{(j_1)}$, where j_1 is the other site belonging to the same corner. From the values in Table 3.1, $H(\omega_1) - H(\omega_0) = J + h$ and $H(\omega_2) - H(\omega_1) = -(J - h)$. By iterating this procedure along the considered side, a bar of the cluster is erased and we obtain the configuration $\eta \equiv \omega_k$ such that $\eta = \mathcal{E}_{B_{m-1}}(r)$ for $m \neq 0$, otherwise $\eta = \mathcal{E}_{B_5}(r-1)$ for $m = 0$. Note that the length of the path is equal to the cardinality k of the bar.
In order to determine where the maximum is attained, we rewrite for $n = 2, \ldots, k$

$$H(\omega_n) - H(\omega_0) = \begin{cases} \sum_{t=2, t\,even}^{n} (H(\omega_t) - H(\omega_{t-2})) & \text{if even n,} \\ \sum_{t=2, t\,even}^{n-1} (H(\omega_t) - H(\omega_{t-2})) + H(\omega_n) - H(\omega_{n-1}) & \text{if odd n.} \end{cases} \tag{4.2.6}$$

From the values in Table 3.1, we obtain for every $s = 2, \cdots, k-1$

$$H(\omega_s) - H(\omega_{s-2}) = [H(\omega_s) - H(\omega_{s-1})] + [H(\omega_{s-1}) - H(\omega_{s-2})] = 2h. \tag{4.2.7}$$

The previous result can also be obtained by using (3.2.19) and observing that flipping two spins, as described above, corresponds to decreasing $N^+(\sigma)$ and leads to a cluster with a Peierls contour of the same length. Thus, we have

$$H(\omega_n) - H(\omega_0) = \begin{cases} 2h\frac{n-1}{2} + (J+h) = J + nh & \text{if odd } n = 1, \cdots, k-2, \\ 2h\frac{n}{2} = nh & \text{if even } n = 2, \cdots, k-1, \\ -J + nh & \text{if } n = k. \end{cases} \tag{4.2.8}$$

The absolute maximum is attained in ω_{k-2}. By Remark 4.1.19 it follows

- $k = 2r-1$, if the initial configuration is $\mathcal{E}_{B_1}(r)$;
- $k = 2r+1$, if the initial configuration is $\mathcal{E}_{B_m}(r)$ for $m = 2, 3, 4, 5$;
- $k = 2r+3$, if the initial configuration is $\mathcal{E}(r+1)$.

and we have

$$\Phi(\overline{\omega}) - H(\omega_0) = H(\omega_{k-2}) - H(\omega_0) = J + (k-2)h. \tag{4.2.9}$$

Thus $\Phi(\overline{\omega})$ depends only on the cardinality k, that is an increasing function of the radius r of the quasi-regular hexagon. The cardinality of the longest bar among those of the quasi-regular hexagon in a configuration in Z_1 is $2r^* + 1$ (obtained removing B_5 from $E_{B_5}(r^*)$). Note that the maximum is not obtained for $k = 2r^* + 3$, since $\mathcal{E}(r^* + 1) \notin Z_1$. Let us check that $\omega_k \in I_\sigma \cap (Z_1 \cup \{\underline{-1}\})$. Since $k \leq 2r^* + 1$ with $r^* = \lfloor J/2h - 1/2 \rfloor$ and by (4.2.8), we get

$$H(\omega_0) - H(\omega_k) = J - kh \geq J - (2r^* + 1)h > 0. \tag{4.2.10}$$

Finally, by equations (4.2.10) and (4.2.9), we have

$$V_\sigma \leq \Phi(\overline{\omega}) - H(\sigma) = J + (k-2)h. \tag{4.2.11}$$

Thus, we find $V^*_{Z_1} = \max_{\sigma \in Z_1} V_\sigma$ by choosing $k - 2 = (2r^* + 1) - 2$ and recalling $r^* = \lfloor J/2h - 1/2 \rfloor$, we have

$$V^*_{Z_1} \leq 2J - 2h. \tag{4.2.12}$$

Case Z_2. For any configuration $\sigma \in Z_2$ we construct a path $\overline{\omega} \in \Theta(\sigma, I_\sigma \cap (Z_2 \cup \{\underline{+1}\}))$. Starting from $\sigma \equiv \omega_0 \in Z_2$, let us define ω_1. Consider a corner in one of the longest sides of the cluster in $\mathcal{E}_{B_m}(r)$ and let j be a site belonging to this corner. Let j_1 be the site at distance one from j such that $\sigma(j_1) = -1$. We define $\omega_1 := \omega_0^{(j_1)}$, *i.e.*, $\sigma(j_1)$ switches the sign. We consider j_2 the site at distance one from j_1 such that $\sigma(j_2) = -1$ and $d(j_2, j') = 2$ where $j' \neq j$ is another site of the initial cluster. We define $\omega_2 := \omega_1^{(j_2)}$, $\omega_3 := \omega_2^{(j_3)}$, where j_3 is the site at distance one from j_2 such that $\sigma(j_3) = -1$ and $d(j_3, j') = 1$ where $j' \neq j$ is another site of the initial cluster. By iterating this procedure along the considered side, a bar is added to the initial cluster. We obtain the configuration $\eta \equiv \omega_k$ such that $\eta = \mathcal{E}_{B_{m+1}}(r)$ for $m \neq 5$, otherwise $\eta = \mathcal{E}(r+1)$ for $m = 5$. Note that the length of the path is equal to the cardinality k of the bar.
In order to determine where the maximum is attained, we rewrite for $n = 2, \ldots, k$

$$H(\omega_n) - H(\omega_0) = \begin{cases} \sum_{t=2, t\,even}^{n} (H(\omega_t) - H(\omega_{t-2})) & \text{if even n,} \\ \sum_{t=2, t\,even}^{n-1} (H(\omega_t) - H(\omega_{t-2})) + H(\omega_n) - H(\omega_{n-1}) & \text{if odd n.} \end{cases} \tag{4.2.13}$$

From the values in Table 3.1 we obtain $H(\omega_1) - H(\omega_0) = J - h$, $H(\omega_2) - H(\omega_0) = 2J - 2h$, and for every $s = 3, \cdots, k$

$$H(\omega_s) - H(\omega_{s-2}) = [H(\omega_s) - H(\omega_{s-1})] + [H(\omega_{s-1}) - H(\omega_{s-2})] = -2h. \tag{4.2.14}$$

The previous result can also be obtained by using (3.2.19) and observing that flipping two spins, as described above, corresponds to increase $N^+(\sigma)$ and leads to a cluster with a Peierls contour of the same length. Thus, we have

$$H(\omega_n) - H(\omega_0) = \begin{cases} J - h, & \text{if } n = 1, \\ 2J - 2h, & \text{if } n = 2, \\ -2h\frac{n-2}{2} + (2J - 2h) = 2J - nh, & \text{if even } n = 4, \cdots, k-1, \\ -2h\frac{n-1}{2} + (J - h) = J - nh, & \text{if odd } n = 3, \cdots, k. \end{cases} \tag{4.2.15}$$

The absolute maximum is attained in ω_2 and we have

$$\Phi(\overline{\omega}) - H(\omega_0) = H(\omega_2) - H(\omega_0) = 2J - 2h. \tag{4.2.16}$$

Finally, let us check that $\omega_k \in I_\sigma \cap (Z_2 \cup \{\underline{+1}\})$. If $\sigma \in Z_2 \setminus \mathcal{E}(r^*+1)$, then the cardinality of the smallest bar among those of the quasi-regular hexagon in a configuration in Z_2 is $k_{\min} = 2(r^*+1)+1$. Since $r^* = \lfloor J/2h - 1/2 \rfloor$ and by (4.2.15), we have

$$H(\omega_0) - H(\omega_k) = kh - J \geq k_{\min} h - J > 0, \tag{4.2.17}$$

thus

$$V_\sigma \leq \Phi(\overline{\omega}) - H(\sigma) = 2J - 2h. \tag{4.2.18}$$

Now we consider $\mathcal{E}(r^*+1)$, we note that $H(\mathcal{E}(r^*+1)) < H(\mathcal{E}_{B_1}(r^*+1))$. Thus we need to consider a new path $\overline{\omega}$ that consists of the previously defined $(\mathcal{E}(r^*+1), \ldots, \mathcal{E}_{B_1}(r^*+1))$ connected with an additional part depending on the value of δ, where $\delta \in (0,1)$ is such that $r^* = J/2h - 1/2 - \delta$. If $0 < \delta < \frac{1}{2}$ then we add the bar B_2 as we have done above for B_1 obtaining $\overline{\omega} = (\mathcal{E}(r^*+1), \ldots, \mathcal{E}_{B_1}(r^*+1), \ldots, \mathcal{E}_{B_2}(r^*+1))$. If $\frac{1}{2} < \delta < 1$ in the same manner we add the bars B_2, B_3, B_4, B_5, B_6 obtaining $\overline{\omega} = (\mathcal{E}(r^*+1), \ldots, \mathcal{E}_{B_1}(r^*+1), \ldots, \mathcal{E}_{B_6}(r^*+1) \equiv \mathcal{E}(r^*+2))$. In both cases the last configurations of the new paths belong to $\mathcal{I}_{\mathcal{E}(r^*+1)}$, indeed

$$\begin{aligned} H(\mathcal{E}(r^*+1)) > H(\mathcal{E}_{B_2}(r^*+1)), &\qquad \text{if } \delta \in (0, \frac{1}{2}), \\ H(\mathcal{E}(r^*+1)) > H(\mathcal{E}(r^*+2)), &\qquad \text{if } \delta \in (\frac{1}{2}, 1). \end{aligned}$$

Thus, using equations (4.2.15), (4.2.16) and (4.2.18), we obtain

$$\begin{aligned} V_\sigma \leq 2J - 2h + H(\mathcal{E}_{B_1}(r^*+1)) - H(\mathcal{E}(r^*+1)) = 2J - 2h + 2h\delta < 2J - h, &\qquad \text{for } \delta \in \left(0, \frac{1}{2}\right), \\ V_\sigma \leq 2J - 2h + H(\mathcal{E}_{B_5}(r^*+1)) - H(\mathcal{E}(r^*+1)) = 2J - 10h + 10h\delta < 2J, &\qquad \text{for } \delta \in \left(\frac{1}{2}, 1\right). \end{aligned}$$

Thus we find

$$V^*_{Z_2} = \max_{\sigma \in Z_2} V_\sigma < 2J. \tag{4.2.19}$$

In conclusion, we have $V^*_Z = \max\{V^*_{Z_1}, V^*_{Z_2}\} < 2J$.

Case R_1**.** For any configuration $\sigma \in R_1$ we construct a path $\overline{\omega} \in \Theta(\sigma, I_\sigma \cap (R_1 \cup Z_1)))$. Starting from $\sigma \equiv \omega_0 \in R_1$, let us define ω_1. Consider the corner in one of the shortest sides of the cluster and let j be a site belonging to it. We define $\omega_1 := \omega_0^{(j)}$, *i.e.*, $\sigma(j)$ switches the sign. Consider j' the other site belonging to the corner and define $\omega_2 := \omega_1^{(j')}$, in this way $\sigma(j')$ switches the sign. By iterating this procedure along the shortest side, a bar of the cluster

is erased and we obtain the configuration $\eta \equiv \omega_l$, where l is the cardinality of the considered bar. We observe that the greatest value of l is always smaller than the cardinality k of the greatest bar of the quasi-regular hexagon contained in the cluster, that is $l < k$. Analogously to the case Z_1, $\omega_l \in I_\sigma$. Then $V_\sigma < 2J - 2h$. Therefore,

$$V^*_{R_1} = \max_{\sigma \in R_1} V_\sigma < 2J - 2h. \tag{4.2.20}$$

Case R_2**.** For any configuration $\sigma \in R_2$ we construct a path $\overline{\omega} \in \Theta(\sigma, I_\sigma \cap (R_2 \cup Z_2 \cup \{\underline{+1}\}))$. Starting from $\sigma \equiv \omega_0 \in R_2$, let us define ω_1. Consider the corner in one of the shortest sides of the cluster and let j be a site belonging to it. If the cardinality of the bar l of the shortest side is smaller than $2(r^*+1)-1$, we define $\omega_1 := \omega_0^{(j)}$, *i.e.* $\sigma(j)$ switches the sign. Consider the other site j' belonging to the corner and define $\omega_2 := \omega_1^{(j')}$, in this way $\sigma(j')$ switches the sign. By iterating this procedure along the shortest side, a bar of the cluster is erased and we obtain the configuration $\eta \equiv \omega_l$, where l is the cardinality of the considered bar. Since $l < 2(r^*+1)-1$, we observe that the greatest value of l is always smaller then the cardinality k of the greatest bar of the quasi-regular hexagon contained in the cluster, that is $l < k$. Analogously to the case Z_1, $\omega_l \in I_\sigma$. Thus $V_\sigma < 2J - 2h$.
If the cardinality of the bar l of the shortest side is bigger than $2(r^*+1)-1$, consider the site j_1 at distance one from j and such that $\sigma(j_1) = -1$. We define $\omega_1 := \omega_0^{(j_1)}$, i.e. $\sigma(j_1)$ switches the sign. Consider j_2 the site at distance one from j_1 such that $\sigma(j_2) = -1$ and $d(j_2, j') = 2$ where $j' \neq j$ is another site of the initial cluster. We define $\omega_2 := \omega_1^{(j_2)}$, $\omega_3 := \omega_2^{(j_3)}$, where j_3 is the site at distance one from j_2 such that $\sigma(j_3) = -1$ and $d(j_3, j') = 1$ where $j' \neq j$ is another site of the initial cluster. By iterating this procedure along the considered side, a bar is added to the initial cluster. Analogously to the case Z_2, $\omega_l \in I_\sigma$ since $l > 2(r^*+1)-1$. Thus $V_\sigma \leq 2J - 2h$ and

$$V^*_{R_2} \leq 2J - 2h. \tag{4.2.21}$$

In conclusion, we have $V^*_R = \max\{V^*_{R_1}, V^*_{R_2}\} < 2J$.

Case U_1**.** For every configuration σ in U_1, all clusters are non-interacting and are of the same type of those in Z_1 or R_1. If σ contains a cluster that is not a quasi-regular hexagon, then we take our path to be the path that cuts a bar, analogously to what has been done for R_1. We get a configuration in $\mathcal{I}_\sigma \cap U_1$. Otherwise, if all clusters are quasi-regular hexagons, then we take our path to be the path that cuts a bar of the cluster, analogously to what has been done for Z_1. We get a configuration in $\mathcal{I}_\sigma \cap (U_1 \cup Z_1)$. So, we have

$$V^*_{U_1} = \max\{V^*_{R_1}, V^*_{Z_1}\} < 2J - 2h. \tag{4.2.22}$$

Case U_2. For every configuration σ in U_2, there exists at least a cluster of the same type of those in Z_2 or R_2. If σ contains a cluster of the type of those in R_2, *i.e.* σ contains a cluster that is not a quasi-regular hexagon, we take our path to be the path that cuts a bar as it has been done for R_2. We get a configuration in $\mathcal{I}_\sigma \cap U_2$. Otherwise, if the cluster is like those in Z_2, i.e. the cluster is a quasi-regular hexagon, then we take the path that adds a bar to the quasi-regular hexagon, alike the cases encountered when considering Z_2. We get a configuration in $\mathcal{I}_\sigma \cap (U_2 \cup \{\underline{+1}\})$. So, we have

$$V^*_{U_2} = \max\{V^*_{R_2}, V^*_{Z_2}\} < 2J. \tag{4.2.23}$$

We conclude that

$$V^*_U = \max\{V^*_{U_1}, V^*_{U_2}\} = V^*_Z.$$

Case Y. We analyze four different kinds of configurations.

1. If $\sigma_1 \equiv \omega_0$ is a configuration in Y such that it has a minus strip that contains at least a hexagon of the type of those in Z_2 or R_2, then we take our path to be as that in the case U_2 and we obtain a configuration in $\mathcal{I}_\sigma \cap (Y \cup \{\underline{+1}\})$. So, we have

$$V_{\sigma_1} = V^*_{U_2} < 2J \tag{4.2.24}$$

2. If $\sigma_2 \equiv \omega_0$ is a configuration in Y such that it contains a plus strip with width greater than one, then we take our path as follows. Pick a site j with $\sigma(j) = -1$ at distance one from the strip. We define $\omega_1 = \omega_0^{(j)}$, *i.e.*, $\sigma(j)$ switches the sign. Then pick a site j_1 at distance one from j such that $\sigma(j_1) = -1$ and define $\omega_2 = \omega_1^{(j_1)}$. Consider a site j_2 nearest neighbor of j_1 such that $\sigma(j_2) = -1$ and define $\omega_3 = \omega_2^{(j_2)}$. By iterating these last two steps, we obtain a configuration in $\mathcal{I}_\sigma \cap (Y \cup \{\underline{+1}\})$. In order to determine where the maximum is attained we write for $n = 2, \cdots, L-1$

$$H(\omega_n) - H(\omega_0) = \begin{cases} \sum_{t=2,\, t\, even}^{n} (H(\omega_t) - H(\omega_{t-2})) & \text{if even n,} \\ \sum_{t=2,\, t\, even}^{n} (H(\omega_t) - H(\omega_{t-2})) + H(\omega_n) - H(\omega_{n-1}) & \text{if odd n.} \end{cases} \tag{4.2.25}$$

From the values in Table 3.1 we obtain

$$H(\omega_1) - H(\omega_0) = J - h, \tag{4.2.26}$$

$$H(\omega_2) - H(\omega_0) = 2J - 2h, \tag{4.2.27}$$

$$H(\omega_L) - H(\omega_{L-1}) = -(J + h), \tag{4.2.28}$$

and for every $t = 3, \cdots, L-1$

$$H(\omega_t) - H(\omega_{t-2}) = [H(\omega_t) - H(\omega_{t-1})] + [H(\omega_{t-1}) - H(\omega_{t-2})] = -2h. \quad (4.2.29)$$

The previous result can also be obtained by using (3.2.19) and observing that flipping two spins, as described above, corresponds to increasing $N^+(\sigma)$ and leads to a cluster with a Peierls contour of the same length. Thus, we have

$$H(\omega_n) - H(\omega_0) = \begin{cases} J - h, & \text{if } n = 1, \\ 2J - 2h, & \text{if } n = 2, \\ -2h\frac{n-2}{2} + (2J - 2h) = 2J - nh, & \text{if even } n = 4, \cdots, L-1, \\ -2h\frac{n-1}{2} + (J - h) = J - nh, & \text{if odd } n = 3, \cdots, L-1, \\ -2h\frac{n-4}{2} + (2J - 2h) - (2J + 2h) = -Lh, & \text{if } n = L. \end{cases} \quad (4.2.30)$$

The maximum of the last equations is obtained for $n = 2$ and it is attained in ω_2. Using (4.2.30), we prove that $\omega_L \in I_\sigma \cap (Y \cup \{\underline{+1}\})$

$$H(\omega_0) - H(\omega_L) = Lh > 0. \quad (4.2.31)$$

Thus

$$V_{\sigma_2} \leq H(\omega_2) - H(\omega_0) = 2J - 2h. \quad (4.2.32)$$

3. If $\sigma_3 \equiv \omega_0$ is a configuration in Y such that it contains a plus strip with width one, then we take our path as follows. Pick a site j in the strip and define $\omega_1 := \omega_0^{(j)}$, *i.e.*, $\sigma(j)$ switches the sign. The difference of the energy given by the Table 3.1 is $H(\omega_1) - H(\omega_0) = J + h$. Considering $j_2, j_3, \ldots$ the nearest sites in the strip, we define $\omega_2 := \omega_1^{j_2}$, $\omega_3 := \omega_2^{(j_3)}$ and so on until we obtain a configuration in $\mathcal{I}_\sigma \cap (Y \cup Z_1 \cup U_1 \cup \{\underline{-1}\})$. Finally, let us check that $\omega_L \in I_\sigma \cap (Y \cup \{\underline{+1}\})$. Using Table 3.1, we get

$$\begin{aligned} H(\omega_L) - H(\omega_0) &= [H(\omega_L) - H(\omega_{L-1})] + \sum_{t=2}^{L-1} (H(\omega_t) - H(\omega_{t-1}) + [H(\omega_1) - H(\omega_0)] \\ &= -(3J - h) - (L-2)(J - h) + (J + h) = -L(J - h) < 0. \end{aligned} \quad (4.2.33)$$

Thus

$$V_{\sigma_3} \leq J + h. \tag{4.2.34}$$

We conclude that

$$V_Y^* = \max\{V_{\sigma_1}, V_{\sigma_2}, V_{\sigma_3}\} < 2J.$$

□

Proof of Theorem 3.3.2. By applying [70, Theorem 3.1] for $V^* = 2J$ and Lemma 4.2.7, we get (3.3.1). □

4.3 Identification of maximal stability level

4.3.1 Reference path

In this section we define our *reference path*, that is a sequence of configurations from $\underline{-1}$ to $\underline{+1}$, that are increasing clusters *as close as possible to quasi-regular hexagonal shape*. We first describe intuitively this path: starting from $\underline{-1}$ we flip the spin at the origin and then consecutively fill (flipping the spins from minus to plus) a standard cluster, see Figure 4.7. More precisely, let $\omega^* \in \Theta(\underline{-1}, \underline{+1})$ be the path defined as follows. Starting from the origin, we add clockwise six triangular units to obtain the first regular hexagon with radius $r = 1$, that is $\mathcal{E}(1)$. Then for each $r = 1, \ldots, m$ we construct the bar on the top of the hexagon $\mathcal{E}(r)$, adding consecutive triangular units until we obtain $\mathcal{E}_{B_1}(r)$. Next we fill the bar on the top right adding consecutive triangular units until we get $\mathcal{E}_{B_2}(r)$. We go on in the same manner adding bars clockwise, until we get $\mathcal{E}_{B_3}(r)$,...,$\mathcal{E}_{B_6}(r) \equiv \mathcal{E}(r+1)$. We iterate this procedure until the hexagon is large enough to wrap around the torus along one direction, giving rise to two triangles of minuses with side length $\frac{L}{2}$. Now the reference path fills six triangular units "covering" all the $\frac{5}{3}\pi$ angles. As a result, it is possible to identify six bars of length two, each adjacent to one of the filled triangular units. For each initial triangle of minuses choose only one of the previous bars and fill it. We obtain two bars of length three, each intersecting the previous bars in the external boundary. Iterate this procedure filling at each step the bars of length four, five, ..., $\frac{L}{2}$.
All configurations in this path contain a standard cluster with radius $r < \frac{L}{2}$. Note that the standard cluster $\mathcal{E}(\frac{L}{2})$ wraps around the torus.

Proposition 4.3.1. *The maximum of the energy in ω^* between two consecutive quasi-regular hexagons $\Phi_{\omega^*}(\mathcal{E}_{B_i}(r), \mathcal{E}_{B_{i+1}}(r))$ for every $i = 0, \ldots, 5$ is achieved in the standard polyiamond obtained adding to $\mathcal{E}_{B_i}(r)$ one elementary rhombus with two pluses along the longest side consecutive to B_i clockwise.*

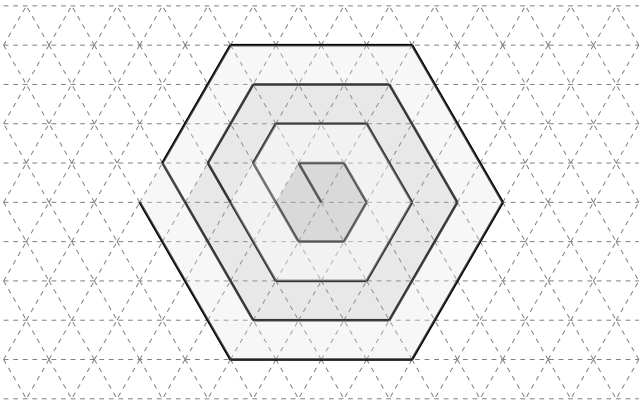

Figure 4.7 The construction of a standard polyiamond.

Proposition 4.3.2. *The maximum of the energy in ω^* between two consecutive quasi-regular hexagons $\Phi_{\omega^*}(\mathcal{E}_{B_i}(r), \mathcal{E}_{B_{i-1}}(r))$ for every $i = 1, \dots, 6$ is achieved in the standard polyiamond obtained removing counter-clockwise from $\mathcal{E}_{B_i}(r)$ a number of triangular units equals to $||B_i|| - 2$.*

Proof of Proposition 4.3.1. Let $E_{B_i}(r)$ and $E_{B_{i+1}}(r)$ be two quasi-regular hexagons for some $r \in \mathbb{N}$ and some $i = 0, \dots, 5$. Let A_n be the area obtained adding n triangular units to the area of the quasi-regular hexagon $E_{B_i}(r)$, where $n = 0, \dots, ||B_{i+1}||$. Note that A_n is the area of the standard polyiamond $S(A_n)$. We observe that $S(A_0) \equiv E_{B_i}(r)$ and $S(A_{||B_{i+1}||}) \equiv E_{B_{i+1}}(r)$. By Table 3.1, we have

$$H(\mathcal{S}(A_n)) - H(\mathcal{S}(A_{n-1})) = \begin{cases} J - h, & \text{if } n = 1, \\ J - h, & \text{if } n \text{ is even}, \\ -(J + h), & \text{if } n \neq 1 \text{ is odd}. \end{cases} \tag{4.3.1}$$

It follows that

$$H(\mathcal{S}(A_n)) - H(\mathcal{E}_{B_i}(r)) = \begin{cases} J - nh, & \text{if } n \text{ is odd}, \\ 2J - nh, & \text{if } n \text{ is even}. \end{cases} \tag{4.3.2}$$

Since the r.h.s. of the last equation decreases with n in both the odd and the even case, it is immediate to check that the maximum is attained for $n = 2$ namely in $\mathcal{S}(A_2)$.

□

Proof of Proposition 4.3.2. Let $E_{B_i}(r)$ and $E_{B_{i-1}}(r)$ be two quasi-regular hexagons for some $r \in \mathbb{N}$ and some $i = 1, \dots, 6$. Let A_n be the area obtained adding n triangular units to

the area of the quasi-regular hexagon $E_{B_{i-1}}(r)$, where $n = 0, \dots, ||B_i||$. Note that $S(A_n)$ can be obtained either by removing $||B_i|| - n$ triangular units from $E_{B_i}(r)$ or by adding n triangular units to $E_{B_{i-1}}(r)$. We recall that *removing* a triangular unit means to flip a plus spin into a minus spin. By Table 3.1, we have

$$H(\mathcal{S}(A_{n-1})) - H(\mathcal{S}(A_n)) = \begin{cases} J + h, & \text{if } n \neq ||B_i|| \text{ is odd,} \\ -(J-h), & \text{if } n \text{ is even,} \\ -(J-h), & \text{if } n = ||B_i||. \end{cases} \tag{4.3.3}$$

It follows that

$$H(\mathcal{S}(A_n)) - H(\mathcal{E}_{B_i}(r)) = \begin{cases} J + nh, & \text{if } n \neq ||B_i|| \text{ is odd,} \\ nh, & \text{if } n \text{ is even,} \\ -(J-nh), & \text{if } n = ||B_i||. \end{cases} \tag{4.3.4}$$

Since the r.h.s. of the last equation increases with n in all three cases and since $||B_i||$ is odd by Definition 4.1.11, the maximum is attained removing $||B_i|| - 2$ triangular units from $E_{B_i}(r)$, namely in $\mathcal{S}(A_2)$. □

Recalling Definition (3.2.21), from now on the strategy of the proof is to divide the reference path ω^* into three regions depending on r:

- the region $r \leq r^*$ will be considered in Proposition 4.3.3;
- the region $r = r^* + 1$ will be considered in Proposition 4.3.5;
- the region $r \geq r^* + 2$ will be considered in Proposition 4.3.4.

Proposition 4.3.3. *If $r \leq r^*$, then the communication height between two consecutive regular hexagons $\Phi_{\omega^*}(\mathcal{E}(r), \mathcal{E}(r+1))$ along the path ω^* is achieved in a configuration with a standard cluster such that the number of its triangular units is $\tilde{A} = 6r^2 + 10r + 5$, that is $\Phi_{\omega^*}(\mathcal{E}(r), \mathcal{E}(r+1)) = \Phi_{\omega^*}(\mathcal{E}_{B_5}(r), \mathcal{E}(r+1)) = H(\mathcal{S}(\tilde{A})) - H(\underline{-1})$. Moreover, $\Phi_{\omega^*}(\underline{-1}, \mathcal{E}(r^*+1)) = \Phi_{\omega^*}(\mathcal{E}(r^*), \mathcal{E}(r^*+1)) = H(\mathcal{S}(A_1)) - H(\underline{-1})$ is achieved in a configuration with a standard cluster $\mathcal{S}(A_1)$ such that $A_1 := 6{r^*}^2 + 10r^* + 5$.*

Proposition 4.3.4. *If $r \geq r^* + 2$, then the communication height between two consecutive regular hexagons $\Phi_{\omega^*}(\mathcal{E}(r), \mathcal{E}(r+1))$ along the path ω^* is achieved in a configuration with a standard cluster such that the number of its triangular units is $\tilde{A} = 6r^2 + 2$, that is $\Phi_{\omega^*}(\mathcal{E}(r), \mathcal{E}(r+1)) = \Phi_{\omega^*}(\mathcal{E}(r), \mathcal{E}_{B_1}(r)) = H(\mathcal{S}(\tilde{A})) - H(\underline{-1})$. Moreover, $\Phi_{\omega^*}(\mathcal{E}(r^*+2), \underline{+1}) = \Phi_{\omega^*}(\mathcal{E}(r^*+2), \mathcal{E}(r^*+3)) = H(\mathcal{S}(A_2)) - H(\underline{-1})$ is achieved in a configuration with a standard cluster $\mathcal{S}(A_2)$ such that $A_2 := 6(r^*+2)^2 + 2$.*

Proposition 4.3.5. *If $r = r^* + 1$, then $r = \lfloor J/2h + 1/2 \rfloor$ and the communication height $\Phi_{\omega^*}(\mathcal{E}(r^*+1), \mathcal{E}(r^*+2))$ along the path ω^* is achieved in a configuration with a standard cluster $\mathcal{S}(A_3)$ with $A_3 := 6(r^*+1)^2 + 2(r^*+1) + 1$.*

Proof of Proposition 4.3.3. Let m be the number of site pairs (i, j) such that $d(i, j) = 1$ with $i, j \in \Lambda$, and let $p(S(A))$ be the perimeter of the standard hexagon $S(A)$. By Definition 3.2.19, we have:

$$H(\mathcal{S}(A)) - H(\underline{-1}) = Jp(S(A)) - hA. \tag{4.3.5}$$

By Remark 4.1.19, it follows that:

$$H(\mathcal{S}(A)) - H(\underline{-1}) = \begin{cases} -6r^2h + 6rJ + 2J - 2h & \text{for } A = 6r^2 + 2 \\ -6r^2h + 6rJ - 2rh + 3J - h & \text{for } A = 6r^2 + 2r + 1 \\ -6r^2h + 6rJ - 4rh + 4J - 2h & \text{for } A = 6r^2 + 4r + 2 \\ -6r^2h + 6rJ - 6rh + 5J - 3h & \text{for } A = 6r^2 + 6r + 3 \\ -6r^2h + 6rJ - 8rh + 6J - 4h & \text{for } A = 6r^2 + 8r + 4 \\ -6r^2h + 6rJ - 10rh + 7J - 5h & \text{for } A = 6r^2 + 10r + 5 \end{cases} \tag{4.3.6}$$

We compare $\Phi_{\omega^*}(\mathcal{E}(r), \mathcal{E}_{B_1}(r))$ with $\Phi_{\omega^*}(\mathcal{E}_{B_1}(r), \mathcal{E}_{B_2}(r))$. By Proposition 4.3.1, we have:

$$\Phi_{\omega^*}(\mathcal{E}(r), \mathcal{E}_{B_1}(r)) = H(\mathcal{S}(6r^2+2)) - H(\underline{-1})$$
$$\Phi_{\omega^*}(\mathcal{E}_{B_1}(r), \mathcal{E}_{B_2}(r)) = H(\mathcal{S}(6r^2+2r+1)) - H(\underline{-1}).$$

Using (4.3.6) we get that if $r \leq \frac{J}{2h} + \frac{1}{2}$

$$\Phi_{\omega^*}(\mathcal{E}(r), \mathcal{E}_{B_1}(r)) \leq \Phi_{\omega^*}(\mathcal{E}_{B_1}(r), \mathcal{E}_{B_2}(r)) \tag{4.3.7}$$

Since we assume $r \leq r^*$, the inequality (4.3.7) is satisfied.

We compare $\Phi_{\omega^*}(\mathcal{E}_{B_1}(r), \mathcal{E}_{B_2}(r))$ with $\Phi_{\omega^*}(\mathcal{E}_{B_2}(r), \mathcal{E}_{B_3}(r))$. By Proposition 4.3.1, we have:

$$\Phi_{\omega^*}(\mathcal{E}_{B_1}(r), \mathcal{E}_{B_2}(r)) = H(\mathcal{S}(6r^2+2r+1)) - H(\underline{-1})$$
$$\Phi_{\omega^*}(\mathcal{E}_{B_2}(r), \mathcal{E}_{B_3}(r)) = H(\mathcal{S}(6r^2+4r+2)) - H(\underline{-1}).$$

Using (4.3.6) we get that if $r \leq \frac{J}{2h} - \frac{1}{2}$

$$\Phi_{\omega^*}(\mathcal{E}_{B_1}(r), \mathcal{E}_{B_2}(r)) \leq \Phi_{\omega^*}(\mathcal{E}_{B_2}(r), \mathcal{E}_{B_3}(r)). \tag{4.3.8}$$

Since we assume $r \leq r^*$, the inequality (4.3.8) is satisfied.

We compare $\Phi_{\omega^*}(\mathcal{E}_{B_2}(r), \mathcal{E}_{B_3}(r))$ with $\Phi_{\omega^*}(\mathcal{E}_{B_3}(r), \mathcal{E}_{B_4}(r))$. By Proposition 4.3.1, we have:

$$\begin{aligned}
\Phi_{\omega^*}(\mathcal{E}_{B_2}(r), \mathcal{E}_{B_3}(r)) &= H(\mathcal{S}(6r^2 + 4r + 2)) - H(\underline{-1}) \\
\Phi_{\omega^*}(\mathcal{E}_{B_3}(r), \mathcal{E}_{B_4}(r)) &= H(\mathcal{S}(6r^2 + 6r + 3)) - H(\underline{-1}).
\end{aligned}$$

Using (4.3.6) we get that if $r \leq \frac{J}{2h} - \frac{1}{2}$

$$\Phi_{\omega^*}(\mathcal{E}_{B_2}(r), \mathcal{E}_{B_3}(r)) \leq \Phi_{\omega^*}(\mathcal{E}_{B_3}(r), \mathcal{E}_{B_4}(r)). \tag{4.3.9}$$

Since we assume $r \leq r^*$, the inequality (4.3.9) is satisfied.

We compare $\Phi_{\omega^*}(\mathcal{E}_{B_3}(r), \mathcal{E}_{B_4}(r))$ with $\Phi_{\omega^*}(\mathcal{E}_{B_4}(r), \mathcal{E}_{B_5}(r))$. By Proposition 4.3.1, we have:

$$\begin{aligned}
\Phi_{\omega^*}(\mathcal{E}_{B_3}(r), \mathcal{E}_{B_4}(r)) &= H(\mathcal{S}(6r^2 + 6r + 3)) - H(\underline{-1}) \\
\Phi_{\omega^*}(\mathcal{E}_{B_4}(r), \mathcal{E}_{B_5}(r)) &= H(\mathcal{S}(6r^2 + 8r + 4)) - H(\underline{-1}).
\end{aligned}$$

Using (4.3.6) we get that if $r \leq \frac{J}{2h} - \frac{1}{2}$

$$\Phi_{\omega^*}(\mathcal{E}_{B_3}(r), \mathcal{E}_{B_4}(r)) \leq \Phi_{\omega^*}(\mathcal{E}_{B_4}(r), \mathcal{E}_{B_5}(r)). \tag{4.3.10}$$

Since we assume $r \leq r^*$, the inequality (4.3.10) is satisfied.

We compare $\Phi_{\omega^*}(\mathcal{E}_{B_4}(r), \mathcal{E}_{B_5}(r))$ with $\Phi_{\omega^*}(\mathcal{E}_{B_5}(r), \mathcal{E}(r+1))$. By Proposition 4.3.1, we have:

$$\begin{aligned}
\Phi_{\omega^*}(\mathcal{E}_{B_4}(r), \mathcal{E}_{B_5}(r)) &= H(\mathcal{S}(6r^2 + 8r + 4)) - H(\underline{-1}) \\
\Phi_{\omega^*}(\mathcal{E}_{B_5}(r), \mathcal{E}(r+1)) &= H(\mathcal{S}(6r^2 + 10r + 5)) - H(\underline{-1}).
\end{aligned}$$

Using (4.3.6) we get that if $r \leq \frac{J}{2h} - \frac{1}{2}$

$$\Phi_{\omega^*}(\mathcal{E}_{B_4}(r), \mathcal{E}_{B_5}(r)) \leq \Phi_{\omega^*}(\mathcal{E}_{B_5}(r), \mathcal{E}(r+1)). \tag{4.3.11}$$

Since we assume $r \leq r^*$, the inequality (4.3.11) is satisfied.
Thus the communication height between two consecutive regular hexagons along the path ω^* is achieved in $\mathcal{S}(\tilde{A})$ with $\tilde{A} = 6r^2 + 10r + 5$, that is

$$\Phi_{\omega^*}(\mathcal{E}(r), \mathcal{E}(r+1)) = \Phi_{\omega^*}(\mathcal{E}_{B_5}(r), \mathcal{E}(r+1)) = H(\mathcal{S}(\tilde{A})) - H(\underline{-1}).$$

The maximum of the function $H(\mathcal{S}(\tilde{A})) - H(\underline{-1}) = -6r^2h + 6rJ - 10rh + 7J - 5h$ is obtained in $r_{\max} = \frac{J}{2h} - \frac{5}{6}$. However r must be integer and $r \leq r^*$, therefore the maximum is attained in r^* and

$$\Phi_{\omega^*}(\underline{-1}, \mathcal{E}(r^*+1)) = \Phi_{\omega^*}(\mathcal{E}(r^*), \mathcal{E}(r^*+1)) = H(\mathcal{S}(A_1)) - H(\underline{-1})$$

where $\mathcal{S}(A_1)$ is a configuration with a standard cluster such that $A_1 := 6{r^*}^2 + 10r^* + 5$. □

Proof of Proposition 4.3.4. We compare $\Phi_{\omega^*}(\mathcal{E}(r), \mathcal{E}_{B_1}(r))$ with $\Phi_{\omega^*}(\mathcal{E}_{B_1}(r), \mathcal{E}_{B_2}(r))$. By Proposition 4.3.1 we have:

$$\Phi_{\omega^*}(\mathcal{E}(r), \mathcal{E}_{B_1}(r)) = H(\mathcal{S}(6r^2+2)) - H(\underline{-1})$$
$$\Phi_{\omega^*}(\mathcal{E}_{B_1}(r), \mathcal{E}_{B_2}(r)) = H(\mathcal{S}(6r^2+2r+1)) - H(\underline{-1}).$$

Using (4.3.6) we get that if $r \geq \frac{J}{2h} + \frac{1}{2}$

$$\Phi_{\omega^*}(\mathcal{E}(r), \mathcal{E}_{B_1}(r)) \geq \Phi_{\omega^*}(\mathcal{E}_{B_1}(r), \mathcal{E}_{B_2}(r)). \tag{4.3.12}$$

Since we assume $r \geq r^* + 2$, the inequality (4.3.12) is satisfied.

We compare $\Phi_{\omega^*}(\mathcal{E}_{B_1}(r), \mathcal{E}_{B_2}(r))$ with $\Phi_{\omega^*}(\mathcal{E}_{B_2}(r), \mathcal{E}_{B_3}(r))$. By Proposition 4.3.1 we have:

$$\Phi_{\omega^*}(\mathcal{E}_{B_1}(r), \mathcal{E}_{B_2}(r)) = H(\mathcal{S}(6r^2+2r+1)) - H(\underline{-1}))$$
$$\Phi_{\omega^*}(\mathcal{E}_{B_2}(r), \mathcal{E}_{B_3}(r)) = H(\mathcal{S}(6r^2+4r+2)) - H(\underline{-1}).$$

Using (4.3.6) we get that if $r \geq \frac{J}{2h} - \frac{1}{2}$

$$\Phi_{\omega^*}(\mathcal{E}_{B_1}(r), \mathcal{E}_{B_2}(r)) \geq \Phi_{\omega^*}(\mathcal{E}_{B_2}(r), \mathcal{E}_{B_3}(r)). \tag{4.3.13}$$

Since we assume $r \geq r^* + 2$, the inequality (4.3.13) is satisfied.

We compare $\Phi_{\omega^*}(\mathcal{E}_{B_2}(r), \mathcal{E}_{B_3}(r))$ with $\Phi_{\omega^*}(\mathcal{E}_{B_3}(r), \mathcal{E}_{B_4}(r))$. By Proposition 4.3.1 we have:

$$\Phi_{\omega^*}(\mathcal{E}_{B_2}(r), \mathcal{E}_{B_3}(r)) = H(\mathcal{S}(6r^2+4r+2)) - H(\underline{-1})$$
$$\Phi_{\omega^*}(\mathcal{E}_{B_3}(r), \mathcal{E}_{B_4}(r)) = H(\mathcal{S}(6r^2+6r+3)) - H(\underline{-1}).$$

Using (4.3.6) we get that if $r \geq \frac{J}{2h} - \frac{1}{2}$

$$\Phi_{\omega^*}(\mathcal{E}_{B_2}(r), \mathcal{E}_{B_3}(r)) \geq \Phi_{\omega^*}(\mathcal{E}_{B_3}(r), \mathcal{E}_{B_4}(r)). \tag{4.3.14}$$

Since we assume $r \geq r^* + 2$, the inequality (4.3.14) is satisfied.

We compare $\Phi_{\omega^*}(\mathcal{E}_{B_3}(r), \mathcal{E}_{B_4}(r))$ with $\Phi_{\omega^*}(\mathcal{E}_{B_4}(r), \mathcal{E}_{B_5}(r))$. By Proposition 4.3.1 we have:

$$\Phi_{\omega^*}(\mathcal{E}_{B_3}(r), \mathcal{E}_{B_4}(r)) = H(\mathcal{S}(6r^2+6r+3)) - H(\underline{-1})$$
$$\Phi_{\omega^*}(\mathcal{E}_{B_4}(r), \mathcal{E}_{B_5}(r)) = H(\mathcal{S}(6r^2+8r+4)) - H(\underline{-1}).$$

Using (4.3.6) we get that if $r \geq \frac{J}{2h} - \frac{1}{2}$

$$\Phi_{\omega^*}(\mathcal{E}_{B_3}(r), \mathcal{E}_{B_4}(r)) \geq \Phi_{\omega^*}(\mathcal{E}_{B_4}(r), \mathcal{E}_{B_5}(r)). \tag{4.3.15}$$

Since we assume $r \geq r^* + 2$, the inequality (4.3.15) is satisfied.

We compare $\Phi_{\omega^*}(\mathcal{E}_{B_4}(r), \mathcal{E}_{B_5}(r))$ with $\Phi_{\omega^*}(\mathcal{E}_{B_5}(r), \mathcal{E}(r+1))$. By Proposition 4.3.1 we have:

$$\Phi_{\omega^*}(\mathcal{E}_{B_4}(r), \mathcal{E}_{B_5}(r)) = H(\mathcal{S}(6r^2+8r+4)) - H(\underline{-1})$$
$$\Phi_{\omega^*}(\mathcal{E}_{B_5}(r), \mathcal{E}(r+1)) = H(\mathcal{S}(6r^2+10r+5)) - H(\underline{-1}).$$

Using (4.3.6) we get that if $r \geq \frac{J}{2h} - \frac{1}{2}$

$$\Phi_{\omega^*}(\mathcal{E}_{B_4}(r), \mathcal{E}_{B_5}(r)) \geq \Phi_{\omega^*}(\mathcal{E}_{B_5}(r), \mathcal{E}(r+1)). \tag{4.3.16}$$

Since we assume $r \geq r^* + 2$, the inequality (4.3.16) is satisfied.

Thus the communication height between two consecutive regular hexagons along the path ω^* is achieved in $\mathcal{S}(\tilde{A})$ with $\tilde{A} = 6r^2 + 2$, that is

$$\Phi_{\omega^*}(\mathcal{E}(r), \mathcal{E}(r+1)) = \Phi_{\omega^*}(\mathcal{E}(r), \mathcal{E}_{B_1}(r)) = H(\mathcal{S}(\tilde{A})) - H(\underline{-1}).$$

The maximum of the function $H(\mathcal{S}(\tilde{A})) - H(\underline{-1}) = -6r^2h + 6rJ + 2J - 2h$ is obtained in $r_{\max} = \frac{J}{2h}$, but r must be integer and $r \geq r^* + 2$, therefore the maximum is attained in $r^* + 2$ and

$$\Phi_{\omega^*}(\mathcal{E}(r^*+2), \underline{+1}) = \Phi_{\omega^*}(\mathcal{E}(r^*+2), \mathcal{E}(r^*+3)) = H(\mathcal{S}(A_2)) - H(\underline{-1})$$

where $\mathcal{S}(A_2)$ is a configuration with a standard cluster such that $A_2 := 6(r^*+2)^2 + 2$. □

Proof of Proposition 4.3.5. We analyze $\Phi_{\omega^*}(\mathcal{E}(r^*+1), \mathcal{E}(r^*+2))$. With the same arguments of the proofs of Propositions 4.3.3 and 4.3.4, we consider the Equation (4.3.12) which holds if and only if $r \geq \frac{J}{2h} + \frac{1}{2}$. In this case, we consider $r = r^* + 1 = \lfloor \frac{J}{2h} + \frac{1}{2} \rfloor$, thus we have

$$\Phi_{\omega^*}(\mathcal{E}(r), \mathcal{E}_{B_1}(r)) < \Phi_{\omega^*}(\mathcal{E}_{B_1}(r), \mathcal{E}_{B_2}(r)). \tag{4.3.17}$$

Equations (4.3.13) - (4.3.16) hold if and only if $r \geq \frac{J}{2h} - \frac{1}{2}$

$$\begin{aligned}\Phi_{\omega^*}(\mathcal{E}_{B_1}(r), \mathcal{E}_{B_2}(r)) &> \Phi_{\omega^*}(\mathcal{E}_{B_2}(r), \mathcal{E}_{B_3}(r)) \\ &> \Phi_{\omega^*}(\mathcal{E}_{B_3}(r), \mathcal{E}_{B_4}(r)) \\ &> \Phi_{\omega^*}(\mathcal{E}_{B_4}(r), \mathcal{E}_{B_5}(r)) \\ &> \Phi_{\omega^*}(\mathcal{E}_{B_5}(r), \mathcal{E}(r+1)).\end{aligned}$$

Then the communication height along the path ω^* between two consecutive regular hexagons with radius $r^* + 1$ is

$$\Phi_{\omega^*}(\mathcal{E}(r^*+1), \mathcal{E}(r^*+2)) = \Phi_{\omega^*}(\mathcal{E}_{B_1}(r^*+1), \mathcal{E}_{B_2}(r^*+1))$$

and, by Proposition 4.3.1, it is achieved in $\mathcal{S}(A_3)$, such that $A_3 := 6(r^*+1)^2 + 2(r^*+1) + 1$. □

Corollary 4.3.6. *Let $\delta \in (0,1)$ such that $\frac{J}{2h} - \frac{1}{2} - \delta$ is integer. The maximum $\Phi_{\omega^*}(\underline{-1}, \underline{+1})$ along the path ω^* is achieved in a configuration with a standard cluster with area A_i^* for $i \in \{1,2\}$ (see Figure 4.8 and 4.9), where*

1. $A_1^* = A_1 = 6{r^*}^2 + 10r^* + 5$, *if* $0 < \delta < \frac{1}{2}$;
2. $A_2^* = A_3 = 6(r^*+1)^2 + 2(r^*+1) + 1$, *if* $\frac{1}{2} < \delta < 1$.

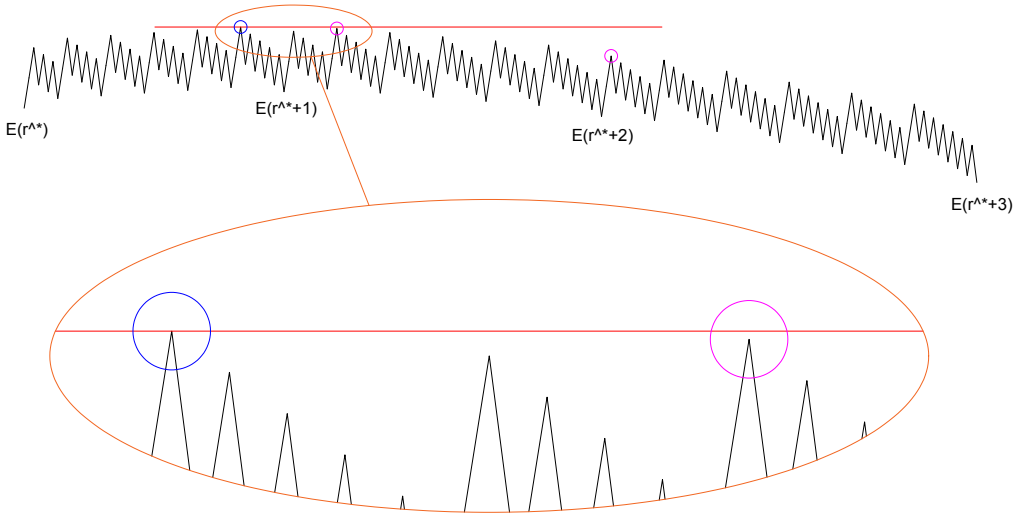

Figure 4.8 An example of the energy landscape between $\mathcal{E}(r^*)$ and $\mathcal{E}(r^*+3)$ for the values of the external magnetic field $h = 5/7$ and the ferromagnetic interaction $J = 7$, thus $\delta \in (0, 1/2)$. We zoom in some part of the energy landscape, in order to compare the saddles and we highlight the maximal saddle in blue.

Proof of Corollary 4.3.6. We compare $\Phi_{\omega^*}(\underline{-1}, \mathcal{E}(r^*+1))$, $\Phi_{\omega^*}(\mathcal{E}(r^*+1), \mathcal{E}(r^*+2))$ and $\Phi_{\omega^*}(\mathcal{E}(r^*+2), \underline{+1})$. By Proposition 4.3.3, we have

$$\begin{aligned}\Phi_{\omega^*}(\underline{-1}, \mathcal{E}(r^*+1)) &= H(\mathcal{S}(A_1)) - H(\underline{-1}) \\ &= -6r^{*2}h + 6r^*J - 10r^*h + 7J - 5h. \end{aligned} \tag{4.3.18}$$

By Proposition 4.3.5, we have

$$\begin{aligned}\Phi_{\omega^*}(\mathcal{E}(r^*+1), \mathcal{E}(r^*+2)) &= H(\mathcal{S}(A_3)) - H(\underline{-1}) \\ &= -6(r^*+1)^2h + 6(r^*+1)J - 2(r^*+1)h + 3J - h. \end{aligned} \tag{4.3.19}$$

By Proposition 4.3.4, we have

$$\begin{aligned}\Phi_{\omega^*}(\mathcal{E}(r^*+2), \underline{+1}) &= H(\mathcal{S}(A_2)) - H(\underline{-1}) \\ &= -6(r^*+2)^2h + 6(r^*+2)J + 2J - 2h. \end{aligned} \tag{4.3.20}$$

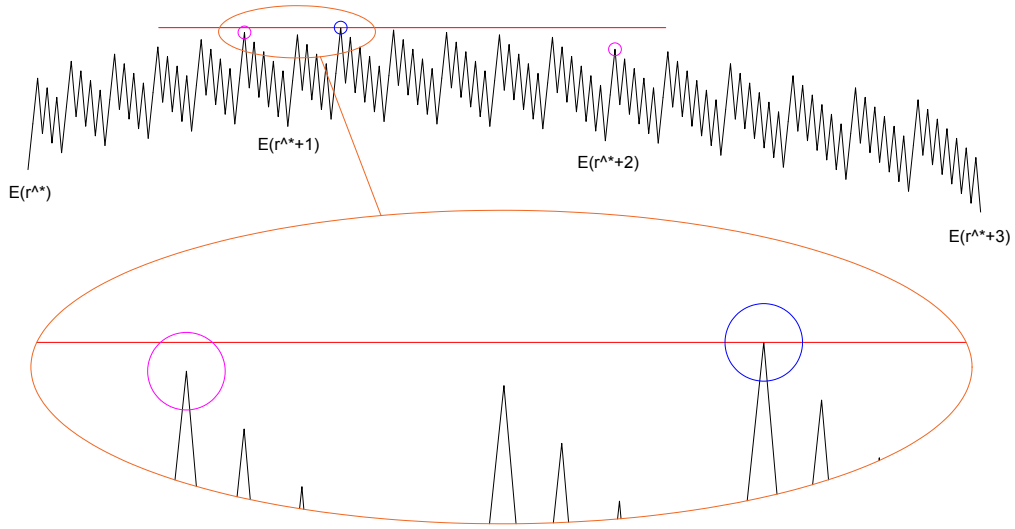

Figure 4.9 An example of the energy landscape between $\mathcal{E}(r^*)$ and $\mathcal{E}(r^*+3)$ for the values of the external magnetic field $h=1$, the ferromagnetic interaction $J=21/2$, thus $\delta \in (1/2,1)$. We zoom in some part of the energy landscape, in order to compare the saddles and we highlight the maximal saddle in blue.

Recalling Definition 3.2.21 and comparing equations (4.3.18), (4.3.19), (4.3.20), we obtain

$$\Phi_{\omega^*}(\underline{-1},\mathcal{E}(r^*+1)) > \Phi_{\omega^*}(\mathcal{E}(r^*+2),\underline{+1}), \tag{4.3.21}$$

$$\Phi_{\omega^*}(\mathcal{E}(r^*+1),\mathcal{E}(r^*+2)) > \Phi_{\omega^*}(\mathcal{E}(r^*+2),\underline{+1}). \tag{4.3.22}$$

Thus $\Phi_{\omega^*}(\mathcal{E}(r^*+2),\underline{+1})$ can not be the maximum. As it can be seen in the figures 4.8 and 4.9 and by standard computations, we have

$$\Phi_{\omega^*}(\underline{-1},\mathcal{E}(r^*+1)) > \Phi_{\omega^*}(\mathcal{E}(r^*+1),\mathcal{E}(r^*+2)), \qquad \text{if } 0<\delta<\frac{1}{2} \tag{4.3.23}$$

$$\Phi_{\omega^*}(\mathcal{E}(r^*+1),\mathcal{E}(r^*+2)) > \Phi_{\omega^*}(\underline{-1},\mathcal{E}(r^*+1)), \qquad \text{if } \frac{1}{2}<\delta<1 \tag{4.3.24}$$

So, if $0<\delta<\frac{1}{2}$, then the maximum $\Phi_{\omega^*}(\underline{-1},\underline{+1}) = \Phi_{\omega^*}(\underline{-1},\mathcal{E}(r^*+1))$ is achieved in a configuration with the standard cluster $\mathcal{S}(6r^{*2}+10r^*+5)$. If $\frac{1}{2}<\delta<1$, then the maximum $\Phi_{\omega^*}(\underline{-1},\underline{+1}) = \Phi_{\omega^*}(\mathcal{E}(r^*+1),\mathcal{E}(r_2^*+1))$ is achieved in a configuration with the standard cluster $\mathcal{S}(6(r^*+1)^2+2(r^*+1)+1)$. Moreover, we observe that if $\delta=\frac{1}{2}$, then the maximum

$\Phi_{\omega^*}(\underline{-1},\underline{+1}) = \Phi_{\omega^*}(\underline{-1},\mathcal{E}(r^*+1)) = \Phi_{\omega^*}(\mathcal{E}(r^*+1),\mathcal{E}(r^*+2))$ is achieved in two configurations with the standard clusters $\mathcal{S}(6{r^*}^2+10r^*+5)$ and $\mathcal{S}(6(r^*+1)^2+2(r^*+1)+1)$. □

4.3.2 Lower bound of maximal stability level

Let $\sigma \in \mathcal{X}$ and denote by $\mathcal{F}(Q)$ the set of ground states in $Q \subseteq \mathcal{X}$, that is

$$\mathcal{F}(Q) := \{y \in Q | \min_{x \in Q} H(x) = H(y)\}. \tag{4.3.25}$$

For n integer, $0 \le n \le |\Lambda|$, we introduce the following set

$$\mathcal{V}_n := \{\sigma \in \mathcal{X} | N^+(\sigma) = n\}, \tag{4.3.26}$$

namely $\mathcal{V}_n$ is the set of configurations with a number of plus spins fixed at the value n. The number of pluses corresponds to the area of the cluster.

Lemma 4.3.7. *Assume that Condition 3.3.1 is satisfied. We have*

1. *Let $\sigma \in \mathcal{V}_{A_i^*}$ for $i \in \{1,2\}$, we have that the set $N^+(\sigma)$ is not a nearest neighbor connected subset of Λ winding around the torus Λ;*
2. *$\mathcal{V}_{A_i^*} \supset \mathcal{S}(A_i^*)$, for $i \in \{1,2\}$;*
3. *$H(\mathcal{F}(\mathcal{V}_{A_i^*})) = H(\underline{-1}) + \Gamma^{Hex}$, for $i \in \{1,2\}$.*

Proof of Lemma 4.3.7. 1. Recalling the two cases of critical area in Corollary 4.3.6 and observing that $r^* < \frac{J}{2h}$, we have

a. Consider $A_1^* = 6{r^*}^2 + 10r^* + 5$ and let $\sigma \in \mathcal{V}_{A_1^*}$

$$\begin{aligned} |N^+(\sigma)| = 6{r^*}^2 + 10r^* + 5 < 6(r^*+1)^2 < 6\Big(\frac{J}{2h}+1\Big)^2 \\ \le 6\Big(\frac{J}{h}\Big)^2 < \Big(\frac{4J}{h}\Big)^2 \end{aligned} \tag{4.3.27}$$

where in the third inequality we have used that, by Condition 3.3.1, $J \ge 2h$. The item follows since, by Condition 3.3.1, we have that $|\Lambda| \ge \left(\frac{4J}{h}\right)^2$.

b. Consider $A_2^* = 6(r^*+1)^2 + 2(r^*+1) + 1$ and let $\sigma \in \mathcal{V}_{A_2^*}$

$$\begin{aligned} |N^+(\sigma)| = 6(r^*+1)^2 + 2(r^*+1) + 1 < 6(r^*+2)^2 < 6\Big(\frac{J}{2h}+2\Big)^2 \\ \le 6\Big(\frac{3J}{2h}\Big)^2 < \Big(\frac{4J}{h}\Big)^2 \end{aligned} \tag{4.3.28}$$

where in the third inequality we have used that, by Condition 3.3.1, $J \geq 2h$. The item follows since, by Condition 3.3.1, we have that $|\Lambda| \geq \left(\frac{4J}{h}\right)^2$.

2. By Equation (4.3.26) and Definition 4.1.16 of standard polyamond $S(A_i^*)$ and the corresponding cluster in $\mathcal{S}(A_i^*)$, we have $\mathcal{V}_{A_i^*} \supset \mathcal{S}(A_i^*)$, for $i \in \{1,2\}$.

3. Let m be the number of site pairs of Λ at lattice distance one, and let $p(C)$ be the perimeter of the cluster C in a configuration $\sigma(C) \in \mathcal{V}_{A_i^*}$. By (3.2.19) we have:

$$\begin{aligned}\min_{\sigma(C)\in\mathcal{V}_{A_i^*}} H(\sigma(C)) &= \min_{\sigma(C)\in\mathcal{V}_{A_i^*}} \left[H(\underline{-1}) + Jp(C) - hA_i^*\right] \\ &= H(\underline{-1}) - hA_i^* + J \min_{\sigma(C)\in\mathcal{V}_{A_i^*}} p(C) \\ &= H(\underline{-1}) - hA_i^* + Jp(S(A_i^*)), \end{aligned} \tag{4.3.29}$$

where in the last equality we use Theorem 4.1.22. Using Remark 4.1.19 and the values of A_i^* given in Corollary 4.3.6, we compute $p(S(A_i^*))$ for $i = 1, 2$, obtaining

$$-hA_i^* + Jp(S(A_i^*)) = \begin{cases} -6r^{*2}h + 6r^*J - 10r^*h + 7J - 5h & \text{for } i = 1 \\ -6(r^*+1)^2h + 6(r^*+1)J - 2(r^*+1)h + 3J - h & \text{for } i = 2 \end{cases}$$

Recalling Definition 3.2.21, we observe that these values correspond to the Definition 3.2.23. Therefore

$$H(\mathcal{F}(\mathcal{V}_{A_i^*})) = H(\underline{-1}) + \Gamma^{Hex}. \tag{4.3.30}$$

□

Lemma 4.3.8. *Assume that Condition 3.3.1 is satisfied. We have that* $\Phi_{\omega^*}(\underline{-1}, \underline{+1}) - H(\underline{-1}) = \Gamma^{Hex}$.

Proof of Lemma 4.3.8. By Corollary 4.3.6, we have two values of A_i^* depending on the two parameters J, h. We analyze two different cases:

· $A_1^* = 6r^{*2} + 10r^* + 5$. By Corollary 4.3.6, we have

$$\Phi_{\omega^*}(\underline{-1}, \underline{+1}) - H(\underline{-1}) = H(\mathcal{S}(A_1^*)) - H(\underline{-1}) = -6r^{*2}h + 6r^*J - 10r^*h + 7J - 5h \tag{4.3.31}$$

and this value corresponds to that of Definition 3.2.23.

· $A_2^* = 6(r^*+1)^2 + 2(r^*+1) + 1$. By Corollary 4.3.6, we have

$$\Phi_{\omega^*}(\underline{-1}, \underline{+1}) - H(\underline{-1}) = H(\mathcal{S}(A_2^*)) - H(\underline{-1})$$

$$= -6(r^*+1)^2h + 6(r^*+1)J - 2(r^*+1)h + 3J - h \tag{4.3.32}$$

and this value corresponds to that of Definition 3.2.23.

□

4.4 Metastable state, gate, transition time and spectral gap

The present Section is devoted to the proofs of those theorems introduced in Section 3.3 concerning respectively: the identification of the metastable state (Theorem 3.3.3), the behavior of the transition time (Theorems 3.3.4, 3.3.5 and 3.3.6), the estimates for the mixing time and the spectral gap (Theorem 3.3.7) and the identification of the critical configurations that exhibit a gate property (Theorem 3.3.8).

Proof of Theorem 3.3.3. In Section 4.3.1 we computed the value of Γ to be Γ^{Hex}, see Definition (3.2.23). There, we also proved that

$$\Phi(\underline{-1}, \underline{+1}) - H(\underline{-1}) = \Gamma^{Hex}. \tag{4.4.1}$$

Thus, the first assumption of [30, Theorem 2.4] is satisfied for the choice of $A = \{\underline{-1}\}$ and $a = \Gamma^{Hex}$. The second assumption of [30, Theorem 2.4] is satisfied thanks to Lemma 4.2.7, since either $\mathcal{X} \setminus \{\underline{-1}, \underline{+1}\} = \emptyset$ or

$$V_\sigma < \Gamma^{Hex} \text{ for all } \sigma \in \mathcal{X} \setminus \{\underline{-1}, \underline{+1}\}. \tag{4.4.2}$$

Finally, by applying [30, Theorem 2.4], we conclude that $\Gamma_m = \Gamma^{Hex}$ and $\mathcal{X}^m = \{\underline{-1}\}$. □

Proof of Theorem 3.3.4. Apply [70, Theorem 4.1] with $\eta_0 = \{\underline{-1}\}$ and $\Gamma = \Gamma^{Hex}$. □

Proof of Theorem 3.3.6. By Theorem 3.3.2, the assumptions of [70, Theorem 4.15] are verified taking $\eta_0 = \{\underline{-1}\}$ and $T'_\beta = e^{\beta(V^*+\epsilon)}$. Then (3.3.5) and (3.3.6) follow from [70, Theorem 4.15]. □

Proof of Theorem 3.3.7. By [77, Lemma 3.24 and Example 3], since $\Gamma_m = \Gamma^{Hex}$ thanks to Theorem 3.3.3, we get the result. □

Proof of Theorem 3.3.8. Recalling the two cases in Corollary 4.3.6, we analyze for $i \in \{1, 2\}$ the elements of $\mathcal{V}_{A_i^*}$ with minimal perimeter (otherwise the configuration has, at least, energy $H(\underline{-1}) + \Gamma^{Hex} + 2h$). By Lemma 5.2.5, we have that every optimal path from $\underline{-1}$ to $\underline{+1}$

intersects the configurations with cluster of area $A_i^* - 2$ and minimal perimeter (otherwise the configuration has, at least, energy $H(\underline{-1}) + \Gamma^{Hex} + 2h$) consisting of the quasi-regular hexagons $E_{B_5}(r^*)$ if $i = 1$ and $E_{B_1}(r^* + 1)$ if $i = 2$. Adding two triangular units to these quasi-regular hexagons, we obtain an element $\sigma(C^*)$ of $\mathcal{V}_{A_i^*}$, see Figure 4.10. $\sigma(C^*)$ is a configuration with a cluster C^* which is composed by a quasi-regular hexagonal cluster and two triangular units attached to it according to one of the following cases:

(1) the two triangular units form an elementary rhombus which is attached to one of the longest sides of the quasi-regular hexagonal cluster, $\tilde{\mathcal{S}}(A_i^*)$;

(2) the two triangular units are attached to one of the longest sides of the quasi-regular hexagonal cluster at triangular lattice distance 2, $\tilde{\mathcal{D}}(A_i^*)$;

(3) the two triangular units are attached to the same side of the quasi-regular hexagonal cluster at triangular lattice distance grater than 2;

(4) the two triangular units are attached to two different sides of the quasi-regular hexagonal cluster;

(5) the two triangular units form an elementary rhombus which is attached to one of the sides, other than the longest, of the quasi-regular hexagonal cluster;

(6) the two triangular units are attached at triangular lattice distance 2 to the same side, other than the longest, of the quasi-regular hexagonal cluster.

We note that in all the above cases C^* has minimal perimeter, since C^* has the same perimeter of a standard hexagon with the same area. In the remainder we analyze the previous cases from a dynamical point of view. We will show that all optimal paths must go through a configuration as in case (1) or (2), whereas optimal paths visiting configurations as those of cases (3), (4), (5), and (6) (*dead ends*) must go back to configurations as those of the first two cases before reaching $\underline{+1}$.
Let ω_0 be the configuration that contains the quasi-regular hexagon of area $A_i^* - 2$. ω_1 is obtained from ω_0 flipping a minus spin adjacent to the cluster and ω_2 is obtained from ω_1 flipping another minus spin to reach a configuration as those of the cases described above. By Table 3.1, we have

$$H(\omega_2) - H(\omega_0) = [H(\omega_2) - H(\omega_1)] + [H(\omega_1) - H(\omega_0)] = 2J - 2h. \tag{4.4.3}$$

We observe that $H(\omega_2) - H(\underline{-1}) = H(\sigma(C^*)) - H(\underline{-1})$ is equal to Γ^{Hex} by Corollary 4.3.6, Lemma 4.3.7 and Lemma 4.3.8. Next, we consider a configuration ω_3 obtained from ω_2 flipping another minus spin. We observe that the perimeter of the cluster decreases only if

we add a plus spin in a site belonging to an internal angle of $\frac{5}{3}\pi$ (of the cluster). This spin flip can be done only in the cases (1) and (2) above, see Figure 4.10. In these two cases, we

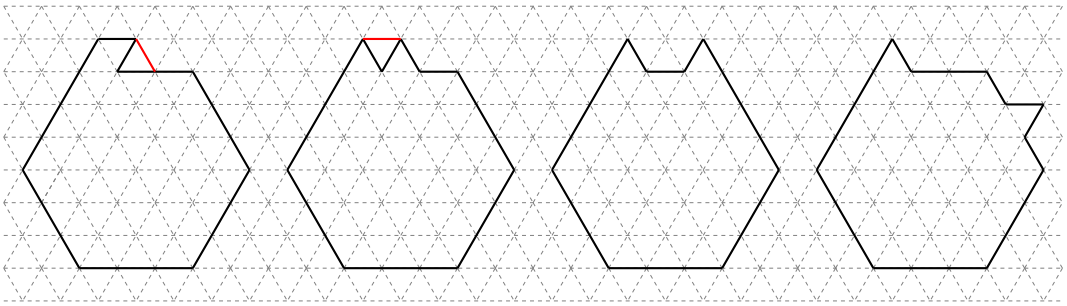

Figure 4.10 From left to right we depict configurations in cases (1),(2),(3),(4) where two triangular units are added to the quasi-regular hexagon. In red the third triangular unit that can be added only in cases (1) and (2) decreasing the energy.

obtain ω_3 adding the third triangular unit to cover the internal angle of $\frac{5}{3}\pi$. Therefore, the energy of the system is lowered by $J+h$, see Table 3.1:

$$H(\omega_3) - H(\omega_2) = -(J+h). \tag{4.4.4}$$

Thus, we have

$$H(\omega_3) - H(\underline{-1}) = [H(\omega_3) - H(\omega_2)] + [H(\omega_2) - H(\underline{-1})] = -(J+h) + \Gamma^{Hex} < \Gamma^{Hex}. \tag{4.4.5}$$

In cases (3) and (4) the cluster does not have an angle of $\frac{5}{3}\pi$. This implies that when we add another triangular unit, the energy of the system can only increase. Thus, we have

$$H(\omega_3) - H(\omega_2) \geq J - h, \tag{4.4.6}$$

and

$$H(\omega_3) - H(\underline{-1}) = [H(\omega_3) - H(\omega_2)] + [H(\omega_2) - H(\underline{-1})] \geq J - h + \Gamma^{Hex} > \Gamma^{Hex}. \tag{4.4.7}$$

To rule out cases (5) and (6), we show that the two triangular units have to be attached along one of the longest sides of the quasi-regular hexagon. In particular, recalling Corollary 4.3.6 and Definition 3.2.24, if $\delta \in (0, \frac{1}{2})$ we must attach the two triangular units along the longest side of $E_{B_5}(r^*)$. Indeed, recalling Definition 4.1.11, the longest side of $E_{B_5}(r^*)$ has length r^*+2 and it has the same length of the larger base of the bar B_6, that has cardinality $2r^*+3$. Any other side s of $E_{B_5}(r^*)$ has length r^*+1, so the bar B with the larger base r^*+1 has cardinality $l = 2r^* - 1$. Suppose by contradiction that there exits a path

$\tilde{\omega} := (\omega_0, \dots, \omega_2, \dots, \omega_l, \dots, \omega_{l+2}, \dots, \omega_{2r^*+3})$ that intersects the configurations described in case (5) and (6) with $\Phi_{\tilde{\omega}} \leq H(\underline{-1}) + \Gamma^{Hex}$. Let $\omega_0 := \mathcal{E}_{B_5}(r^*)$, ω_2 be the configuration with the two triangular units attached along s, $\omega_3, \dots, \omega_l$ be the configurations obtained filling the new bar B and let ω_{l+2} be the configuration obtained from ω_l attaching two triangular units. Recalling (4.2.15) and (3.2.21), we have the following contradiction

$$\begin{aligned} H(\omega_{l+2}) - H(\underline{-1}) &= [H(\omega_{l+2}) - H(\omega_l)] + [H(\omega_l) - H(\omega_2)] + [H(\omega_2) - H(\underline{-1})] \\ &= [2J - 2h] + [-J - (l-2)h] + \Gamma^{Hex} = J - lh + \Gamma^{Hex} = \\ &= J - (2r^* - 1)h + \Gamma^{Hex} = 2h(\delta + 1) + \Gamma^{Hex} > \Gamma^{Hex}. \end{aligned} \tag{4.4.8}$$

Analogously, if $\delta \in (\frac{1}{2}, 1)$ we must attach the two triangular units along one of the longest sides of $E_{B_1}(r^* + 1)$. Indeed, recalling Definition 4.1.11, there exist two longest sides of $E_{B_1}(r^* + 1)$ with length $r^* + 2$ and each of these sides has the same length of the larger base of a bar with cardinality $2(r^* + 1) + 1$. The other sides s of $E_{B_1}(r^* + 1)$ have length $r^* + 1$ and the corresponding bars have cardinality $2(r^* + 1) - 1$. Suppose by contradiction that there exits a path $\tilde{\omega} := (\omega_0, \dots, \omega_2, \dots, \omega_l, \dots, \omega_{l+2}, \dots, \omega_{2r^*+3})$ that intersects the configurations described in case (5) and (6) with $\Phi_{\tilde{\omega}} \leq H(\underline{-1}) + \Gamma^{Hex}$. Let $\omega_0 := \mathcal{E}_{B_1}(r^* + 1)$, ω_2 be the configuration with the two triangular units attached along s, $\omega_3, \dots, \omega_l$ be the configurations obtained filling the new bar B and let ω_{l+2} be the configuration obtained from ω_l attaching two triangular units. Recalling (4.2.15) and (3.2.21), we have the following contradiction

$$\begin{aligned} H(\omega_{l+2}) - H(\underline{-1}) &= [H(\omega_{l+2}) - H(\omega_l)] + [H(\omega_l) - H(\omega_2)] + [H(\omega_2) - H(\underline{-1})] \\ &= [2J - 2h] + [-J - (l-2)h] + \Gamma^{Hex} = J - lh + \Gamma^{Hex} = \\ &= J - (2(r^* + 1) - 1)h + \Gamma^{Hex} = 2h\delta + \Gamma^{Hex} > \Gamma^{Hex}. \end{aligned} \tag{4.4.9}$$

Therefore, the two triangular units have to be attached along one of the longest sides of the quasi-regular hexagon as in case (1) and (2). Recalling Definition 3.2.4 and 3.2.5, let $\mathcal{W}(\underline{-1}, \underline{+1})$ be a minimal gate for the transition from $\underline{-1}$ to $\underline{+1}$. By the previous analysis, we have that all configurations as those in the cases (3), (4), (5), (6) are not in $\mathcal{W}(\underline{-1}, \underline{+1})$. Moreover, observing that configurations as those of case (1) correspond to the configurations $\tilde{\mathcal{S}}(A_i^*)$ and configurations as those of case (2) correspond to the configurations $\tilde{\mathcal{D}}(A_i^*)$ (see Figure 3.3), we conclude $\mathcal{W}(\underline{-1}, \underline{+1}) = \tilde{\mathcal{S}}(A_i^*) \cup \tilde{\mathcal{D}}(A_i^*)$. □

4.4.1 Sharp estimate of the transition time

To prove Theorem 3.3.5, we estimate the *capacity* between $\underline{-1}$ and $\underline{+1}$ which is linked to the mean hitting time of the stable state through the following formula (see [12, Corollary 7.11]):

$$\mathbb{E}_{\underline{-1}}[\tau_{\underline{+1}}] = \frac{1}{\mathrm{CAP}(\underline{-1},\underline{+1})} \sum_{\sigma\in\mathcal{X}} \mu(\sigma) h_{\underline{-1},\underline{+1}}(\sigma). \tag{4.4.10}$$

For a detailed discussion of the strategy outlined below to estimate the capacity refer to [12].

Capacity as the minimum of the Dirichlet form. Let $h : \mathcal{X} \to \mathbb{R}$ and consider the following *Dirichlet form*

$$\mathfrak{E}(h) = \frac{1}{2} \sum_{\sigma,\eta\in\mathcal{X}} \mu(\sigma) p(\sigma,\eta) [h(\sigma) - h(\eta)]^2 \tag{4.4.11}$$

$$= \frac{1}{2} \sum_{\sigma,\eta\in\mathcal{X}} \frac{e^{-\beta H(\sigma)}}{Z} \frac{e^{-\beta[H(\eta)-H(\sigma)]_+}}{|\Lambda|} [h(\sigma) - h(\eta)]^2 \tag{4.4.12}$$

where Z is the partition function $Z := \sum_{\eta\in\mathcal{X}} e^{-\beta H(\eta)}$.
Given two non-empty disjoint sets A, B the *capacity* of the pair A, B is defined by

$$\mathrm{CAP}(A,B) := \min_{\substack{h:\mathcal{X}\to[0,1] \\ h_{|A}=1, h_{|B}=0}} \mathfrak{E}(h). \tag{4.4.13}$$

From this definition it follows immediately that the capacity is a *symmetric* function of the sets A and B.
The right hand side of (4.4.13) has a unique minimizer $h^*_{A,B}$ called *equilibrium potential* of the pair A, B given by

$$h^*_{A,B}(\eta) = \mathbb{P}_\eta(\tau_A < \tau_B), \tag{4.4.14}$$

for any $\eta \notin A \cup B$.

Hence, inserting a general test function h in the Dirichlet form, one obtains an *upper bound* for the capacity. Obviously, the closer h is to the equilibrium potential, the sharper is the bound.

Capacity as the maximum of the expectation of a flow dependent variable. A remarkable property of capacity is that it can be characterized also by another variational principle, useful to obtain *a lower bound*. Think to $\mathcal{X}$ as the vertex set of a graph $(\mathcal{X},\mathcal{L})$ whose edge

set $\mathcal{L}$ consists of all pairs (σ,η) with $\sigma,\eta\in\mathcal{X}$ for which $P(\sigma,\eta)>0$ (see also [75, 15, 10] for further details and applications to several models).

Definition 4.4.1. *Given two non-empty disjoint sets $A,B\subset\mathcal{X}$, a loop-free non-negative unit flow, f, from A to B is a function $f\colon\ E\to[0,\infty)$ such that:*

(a) $(f(e)>0\Longrightarrow f(-e)=0)\ \forall e\in E$.

(b) f *satisfies Kirchoff's law:*

$$\sum_{\sigma'\in\mathcal{X}} f(\sigma,\sigma')=\sum_{\sigma''\in\mathcal{X}} f(\sigma'',\sigma),\qquad \forall\sigma\in\mathcal{X}\backslash(A\cup B). \tag{4.4.15}$$

(c) f *is normalized:*

$$\sum_{\sigma\in A}\sum_{\sigma'\in\mathcal{X}} f(\sigma,\sigma')=1=\sum_{\sigma\in\mathcal{X}}\sum_{\sigma\in B} f(\sigma'',\sigma). \tag{4.4.16}$$

(d) Any path from A to B along edges e such that $f(e)>0$ is self-avoiding.

The space of all loop-free non-negative unit flows from A to B is denoted by $\mathbb{U}_{A,B}$.

A loop-free non-negative unit flow f is naturally associated with a probability measure $\mathbb{P}^f$ on self-avoiding paths, γ. To see this, define $F(\sigma)=\sum_{\sigma'\in\mathcal{X}} f(\sigma,\sigma')$, $\sigma\in\mathcal{X}\setminus B$. Then $\mathbb{P}^f$ is the Markov chain $(\sigma_n)_{n\in\mathbb{N}_0}$ with initial distribution $\mathbb{P}^f(\sigma_0)=F(\sigma_0)\mathbb{1}_A(\sigma_0)$, transition probabilities

$$q^f(\sigma,\sigma')=\frac{f(\sigma,\sigma')}{F(\sigma)},\qquad \sigma\in\mathcal{X}\setminus B, \tag{4.4.17}$$

such that the chain is stopped upon arrival in B. In terms of this probability measure, we have the following proposition:

Proposition 4.4.2 (Berman–Konsowa principle: flow version)**.** *Let $A,B\subset\mathcal{X}$ be two non-empty disjoint sets. Then, with the notation introduced above,*

$$\mathit{CAP}(A,B)=\sup_{f\in\mathbb{U}_{A,B}}\mathbb{E}^f\left(\left[\sum_{e\in\gamma}\frac{f(e_l,e_r)}{\mu(e_l)\,p(e_l,e_r)}\right]^{-1}\right), \tag{4.4.18}$$

where $e=(e_l,e_r)$ and the expectation is with respect to γ.

Thanks to this variational principle, any flow provides a *computable lower bound* for the capacity.

Upper bound. Consider the following sets:

- $\mathcal{X}^* \subset \mathcal{X}$ defined as the subgraph obtained by removing all vertices σ with $\Phi(\underline{-1},\sigma) > \Gamma^{Hex} + H(\underline{-1})$ or with $\Phi(\underline{+1},\sigma) > \Gamma^{Hex} + H(\underline{-1})$ together with all edges incident to these vertices (note that, in particular, $\mathcal{X}^*$ does not contain vertices with $H(\sigma) > \Gamma^{Hex} + H(\underline{-1})$); and all edges incident to these vertices;
- $A := \{\sigma \in \mathcal{X} \,|\, \Phi(\underline{-1},\sigma) < \Gamma^{Hex} + H(\underline{-1})\} \subset \mathcal{X}^*$;
- $B := \{\sigma \in \mathcal{X} \,|\, \Phi(\sigma,\underline{+1}) < \Gamma^{Hex} + H(\underline{-1})\} \subset \mathcal{X}^*$;
- $\mathcal{G}_i \subset \mathcal{X}^*, i = 1,\dots,I$ a collection of sets such that, for all i, $\Phi(\underline{-1},\sigma) = \Phi(\underline{+1},\sigma)$ and $\sigma \sim \eta$ and $\sigma \sim \eta'$, for all $\eta \in A$, $\eta' \in B$ for all $\sigma \in \mathcal{G}_i$;
- $\mathcal{N}_j^A \subset \mathcal{X}^*, j = 1,\dots,J_A$ a collection of sets such that, for all j and for all $\sigma \in \mathcal{N}_j^A$, $\Phi(\underline{-1},\sigma) = \Phi(\underline{+1},\sigma)$ and any path $\omega : \sigma \to \underline{+1}$ must be such that $\omega \cap A \neq \emptyset$;
- $\mathcal{N}_j^B \subset \mathcal{X}^*, j = 1,\dots,J_B$ a collection of sets such that, for all j and for all $\sigma \in \mathcal{N}_j^B$, $\Phi(\underline{+1},\sigma) = \Phi(\underline{-1},\sigma)$ and any path $\omega : \sigma \to \underline{-1}$ must be such that $\omega \cap B \neq \emptyset$.

In words, sets A and B are the cycles with stability level Γ^{Hex} around $\underline{-1}$ and $\underline{+1}$ respectively. Further sets $\mathcal{G}_i$ consists of those configurations belonging to some minimal gate whereas $\mathcal{N}_j^A$ and $\mathcal{N}_j^B$ are *dead ends*, that is, to achieve a transition between $\underline{-1}$ and $\underline{+1}$ starting from one of these sets the dynamics must go back to A or B.
Note that sets $\mathcal{G}_i$, $\mathcal{N}_j^A$ and $\mathcal{N}_j^B$ are not connected via *allowed moves*.
By standard arguments (see [12, Chapter 16]) it is straightforward to check that the sum over $\sigma, \eta \in \mathcal{X}$ in (4.4.11) can be substituted by a sum over $\mathcal{X}^*$ at the price of a factor $[1 + o(1)]$.
To find an upper bound for the capacity we choose a test function h^U defined in the following way:

$$h^U(\sigma) := \begin{cases} 1 & \sigma \in A \cup \{\bigcup_{j=1}^{J_A} \mathcal{N}_j^A\} \\ c_i & \sigma \in \mathcal{G}_i, i = 1,\dots,I \\ 0 & \sigma \in B \cup \{\bigcup_{j=1}^{J_B} \mathcal{N}_j^B\} \end{cases} \tag{4.4.19}$$

It is convenient to call $\mathcal{X}_A := A \cup \{\bigcup_{j=1}^{J_A} \mathcal{N}_j^A\}$, $\mathcal{X}_B := B \cup \{\bigcup_{j=1}^{J_B} \mathcal{N}_j^B\}$.
Consider the case $\delta \in (0, \frac{1}{2})$. By Theorem 3.3.8, it follows that $I = 2$ and $\mathcal{G}_1 \equiv \tilde{\mathcal{S}}(A_1^*)$ and $\mathcal{G}_2 \equiv \tilde{\mathcal{D}}(A_1^*)$. Define $(\mathcal{C}^*)^-$ as the set of configurations where the cluster has the shape of $E_{B_5}(r^*)$ with attached a triangular unit along the longest side and $(\mathcal{C}^*)^+$ as the set of configurations where the cluster has the shape of $E_{B_5}(r^*)$ with an incomplete bar of

cardinality 3 along the longest side. Note that $(\mathcal{C}^*)^- \subset A$ and $(\mathcal{C}^*)^+ \subset B$.

$$\begin{aligned}
\mathrm{CAP}(A,B) &\le (1+o(1))\Big[\min_{c_1,c_2\in[0,1]} \min_{\substack{h:\mathcal{X}^*\to[0,1]\\ h_{|\mathcal{X}_A}=1, h_{|\mathcal{X}_B}=0,\\ h_{|\mathcal{G}_1}=c_1, h_{|\mathcal{G}_2}=c_2}} \frac{1}{2}\sum_{\sigma,\eta\in\mathcal{X}^*}\mu(\sigma)P(\sigma,\eta)[h(\sigma)-h(\eta)]^2\Big] \\
&= (1+o(1))\Big[\min_{c_1,c_2\in[0,1]} \sum_{\substack{\sigma\in\mathcal{X}_A,\\ \eta\in\mathcal{G}_i, i=1,2\\ \sigma\sim\eta}} \frac{e^{-\beta H(\sigma)}}{Z|\Lambda|}(1-c_i)^2 + \sum_{\substack{\sigma\in\mathcal{X}_B,\\ \eta\in\mathcal{G}_i, i=1,2\\ \sigma\sim\eta}} \frac{e^{-\beta H(\sigma)}}{Z|\Lambda|}c_i^2\Big] \\
&= (1+o(1))\Big[\frac{e^{-\beta\Gamma^{Hex}}}{Z|\Lambda|}\min_{c_1,c_2\in[0,1]} \sum_{\substack{\sigma\in(\mathcal{C}^*)^-,\\ \eta\in\mathcal{G}_i, i=1,2}}(1-c_i)^2 + \sum_{\substack{\sigma\in(\mathcal{C}^*)^+,\\ \eta\in\mathcal{G}_i, i=1,2}} c_i^2\Big] \\
&= (1+o(1))\Big[\frac{e^{-\beta\Gamma^{Hex}}}{Z|\Lambda|}\min_{c_1,c_2\in[0,1]} \sum_{\substack{\eta\in\mathcal{G}_i,\\ i=1,2}} |(\mathcal{C}^*)^-\sim\eta|(1-c_i)^2 + \sum_{\substack{\eta\in\mathcal{G}_i,\\ i=1,2}} |(\mathcal{C}^*)^+\sim\eta|c_i^2\Big]
\end{aligned} \tag{4.4.20}$$

where we used the definition of the Gibbs measure (3.2.6) and the expression of the transition probability (3.2.2) and we observed that $\sigma\in\mathcal{X}_A$ and $\eta\in\mathcal{G}_i$ are neighbors only if $\sigma\in(\mathcal{C}^*)^-$ and $\sigma\in\mathcal{X}_B$ and $\eta\in\mathcal{G}_i$ are neighbors only if $\sigma\in(\mathcal{C}^*)^+$.
For all $\eta\in\mathcal{G}_1$ we have that $|(\mathcal{C}^*)^-\sim\eta|=1$, whereas for all $\eta\in\mathcal{G}_2$ we have that $|(\mathcal{C}^*)^-\sim\eta|=2$. Moreover, we have $|(\mathcal{C}^*)^+\sim\eta|=1$ for all $\eta\in\mathcal{G}_1\cup\mathcal{G}_2$. Therefore, we obtain

$$\begin{aligned}
\mathrm{CAP}(A,B) &\le (1+o(1))\Big[\frac{e^{-\beta\Gamma^{Hex}}}{Z|\Lambda|}\min_{c_1,c_2\in[0,1]}\sum_{\eta\in\mathcal{G}_1}(1-c_1)^2+c_1^2+\sum_{\eta\in\mathcal{G}_2}2(1-c_2)^2+c_2^2\Big] \\
&\le (1+o(1))\Big[\frac{e^{-\beta\Gamma^{Hex}}}{Z|\Lambda|}\min_{c_1,c_2\in[0,1]}|\mathcal{G}_1|(2c_1^2-2c_1+1)+|\mathcal{G}_2|(3c_2^2-4c_2+2)\Big]
\end{aligned} \tag{4.4.21}$$

The functions $f(c_1):=2c_1^2-2c_1+1$ and $f(c_2):=3c_2^2-4c_2+2$ are minimized respectively at $c_1=\frac{1}{2}$ and $c_2=\frac{2}{3}$. Moreover, $|\mathcal{G}_1|=6(l-1)|\Lambda|$ and $|\mathcal{G}_2|=3(l-1)|\Lambda|$ where l is the length of the longest side of $E_{B_5}(r^*)$, i.e., $l=r^*+2$. Finally, we have

$$\begin{aligned}
\mathrm{CAP}(A,B) &\le (1+o(1))\Big[\frac{e^{-\beta\Gamma^{Hex}}}{Z|\Lambda|}(6(l-1)|\Lambda|\frac{1}{2}+3(l-1)|\Lambda|\frac{2}{3})\Big] \\
&= (1+o(1))\Big[5(l-1)\frac{e^{-\beta\Gamma^{Hex}}}{Z}\Big].
\end{aligned} \tag{4.4.22}$$

The case $\delta \in (\frac{1}{2}, 1)$ can be treated likewise with the following modifications: the critical area A_1^* becomes A_2^*; $E_{B_5}(r^*)$ is replaced by $E_{B_1}(r^*+1)$; $|\mathcal{G}_1| = 12(l-1)|\Lambda|$ and $|\mathcal{G}_2| = 6(l-1)|\Lambda|$ where l is the length of the longest side of $E_{B_1}(r^*+1)$, i.e., again $l = r^*+2$. We these changes we get

$$\text{CAP}(A, B) \leq (1+o(1))\Big[10(l-1)\frac{e^{-\beta\Gamma^{Hex}}}{Z}\Big]. \tag{4.4.23}$$

Lower bound. For the symmetry of the capacity, it is possible to consider a loop-free unitary flow from $\underline{-1}$ to $\underline{+1}$ to estimate $\text{CAP}(\underline{-1}, \underline{+1}) = \text{CAP}(\underline{+1}, \underline{-1})$.
If $\delta \in (0, 1/2)$, choose the unitary flow f as follows. Distribute the mass of the test flow equally among a suitable subset of optimal paths. Consider a configuration $\sigma \in (\mathcal{C}^*)^+$, consisting of a cluster with the shape of a quasi-regular hexagon $E_{B_5}(r^*)$ with an incomplete bar of cardinality 3 attached along its longest side.
Observe that the triangular units in the incomplete bar of σ are of two types: the first type consists of those triangular units at lattice distance one from $E_{B_5}(r^*)$ (the two extreme of the incomplete bar) whereas the second type consists of those triangular units at lattice distance two from $E_{B_5}(r^*)$ (the central triangular unit of the incomplete bar). Each $\sigma \in (\mathcal{C}^*)^+$ can be univocally identified by the coordinate x of the triangular unit of second type of the incomplete bar. Further, for each $\sigma \in (\mathcal{C}^*)^+$ with incomplete bar centered at x, it is possible to define a (optimal) path in a deterministic way from σ to $\underline{+1}$. In this way it is possible to find a bijection between the set of configurations $(\mathcal{C}^*)^+$ and the set of paths from σ to $\underline{+1}$ for $\sigma \in (\mathcal{C}^*)^+$. Call γ_x the time reversal of the deterministic path from the configuration σ with incomplete bar centered at x to $\underline{+1}$. Note that from $(\mathcal{C}^*)^+$ the path γ_x can be extended towards $\underline{-1}$ either by flipping one of the two spins of the first type (with probability $1/a$), or by flipping the spin of the second type (with probability $1/b$). If one of the two spins of the first type is flipped, creating an elementary rhombus, then the path is extended deterministically by flipping the remaining spins from plus to minus starting from the spin belonging to the second type. Otherwise, if the flipped spin is that of the second type, then the path can be extended by flipping one of the spins of the first type (with probability $1/2$) and then proceeding deterministically to flip the remaining spins from plus to minus.

Let K be the number of negative spins in configurations in $\tilde{\mathcal{S}}(A_1^*) \cup \tilde{\mathcal{D}}(A_1^*)$, set $\nu_0 := \frac{1}{|\Lambda|}$ and consider the unitary flow from $\underline{+1}$ to $\underline{-1}$, defined as follows

$$f(\sigma', \sigma'') = \begin{cases} \nu_0 & \text{if } \sigma' = \gamma_x(k),\, \sigma'' = \gamma_x(k+1) \\ & \text{for some } x \in \Lambda, 0 \le k \le K-1 \\ \frac{\nu_0}{a} & \text{if } \sigma' = \gamma_x(K-1),\, \sigma'' = \gamma_x^i(K) \in \tilde{\mathcal{S}}(A_1^*) \\ & \text{for some } x \in \Lambda \\ \frac{\nu_0}{b} & \text{if } \sigma' = \gamma_x(K-1),\, \sigma'' = \gamma_x^i(K) \in \tilde{\mathcal{D}}(A_1^*) \\ & \text{for some } x \in \Lambda \\ \frac{\nu_0}{a} & \text{if } \sigma' = \gamma_x(K) \in \tilde{\mathcal{S}}(A_1^*),\, \sigma'' = \gamma_x^i(K+1) \\ & \text{for some } x \in \Lambda \\ \frac{\nu_0}{2b} & \text{if } \sigma' = \gamma_x(K) \in \tilde{\mathcal{D}}(A_1^*),\, \sigma'' = \gamma_x^i(K+1) \\ & \text{for some } x \in \Lambda \\ \nu_0 & \text{if } \sigma' = \gamma_x(k),\, \sigma'' = \gamma_x(k+1) \\ & \text{for some } x \in \Lambda,\, K+1 \le k \le |\Lambda|-1 \\ 0, & \text{otherwise.} \end{cases} \tag{4.4.24}$$

where $\gamma_x(k)$ is the k-th configuration visited by the path γ_x and a and b must be chosen so that the flow is unitary.
The flow described above can be used to assign to each path $\gamma = (\gamma(0), ..., \gamma(|\Lambda|))$ with $\gamma(0) = \underline{+1}$ and $\gamma(|\Lambda|) = \underline{-1}$ a probability $\mathbb{P}(\gamma)$ defined as

$$\mathbb{P}(\gamma) := \mathbb{P}^f(\mathbb{X} = \gamma) = \frac{\prod_{i=1}^{|\Lambda|} f(\gamma(i-1), \gamma(i))}{\prod_{i=1}^{|\Lambda|} F(\gamma(i-1))}. \tag{4.4.25}$$

Non null probability paths $\underline{+1} \to \underline{-1}$ can be partitioned into two sets $\mathcal{I}_{\tilde{S}}$ and $\mathcal{I}_{\tilde{D}}$. $\mathcal{I}_{\tilde{S}}$ contains those paths such that $\gamma(K)$ is in $\tilde{\mathcal{S}}(A_1^*)$ whereas $\mathcal{I}_{\tilde{S}}$ contains those paths such that $\gamma(K)$ is in $\tilde{\mathcal{D}}(A_1^*)$. Further let $N_{\tilde{S}}$ and $N_{\tilde{D}}$ the cardinality of $\mathcal{I}_{\tilde{S}}$ and $\mathcal{I}_{\tilde{D}}$ respectively.
Equation (4.4.25) yields

$$\mathbb{P}(\gamma) = f(\gamma(K-1), \gamma(K)), \tag{4.4.26}$$

so that for $\gamma \in \mathcal{I}_{\tilde{S}}$

$$\mathbb{P}(\mathcal{I}_{\tilde{S}}) = N_{\tilde{S}} f(\gamma(K-1), \gamma(K) \in \tilde{\mathcal{S}}(A_1^*)). \tag{4.4.27}$$

and for $\gamma \in \mathcal{I}_{\tilde{D}}$

$$\mathbb{P}(\mathcal{I}_{\tilde{D}}) = N_{\tilde{D}}(\lambda-2) f(\gamma(K-1), \gamma(K) \in \tilde{\mathcal{D}}(A_1^*)). \tag{4.4.28}$$

By Proposition 4.4.2 and by the choice of the flow (4.4.24), we have

$$\begin{aligned}
\text{CAP}(\underline{+1}, \underline{-1}) &\geq \sum_{\gamma \in \mathcal{I}_{\tilde{S}} \cup \mathcal{I}_{\tilde{D}}} \mathbb{P}(\gamma) \left[\sum_{k=0}^{|\Lambda|-1} \frac{f(\gamma(k), \gamma(k+1))}{\mu(\gamma(k)) p(\gamma(k), \gamma(k+1))} \right]^{-1} \\
&\geq \mathbb{P}(\gamma \in \mathcal{I}_{\tilde{S}}) \frac{e^{-\beta \Gamma^{Hex}}}{Z|\Lambda|} \frac{1}{f(\gamma(K-1), \gamma(K) \in \tilde{\mathcal{S}}(A_1^*))} (1+o(1)) \\
&+ \mathbb{P}(\gamma \in \mathcal{I}_{\tilde{D}}) \frac{e^{-\beta \Gamma^{Hex}}}{Z|\Lambda|} \frac{1}{f(\gamma(K-1), \gamma(K) \in \tilde{\mathcal{D}}(A_1^*))} (1+o(1)) \\
&\geq \frac{e^{-\beta \Gamma^{Hex}}}{Z|\Lambda|} \left[\frac{N_R}{\frac{2}{a}+\frac{1}{b}} + \frac{N_T}{\frac{2}{a}+\frac{1}{b}} \right] (1+o(1))
\end{aligned} \tag{4.4.29}$$

The number of the paths in both $\mathcal{I}_{\tilde{S}}$ and $\mathcal{I}_{\tilde{D}}$ is equal to $6|\Lambda|(l-1)$. Hence, it follows

$$\text{CAP}(\underline{+1}, \underline{-1}) \geq \frac{e^{-\beta \Gamma^{Hex}}}{Z} \frac{12ab(l-1)}{2b+a} (1+o(1)). \tag{4.4.30}$$

Choosing $a = 1$ and $b = 5/2$, yields

$$\text{CAP}(\underline{+1}, \underline{-1}) \geq \frac{e^{-\beta \Gamma^{Hex}}}{Z} 5(l-1)(1+o(1)). \tag{4.4.31}$$

that matches the upper bound (4.4.22).
If $\delta \in (1/2, 1)$, it is possible to construct a flow similar to the one described above. In this case, the incomplete bar of length 3 can be attached on one of the two longest sides of $E_{B_1}(r^*+1)$. The same arguments allow to write

$$\text{CAP}(\underline{+1}, \underline{-1}) \geq \frac{e^{-\beta \Gamma^{Hex}}}{Z} \frac{24ab(l-1)}{2b+a} (1+o(1)). \tag{4.4.32}$$

where the factor 24 instead of 12 is due to the fact that the incomplete bar can be attached to either of the longest sides of the quasi-regular hexagons and the number of paths from $\underline{+1}$ to $\underline{-1}$ is, therefore, doubled. Choosing again $a = 1$ and $b = 5/2$, we have

$$\text{CAP}(\underline{+1}, \underline{-1}) \geq \frac{e^{-\beta \Gamma^{Hex}}}{Z} 10(l-1)(1+o(1)). \tag{4.4.33}$$

that matches the upper bound (4.4.23).

5 Polyiamonds with minimum edge-perimeter and maximal area

The problem of finding the shape minimizing the perimeter of a polyiamond given its area is relevant in a handful of fields and a vast literature on the topic has flourished in several communities (see for instance [50, 54, 73, 38, 85]). However, depending on the application, different definitions of perimeter may be taken into account. For instance, one may wish to consider, for the perimeter of a polyiamond, the number of neighboring vertices or, as we do above, the number of boundary edges. The problem of minimizing the perimeter might, therefore, be different.
In this section we leverage on the results in [50] where the properties of the *site-perimeter* of polyiamonds are studied. More formally,

Definition 5.0.1. *Given a polyiamond P, its site-perimeter s(P) is the number of empty triangular units sharing at least one edge with the polyiamond.*

In [50] both polyiamonds with fixed site-perimeter and maximal area and polyiamonds with fixed area and minimal site-perimeter are identified. In particular, they prove that those polyiamonds referred to as quasi-regular hexagons in the previous Sections have both maximal area for fixed site-perimeter and minimal site-perimeter for fixed area. Moreover, they show that those polyiamonds that here we called *standard* have minimal site-perimeter and provide an explicit formula for its value. Here we will show, on one hand, that quasi-regular hexagons are the *only* polyiamonds of maximal area for fixed site-perimeter and, on the other hand, that standard polyiamonds not only minimize the site-perimeter for fixed area, but they also minimize the edge-perimeter establishing Theorem 4.1.22. Moreover, we show that quasi-regular hexagons maximize the area for fixed edge-perimeter as well. In the remainder of this Section we first recall the definitions and the results of [50] (see

Subsection 5.1) and then we show how these results can be extended as mentioned above (see Subsection 5.1.1). Finally we give the proof of Theorem 4.1.22.

5.1 Site-perimeter of polyiamonds: known results

In [50] hexagons, living on the triangular lattice, are identified starting from an equilateral triangle and "cutting the corners" (see [50, Definition 2.1]). In particular hexagons are parametrized by quadruples (a, b, c, d) and $T^d_{a,b,c}$ denotes a hexagon obtained from an equilateral triangle with side length d and removing from its corners the equilateral triangles of side lengths a, b and c (see Figure 5.2). This parametrization allows to express in a straightforward manner the area and the site-perimeter of any hexagon as follows:

$$\begin{aligned} s(T^d_{a,b,c}) &= 3d - a - b - c \\ \|T^d_{a,b,c}\| &= d^2 - a^2 - b^2 - c^2 \end{aligned} \tag{5.1.1}$$

Note that degenerate hexagons are included in this definition. If this is the case the "hexagon" may, indeed, be a triangle, a quadrilateral or a pentagon (see Figure 5.1).

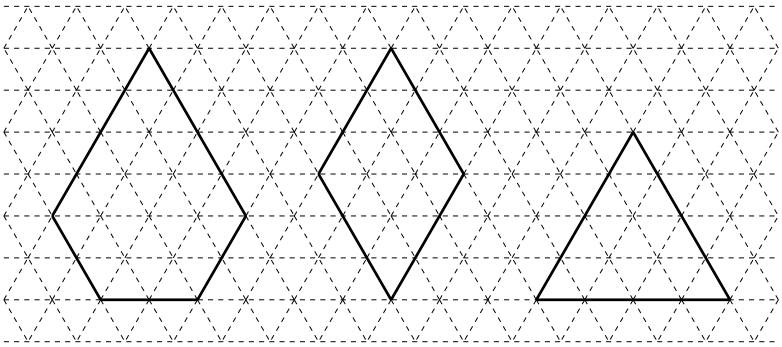

Figure 5.1 Examples of degenerate hexagons.

Remark 5.1.1. *In general there exist two possible parametrizations identifying the same hexagon.*

In [50, Proposition 3.4] the shape of those polyiamonds maximizing the area for a given site-perimeter is identified. In the following we show that these shapes are those that in this paper we called quasi-regular hexagons.
Order the set of quasi-regular hexagons by increasing values of their area and note that going from one quasi-regular hexagon to the next in this sequence, the perimeter (both edge and site) increases by exactly one unit. Consequently each quasi-regular hexagon can be

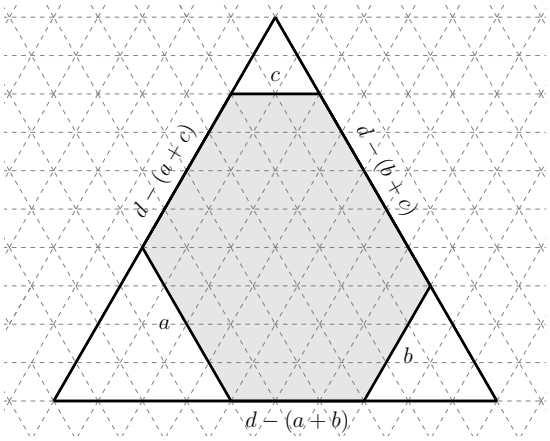

Figure 5.2 The side lengths of the hexagon obtained from the equilateral triangle of side length d cutting the equilateral triangles of side lengths a, b and c.

identified univocally by its perimeter. Write all possible values of the site-perimeter of a quasi-regular hexagon as

$$s = 6r + i, \qquad r \geq 1, \qquad i \in \{0, 1, 2, 3, 4, 5\}. \tag{5.1.2}$$

Note that here $s(P)$ denotes the site-perimeter of polyiamond P whereas in [50] the same notation identifies the area of P.
Since $s = 6r$ is the site-perimeter of the regular hexagon of radius/side length r, $s = 6r + i$ is the site-perimeter of the quasi-regular hexagon obtained by adding i bars to the regular hexagon of radius r.
By constructing, explicitly, the shapes referred to in [50, Proposition 3.4], it is straightforward to check that these are the quasi-regular hexagons (see Fig. 5.3). In particular there is the following correspondence between the notation used in [50] and the notation used in the previous Sections to denote quasi-regular hexagons

$$\begin{aligned}
T^{\lfloor \frac{s}{2} \rfloor}_{r,r,r}, i = 0 \quad &\text{corresponds to} \quad E(r), \\
T^{\lfloor \frac{s}{2} \rfloor}_{r-1,r,r}, i = 1 \quad &\text{corresponds to} \quad E_{B_1}(r), \\
T^{\lfloor \frac{s}{2} \rfloor}_{r,r,r+1}, i = 2 \quad &\text{corresponds to} \quad E_{B_2}(r), \\
T^{\lfloor \frac{s}{2} \rfloor}_{r,r,r}, i = 3 \quad &\text{corresponds to} \quad E_{B_3}(r), \\
T^{\lfloor \frac{s}{2} \rfloor}_{r,r+1,r+1}, i = 4 \quad &\text{corresponds to} \quad E_{B_4}(r), \\
T^{\lfloor \frac{s}{2} \rfloor}_{r,r,r+1}, i = 5 \quad &\text{corresponds to} \quad E_{B_5}(r).
\end{aligned} \tag{5.1.3}$$

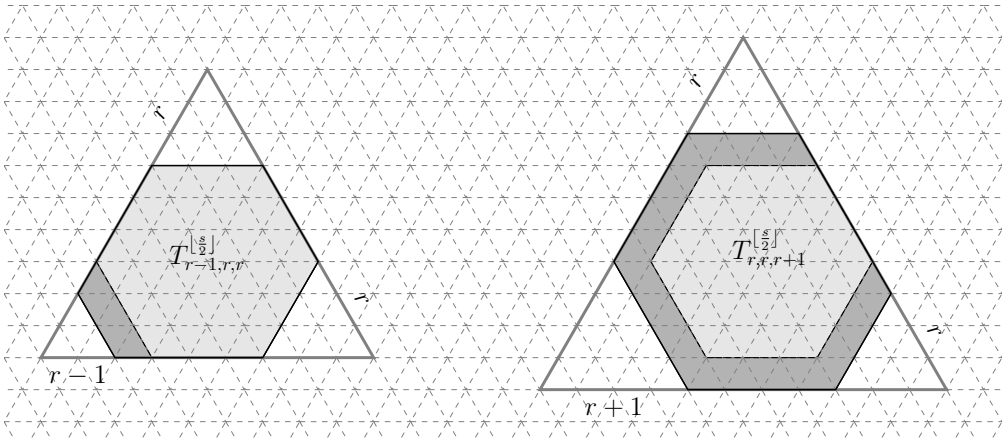

Figure 5.3 Two examples of the correspondences in (5.1.3). On the left the correspondence between $T^{\lfloor \frac{s}{2} \rfloor}_{r-1,r,r}$ and $E_{B_1}(r)$. On the right the correspondence between $T^{\lfloor \frac{s}{2} \rfloor}_{r,r,r+1}$ and $E_{B_5}(r)$.

Since there is only a quasi-regular hexagon for each value of s, the Proposition amounts to saying that quasi-regular hexagons maximize the area for a given site-perimeter.
As a consequence, [50, Proposition 4.5] states, in our notation, that the minimal site-perimeter for a polyiamond of area A is the site-perimeter of the smallest quasi-regular hexagon of area at least A.

5.1.1 Site-perimeter of polyiamonds: further results

We extend the result of [50, Proposition 3.4] as follows

Proposition 5.1.2. *Quasi-regular hexagons are the unique polyiamonds of maximal area for fixed site-perimeter.*

Proof. Let $s = 6r + i$ be the site-perimeter of a hexagon $T^d_{a,b,c}$ and consider the function $M = s^2 - 6\|T^d_{a,b,c}\|$. If the site-perimeter is fixed, polyiamonds of maximal area are those that minimize M. By (5.1.1) one can compute M in terms of the parameters identifying the hexagon as $M = 3(d-a-b-c)^2 + 2((a-b)^2 + (a-c)^2 + (b-c)^2)$. In [50] it is shown that the minimum of M depends on the value of the remainder i (modulo 6). Calling $M^\star$ the minimum of M, by the proof of [50, Proposition 3.4] we know that

$$M^\star = \begin{cases} 0 & \text{if } i \in \{0\} \\ 3 & \text{if } i \in \{3\} \\ 4 & \text{if } i \in \{2,4\} \\ 7 & \text{if } i \in \{1,5\} \end{cases} \tag{5.1.4}$$

Call $\alpha = d-a-b-c$ and $\beta = (a-b)^2+(a-c)^2+(b-c)^2$. This implies that M can be written as $M = 3\alpha^2+2\beta$ where α and β are integers. Therefore for $i \in \{0,\ldots,5\}$ there is a unique pair of integers (α^2,β) for which the optimal value of M is attained.
If $i=0$, we see from (5.1.4) that $M^\star = 0$ and, hence, it must be $\alpha = 0$ and $\beta = 0$. This, in turn, implies $a=b=c=v$ for some positive integer value v and $d = a+b+c = 3v$. Hence, recalling that $s = 3d-a-b-c$, we must have $0 = \alpha = d-a-b-c = \frac{1}{3}(s-2(a+b+c)) = \frac{1}{3}(s-6v)$. The unique solution of this equation is $v = r$. This yields $d = 3r = \frac{s}{2} \in \mathbb{N}$ and, therefore, the unique quadruple (a,b,c,d) parametrizing a hexagon for which the minimum of M is attained is $(r,r,r,\frac{s}{2})$.
If $i=1$, from (5.1.4) we have $M^\star = 7$ amounting to saying $\alpha^2 = 1$ and $\beta = 2$. Assuming, without loss of generality, $a \le b \le c$, the latter implies that, for some v it must be either $a = v-1; b = c = v$ or $a = b = v-1; c = v$.
Consider, first, the case, $a = v-1; b = c = v$. We have $\alpha = \frac{1}{3}(s-2(a+b+c)) = \frac{1}{3}(6(r-v)+3)$. If $\alpha = +1$, then the solution of the equation is $v = r$ implying $d = 3r = \lfloor \frac{s}{2} \rfloor$. This solution corresponds to the quadruple $(r-1,r,r,\lfloor \frac{s}{2} \rfloor)$. If $\alpha = -1$, then it must be $v = r+1$ and the associated quadruple is $(r,r+1,r+1,\lceil \frac{s}{2} \rceil)$.
If we consider the case $a = b = v-1; c = v$, then $\alpha = \frac{1}{3}(6(r-v)+5)$. However no acceptable quadruple can be obtained in this case since α must be integer and $\frac{1}{3}(6(r-v)+5) \notin \mathbb{N}$.
Arguing in the same manner for $i = 2,3,4,5$ it is possible to determine all quadruples for which the minimum of M is attained. In particular we have:

if $i=2$ the only quadruple minimizing M is $(r,r,r+1,\frac{s}{2})$;
if $i=3$ the two quadruples minimizing M are $(r,r,r,\lfloor \frac{s}{2} \rfloor)$ and $(r+1,r+1,r+1,\lceil \frac{s}{2} \rceil)$;
if $i=4$, M is minimized only by the quadruple $(r,r+1,r+1,\frac{s}{2})$;
if $i=5$ the two quadruples minimizing M are $(r,r,r+1,\lfloor \frac{s}{2} \rfloor)$ and $(r+1,r+1,r+2,\lceil \frac{s}{2} \rceil)$.

Note that, for i even, there is only one quadruple minimizing M and, therefore, in these cases the hexagon maximizing the area for fixed site-perimeter is obviously unique.
On the other hand, for i odd, there are two quadruples minimizing M. However, these two quadruples identify the same hexagon. To see this we argue as follows. The parameters a,b and c are the lengths of three non consecutive sides of the hexagon. Therefore there is another parametrization $T^{d'}_{a',b',c'}$, in principle different from $T^{d}_{a,b,c}$, for a hexagon with site-perimeter s, given in terms of the lengths of the other three non consecutive sides for a suitable value d'. Since i is odd, $\frac{s}{2} \notin \mathbb{N}$ thus it is not possible to have $a = a'$, $b = b'$ and $c = c'$ because $s = a+a'+b+b'+c+c'$ would be even. Thus for each hexagon with odd site-perimeter there are, indeed, two quadruples. Since for i odd the minimum of M is always attained

only in two quadruples they must identify the same hexagon (if the two quadruples identify different hexagons, then there should exist four quadruples minimizing M). □

5.2 Proof of Theorem 4.1.22

Edge-perimeter and site-perimeter are closely related. It is straightforward to check that $s(P) \leq p(P)$. Indeed, as shown in Figure 5.4, an empty triangular unit, giving unitary contribution to the site-perimeter, may share 1, 2 or 3 edges with the polyiamond each giving a unitary contribution to the edge-perimeter. More precisely the following proposition holds:

Proposition 5.2.1. *Let $\nu(P)$ be the number of $\frac{5}{3}\pi$ internal angles that are not part of an elementary hole and $e(P)$ the number of elementary holes in P. Then*

$$p(P) = s(P) + \nu(P) + 2e(P) \tag{5.2.1}$$

Proposition 5.2.1 immediately implies

Proposition 5.2.2. *If $s(P)$ is minimal (that is there is no polyiamond with the same area and a smaller site-perimeter) and $p(P) = s(P)$, then $p(P)$ is minimal as well (that is there is no polyiamond with the same area and a smaller edge-perimeter).*

The proof of this statement is straightforward, indeed, call $\alpha(P) = \nu(P) + 2e(P)$ and note that $\alpha(P) \geq 0$. Let $\bar{P}$ be a minimizer of s such that $\alpha(\bar{P}) = 0$ (it, obviously, exists). Assume there is a polyiamond $\tilde{P}$ such that $p(\tilde{P}) < p(\bar{P})$. This is equivalent to saying $s(\tilde{P}) + \alpha(\tilde{P}) < s(\bar{P}) + \alpha(\bar{P}) = s(\bar{P})$ and this is clearly a contradiction since $\alpha \geq 0$.

Proof of Proposition 5.2.1. For the proof we refer to Figure 5.4. Note that in case (c) the contribution of the empty triangular unit to the site-perimeter of the polyiamond is the same (one unit) that the shared edge gives to the edge-perimeter. In case (a) the three edges on the boundary of the polyiamond are adjacent to the same empty triangular unit. Therefore, for each elementary hole the edge-perimeter of the polyiamond increases by two extra units with respect to the site-perimeter. Finally, in case (b) the two edges on the boundary are adjacent to the same empty triangular unit. Hence, for each $\frac{5}{3}\pi$ angle the edge-perimeter of the polyiamond increases by one extra unit with respect to the site-perimeter. □

We have already seen that all quasi-regular hexagons have minimal site-perimeter for fixed area and maximal area for fixed site perimeter. Thanks to Proposition 5.2.1 it is possible to show that these two properties holds also for the edge-perimeter. Moreover, we show that quasi-regular hexagons are the unique polyimonds of maximal area for fixed edge-perimeter. Denote by $\mathcal{Q}$ the set of all quasi-regular hexagons. More formally we have:

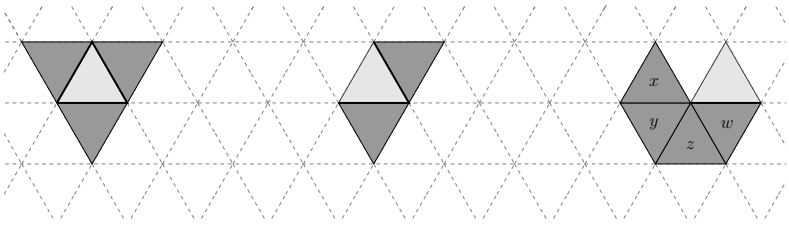

(a) **(b)** **(c)**

Figure 5.4 The three possible cases for the number of edges shared by an empty triangular unit and the polyiamond. If the number of shared edges is 3 (case (a)) the empty triangular unit is an elementary hole of the polyiamond. The empty triangular unit shares 2 edges with the polyiamond if and only if the two edges identify a $\frac{5}{3}\pi$ internal angle (case (b)). The case where the empty triangular unit and the polyiamond share a single edge is represented in (c). Note that this case may correspond to different values of the internal angle (that is an angle of $\frac{\pi}{3}$ when the polyiamond contains only the triangular unit *w*; an angle of $\frac{2\pi}{3}$ when the polyiamond contains the triangular units *w*, *z*; an angle π when the polyiamond contains the triangular units *w*, *z*, *y*; an angle of $\frac{4\pi}{3}$ when the polyiamond contains the triangular units *w*, *z*, *y* and *x*).

Lemma 5.2.3. *Let E be a quasi-regular hexagon and $P \notin \mathcal{Q}$ a polyiamond such that $||P|| \geq ||E||$. Then $p(P) > p(E)$ and $s(P) > s(E)$.*

Proof of Lemma 5.2.3. We give the proof for $p(P)$. The proof for $s(P)$ is analogous. Let A be the area of the quasi-regular hexagon of edge-perimeter $p^\star$. We prove the equivalent statement: if $p(P) \leq p^\star$, then $\|P\| < A$ for all $P \notin \mathcal{Q}$.
Denote by $s(P)$ the site-perimeter of P and by $A^{\max}(s)$ the largest possible value of the area for a polyiamond of site-perimeter s. We consider the cases $p(P) < p^\star$ and $p(P) = p^\star$ separately.
Let $p(P) < p^\star$. By Proposition 5.2.1, we have $s(P) \leq p(P) < p^\star$. Then $\|P\| \leq A^{\max}(s(P)) < A^{\max}(p^\star) = A$. The last inequality follows from [**FuSie**] stating that $A^{\max}(\cdot)$ is a strictly increasing function.
Let $p(P) = p^\star$, then $s(P) \leq p^\star$ and $\|P\| \leq A^{\max}(s(P)) \leq A^{\max}(p^\star) = A$ for all $P \notin \mathcal{Q}$ by Lemma 5.1.2 and, again, by noting that $A^{\max}(\cdot)$ is increasing. □

The previous results serve as building blocks to show that, fixing the area, also all standard polyiamonds, other than quasi-regular hexagons, have minimal edge-perimeter establishing Theorem 4.1.22.

Proof of Theorem 4.1.22. Let E be a quasi-regular hexagon of edge-perimeter $p(E)$ and area $\|E\|$. Consider, at first, the standard polyiamonds obtained by adding an incomplete bar with an odd number of triangular units to E. These polyiamonds have edge-perimeter $p(E)+1$ and area strictly larger than $\|E\|$ and, therefore, their edge-perimeter is minimal

by Lemma 5.2.3. It remains to show that also standard polyiamonds obtained by adding an incomplete bar with an even number of triangular units to a quasi-regular hexagon have minimal edge-perimeter.

Write $A = A_0 + \ell$ where A_0 is the area of the greatest quasi-regular hexagon R'_A containing, at most, A_0 triangular units (that can be obtained via Algorithm 4.1.18) and $\ell \geq 2$ is the (even) number of triangular units in the incomplete bar.

Let $p^\star = p(R'_A)$ and consider a standard polyiamond $\tilde{P}$ with area A and perimeter $p(\tilde{P}) = p^\star + 2$. We will show that there is no polyiamond P such that $\|P\| = A$ and $p(P) < p(\tilde{P}) = p^\star + 2$. If a P as such existed, then it would be immediate to check that it could not have neither $\frac{5}{3}\pi$ internal angles nor elementary holes. Indeed, the polyiamond P_+ obtained by adding a triangular unit in the "corner" or in the elementary hole would have perimeter $p(P_+) < p^\star + 1$ and area $\|P_+\| = A_0 + \ell + 1 > A_0$. This would contradict Lemma 5.2.3. Similarly, it can be seen that P can not have "protuberances" ($\frac{1}{3}\pi$ internal angles). Indeed, the polyiamond P_- obtained from P by removing the protuberance would have perimeter $p(P_-) < p^\star + 1$ and area $\|P_-\| = A_0 + \ell - 1 > A_0$, since $\ell \geq 2$ and, also in this case, Lemma 5.2.3 would be contradicted. Therefore P can only have $\frac{2}{3}\pi$ and $\frac{4}{3}\pi$ internal angles. Consider the sequence of polyiamonds $P =: P_0, P_1, \dots P_m$ where each P_i is obtained from P_{i-1} by adding an elementary rhombus to a corner corresponding to a $\frac{4}{3}\pi$ internal angle until no $\frac{4}{3}\pi$ internal angle is present. Then $p(P_i) = p(P_{i-1})$ for all i and $\|P_i\| = \|P_{i-1}\| + 2 = \|P\| + 2i$. Note that, if some of the P_i had elementary holes, $\frac{5}{3}\pi$ or $\frac{1}{3}\pi$ internal angles we could argue as above and obtain a contradiction. Then P_m should be, necessarily, a (non degenerate) hexagon.

To conclude, we rely on the following

Lemma 5.2.4. *Area and perimeter (both site and edge) of every hexagon have the same parity.*

Proof of Lemma 5.2.4. As already mentioned above, the area and both the site-perimeter and edge-perimeter of a hexagon E are computed to be $\|E\| = d^2 - (a^2 + b^2 + c^2)$ and $p(E) = 3d - (a + b + c)$ respectively, where a, b, c, d are parameters identifying the hexagon. The conclusion follows by observing that d has the same parity of d^2 and $(a + b + c)$ has the same parity of $(a^2 + b^2 + c^2)$. □

Observe that $\|P_m\|$ has the same parity of $\|R'_A\|$ (both ℓ and $2i$ are, indeed, even) whereas the edge-perimeters of these two polyiamonds differ by one and, hence, have different parities. Since P_m is a proper hexagon, this contradicts Lemma 5.2.4 completing the proof. □

We conclude this section by providing a lower bound for the edge-perimeter of *non standard* polyiamonds with area equal to the area of a quasi-regular hexagon.

Lemma 5.2.5. *Let $\bar{p}$ be the edge-perimeter of a quasi-regular hexagon and let $\bar{A}$ be its area. Then, for all $P \notin \mathcal{Q}$ such that $\|P\| = \bar{A}$, $p(P) \geq \bar{p} + 2$.*

Proof. The proof can be done following the same strategy of the proof of Theorem 4.1.22. Let $P \notin \mathcal{Q}$ be a polyiamond of area $\bar{A}$ where $\bar{A}$ is the area of a quasi-regular hexagon. By Lemma 5.2.3 it follows that $p(P) \geq \bar{p} + 1$. We will show that $p(P) = \bar{p} + 1$ can not hold. To this end, suppose $p(P) = \bar{p} + 1$. Then P can not have neither $\frac{5}{3}\pi$ internal angles nor elementary holes. Indeed, if it were the case, the polyiamond obtained by filling the angle or the hole would have area $\bar{A} + 1$ and edge-perimeter at most $\bar{p}$ contradicting Proposition 5.1.2. Consider, then, the sequence of polyiamonds $P =: P_0, P_1, \dots P_m$ where each P_i is obtained from P_{i-1} by adding an elementary rhombus to a corner corresponding to a $\frac{4}{3}\pi$ internal angle until no $\frac{4}{3}\pi$ internal angle is present. Then $p(P_i) = p(P_{i-1})$ for all i and $\|P_i\| = \|P_{i-1}\| + 2 = \|P\| + 2i$. Note that, if some of the P_i had either elementary holes or $\frac{5}{3}\pi$ internal angles we could argue as above and obtain a contradiction. Then P_m must be, necessarily, a hexagon, possibly degenerate, and, therefore, $p(P_m)$ and $\|P_m\|$ must have the same parity by Lemma 5.2.4. By construction, $\|P_m\|$ has the same parity of $\bar{A}$ and $p(P_m)$ has the same parity of $\bar{p} + 1$. Since $\bar{p}$ is the edge-perimeter of a quasi-regular hexagon of area $\bar{A}$, $\bar{p} + 1$ and $\bar{A}$ have different parities contradicting the hypothesis that P_m is a hexagon. □

Remark 5.2.6. *Note that, in the case of site-perimeter, the analogue of the property of the previous lemma does not hold.*

Indeed, a counterexample is given by the polyiamond obtained by removing an elementary rhombus from one corner of the hexagon and moving it on top of a side of the hexagon. The polyiamond obtained in this way has site-perimeter $\bar{p} + 1$.

Conclusions

With the shaken dynamics we exhibit a reversible parallel dynamics which can be defined on arbitrary graphs and whose invariant measure is explicitly given. In particular, this is one of the main features of this dynamics. Indeed, we identify the stationary measure under general conditions, that is in the presence of an external field and on general graphs. Moreover, in the case of the square lattice we control this measure for different boundary conditions.
The second interesting property of our dynamics concern the possibility to tune the geometry of the system. Indeed, the shaken prescription allows to explore different geometries in the systems in two ways:

- with the doubling construction the shaken dynamics turns out to be the marginal of a parallel alternate dynamics defined on a new bipartite graph usually very different from the original one;
- modifying suitably the parameters appearing in the doubled Hamiltonian, it is possible to compare spin systems defined on different geometries. Indeed, when the self-interaction parameter q tends to zero or tends to infinity, the doubling graph changes, cutting the corresponding edge or collapsing the two extremal vertices respectively. In particular, the limit $q \to 0$ leads to a system whose geometry has a different dimension. Finally, when $q = J$, the doubling graph is homogeneous.

Another relevant aspect of the shaken dynamics is the possibility to use this parallel algorithm to solve optimization problems on arbitrary graphs and to sample from the Gibbs measure on the square lattice.
The shaken dynamics belongs to a wide research program aiming at constructing a statistical mechanics model for friction. Even though our dynamics shows interesting properties, clearly this toy model is very far from describing real systems affected by friction. A further step consists in considering a time-dependent external field in the interaction Hamiltonian. With R. D'Autilia, B. Scoppola, E. Scoppola and A. Troiani, we are now studying a simple Curie Weiss model where the Hamiltonian is defined on the set of spin configurations $\mathcal{X}_N$ on the

complete graph K_N, *i.e.*, $\mathcal{X}_N = \{-1,1\}^N$

$$H(\sigma) = -\frac{J}{2} \sum_{i,j\in\{1,\dots,N\}} \sigma_i\sigma_j - h(t) \sum_{i\in\{1,\dots,N\}} \sigma_i \tag{5.2.2}$$

with ferromagnetic interaction $J > 0$ and external field depending on time

$$h(t) = -\alpha_0 + F(t) \tag{5.2.3}$$

with $\alpha_0 > J$, $\beta J > 1$ and $F(t)$ evolving with the following rule depending on the evolution of the mean magnetization $m(t)$

$$F(t+1) = \Big(F(t) + \frac{v}{N}\Big)\mathbb{1}_{\{m(t)<m^*\}}, \quad F(0) = 0 \tag{5.2.4}$$

where $m^* = \sqrt{1-\frac{1}{\beta J}}$. In particular, the mean magnetization evolves according to a *random dynamics* in terms of a random walk on

$$\mathcal{A}_N := \{-1, -1+\frac{2}{N}, \cdots -1+\frac{2k}{N}, \dots, 1-\frac{2}{N}, 1\}$$

corresponding to a random flip of a single spin of the complete graph. This model seems to be more realistic and some preliminary theoretic results seem to be consistent with the physics characterizing stick-slip events. This is the object of a forthcoming work.

Another open problem concerning the shaken dynamics is the study of its convergence to equilibrium. In this regard, it is interesting to investigate the role of the parameter q when studying the decay of metastable states in the low temperature regime. This could lead to detailed estimates of the mixing time. In particular, it is possible to show that the parameter q tunes the shape of the critical droplet. Indeed, in the case of the non homogeneous hexagonal lattice with $q = 2J$ the clusters having minimal perimeter for fixed area have no more the shape of a hexagon but they are diamond clusters. Thus, an extension of the analysis presented in [4] could involve a non uniform interaction among the spins in the Ising Hamiltonian, *i.e.* a non homogeneous hexagonal lattice, and could represent a preliminary step towards the study of the tunneling time of the shaken dynamics in the low temperature regime. On the other hand, the phenomenology of metastability for a stochastic dynamics with parallel updating rule may be different from the one observed in the case of the serial implementation of the single spin flip dynamics. This is the case of the parallel alternate dynamics on the square lattice considered in [28]. Therefore, the analysis of metastability for the stochastic

parallel alternate dynamics on the hexagonal lattice associated to the shaken dynamics could extend the results obtained for the homogeneous square lattice in [28].

References

[1] Michael Aizenman, JT Chayes, L Chayes, and CM Newman. "Discontinuity of the magnetization in one-dimensional $1/|x-y|^2$ Ising and Potts models". In: *Journal of Statistical Physics* 50.1 (1988), pp. 1–40.

[2] Valentina Apollonio, Roberto D'Autilia, Benedetto Scoppola, Elisabetta Scoppola, and Alessio Troiani. "Criticality of measures on 2-d Ising configurations: from square to hexagonal graphs". In: *Journal of Statistical Physics* 177.5 (2019), pp. 1009–1021.

[3] Valentina Apollonio, Roberto D'Autilia, Benedetto Scoppola, Elisabetta Scoppola, and Alessio Troiani. "Shaken dynamics: an easy way to parallel MCMC". In: *arXiv preprint arXiv:1904.06257* (2019).

[4] Valentina Apollonio, Vanessa Jacquier, Francesca Romana Nardi, and Alessio Troiani. "Metastability for the Ising model on the hexagonal lattice". In: *arXiv preprint arXiv:2101.11894* (2021).

[5] Kaveh Bashiri. "A note on the metastability in three modifications of the standard Ising model". In: *arXiv preprint arXiv:1705.07012* (2017).

[6] Johel Beltran and Claudio Landim. "Tunneling and metastability of continuous time Markov chains". In: *Journal of Statistical Physics* 140.6 (2010), pp. 1065–1114.

[7] Johel Beltrán and Claudio Landim. "Tunneling and metastability of continuous time Markov chains II, the nonreversible case". In: *Journal of Statistical Physics* 149.4 (2012), pp. 598–618.

[8] Gérard Ben Arous and Raphaël Cerf. "Metastability of the three dimensional Ising model on a torus at very low temperatures". In: *Electronic Journal of Probability* 1 (1996).

[9] Gianmarco Bet, Vanessa Jacquier, and Francesca R Nardi. "Effect of energy degeneracy on the transition time for a series of metastable states: application to Probabilistic Cellular Automata". In: *arXiv preprint arXiv:2007.08342* (2020).

[10] Alessandra Bianchi, Anton Bovier, Dmitry Ioffe, et al. "Sharp asymptotics for metastability in the random field Curie-Weiss model". In: *Electronic Journal of Probability* 14 (2009), pp. 1541–1603.

[11] Alessandra Bianchi and Alexandre Gaudilliere. "Metastable states, quasi-stationary distributions and soft measures". In: *Stochastic Processes and their Applications* 126.6 (2016), pp. 1622–1680.

[12] Anton Bovier and Frank Den Hollander. *Metastability: a potential-theoretic approach*. Vol. 351. Springer, 2016.

[13] Anton Bovier, Michael Eckhoff, Véronique Gayrard, and Markus Klein. "Metastability and Low Lying Spectra in Reversible Markov Chains". In: *Communications in mathematical physics* 228.2 (2002), pp. 219–255.

[14] Anton Bovier, Michael Eckhoff, Véronique Gayrard, and Markus Klein. "Metastability in reversible diffusion processes I. Sharp asymptotics for capcities and exit times". In: (2004).

[15] Anton Bovier, Frank den Hollander, and Cristian Spitoni. "Homogeneous nucleation for Glauber and Kawasaki dynamics in large volumes at low temperatures". In: *Annals of probability* 38.2 (2010), pp. 661–713.

[16] Anton Bovier and Francesco Manzo. "Metastability in Glauber dynamics in the low-temperature limit: beyond exponential asymptotics". In: *Journal of statistical physics* 107.3 (2002), pp. 757–779.

[17] Raffi Budakian and Seth J Putterman. "Time scales for cold welding and the origins of stick-slip friction". In: *Physical Review B* 65.23 (2002), p. 235429.

[18] Robert Burridge and Leon Knopoff. "Model and theoretical seismicity". In: *Bulletin of the seismological society of america* 57.3 (1967), pp. 341–371.

[19] Marzio Cassandro, Antonio Galves, Enzo Olivieri, and Maria Eulália Vares. "Metastable behavior of stochastic dynamics: a pathwise approach". In: *Journal of statistical physics* 35.5 (1984), pp. 603–634.

[20] Olivier Catoni and Raphaël Cerf. "The exit path of a Markov chain with rare transitions". In: *ESAIM: Probability and Statistics* 1 (1997), pp. 95–144.

[21] Raphaël Cerf and Francesco Manzo. "Nucleation and growth for the Ising model in d dimensions at very low temperatures". In: *Annals of Probability* 41.6 (2013), pp. 3697–3785.

[22] David Cimasoni. "Dimers on graphs in non-orientable surfaces". In: *Letters in Mathematical Physics* 87.1-2 (2009), p. 149.

[23] David Cimasoni. "A generalized Kac–Ward formula". In: *Journal of Statistical Mechanics: Theory and Experiment* 2010.07 (2010), P07023.

[24] David Cimasoni. "The geometry of dimer models". In: *Winter Braids Lecture Notes* 1 (2014), pp. 1–14.

[25] David Cimasoni and Hugo Duminil-Copin. "The critical temperature for the Ising model on planar doubly periodic graphs". In: *Electronic Journal of Probability* 18 (2013).

[26] David Cimasoni and Nicolai Reshetikhin. "Dimers on surface graphs and spin structures. I". In: *Communications in Mathematical Physics* 275.1 (2007), pp. 187–208.

[27] Emilio NM Cirillo. "A note on the metastability of the Ising model: the alternate updating case". In: *Journal of statistical physics* 106.1-2 (2002), pp. 385–390.

[28] Emilio NM Cirillo and Francesca R Nardi. "Metastability for a stochastic dynamics with a parallel heat bath updating rule". In: *Journal of statistical physics* 110.1-2 (2003), pp. 183–217.

[29] Emilio NM Cirillo and Francesca R Nardi. "Relaxation height in energy landscapes: an application to multiple metastable states". In: *Journal of Statistical Physics* 150.6 (2013), pp. 1080–1114.

[30] Emilio NM Cirillo and Francesca R Nardi. “Relaxation height in energy landscapes: an application to multiple metastable states”. In: *Journal of Statistical Physics* 150.6 (2013), pp. 1080–1114.

[31] Emilio NM Cirillo, Francesca R Nardi, and Julien Sohier. “Metastability for general dynamics with rare transitions: escape time and critical configurations”. In: *Journal of Statistical Physics* 161.2 (2015), pp. 365–403.

[32] Emilio NM Cirillo, Francesca R Nardi, and Cristian Spitoni. “Metastability for reversible probabilistic cellular automata with self-interaction”. In: *Journal of Statistical Physics* 132.3 (2008), pp. 431–471.

[33] Emilio NM Cirillo, Francesca R Nardi, and Cristian Spitoni. “Sum of exit times in a series of two metastable states”. In: *The European Physical Journal Special Topics* 226.10 (2017), pp. 2421–2438.

[34] Emilio NM Cirillo and Enzo Olivieri. “Metastability and nucleation for the Blume-Capel model. Different mechanisms of transition”. In: *Journal of statistical physics* 83.3 (1996), pp. 473–554.

[35] F Corbi, F Funiciello, C Faccenna, G Ranalli, and A Heuret. “Seismic variability of subduction thrust faults: Insights from laboratory models”. In: *Journal of Geophysical Research: Solid Earth* 116.B6 (2011).

[36] Paolo Dai Pra, Benedetto Scoppola, and Elisabetta Scoppola. “Sampling from a Gibbs measure with pair interaction by means of PCA”. In: *Journal of Statistical Physics* 149.4 (2012), pp. 722–737.

[37] Paolo Dai Pra, Benedetto Scoppola, and Elisabetta Scoppola. “Fast mixing for the low temperature 2D ising model through irreversible parallel dynamics”. In: *Journal of Statistical Physics* 159.1 (2015), pp. 1–20.

[38] Elisa Davoli, Paolo Piovano, and Ulisse Stefanelli. “Sharp $N^{3/4}$ Law for the Minimizers of the Edge-Isoperimetric Problem on the Triangular Lattice”. In: *Journal of nonlinear science* 27.2 (2017), pp. 627–660.

[39] Pouria Dehghanpour and Roberto H Schonmann. “Metropolis dynamics relaxation via nucleation and growth”. In: *Communications in mathematical physics* 188.1 (1997), pp. 89–119.

[40] C Drummond, J Israelachvili, and Ph Richetti. “Friction between two weakly adhering boundary lubricated surfaces in water”. In: *Physical Review E* 67.6 (2003), p. 066110.

[41] Robert G Edwards and Alan D Sokal. “Generalization of the fortuin-kasteleyn-swendsen-wang representation and monte carlo algorithm”. In: *Physical review D* 38.6 (1988), p. 2009.

[42] Roberto Fernandez, Francesco Manzo, Francesca Nardi, and Elisabetta Scoppola. “Asymptotically exponential hitting times and metastability: a pathwise approach without reversibility”. In: *Electronic Journal of Probability* 20 (2015).

[43] Roberto Fernandez, Francesco Manzo, Francesca Romana Nardi, Elisabetta Scoppola, and Julien Sohier. “Conditioned, quasi-stationary, restricted measures and escape from metastable states”. In: *Annals of Applied Probability* 26.2 (2016), pp. 760–793.

[44] Roberto Fernandez and Andre Toom. “Non-Gibbsianness of the invariant measures of non-reversible cellular automata with totally asymmetric noise”. In: *arXiv preprint math-ph/0101014* (2001).

[45] Michael E Fisher. “Statistical mechanics of dimers on a plane lattice”. In: *Physical Review* 124.6 (1961), p. 1664.

[46] Michael E Fisher. “On the dimer solution of planar Ising models”. In: *Journal of Mathematical Physics* 7.10 (1966), pp. 1776–1781.

[47] Cornelius Marius Fortuin and Piet W Kasteleyn. “On the random-cluster model: I. Introduction and relation to other models”. In: *Physica* 57.4 (1972), pp. 536–564.

[48] RH Fowler and GS Rushbrooke. “An attempt to extend the statistical theory of perfect solutions”. In: *Transactions of the Faraday Society* 33 (1937), pp. 1272–1294.

[49] Ya I Frenkel and TA Kontorova. “see phys. z. sowietunion 13 1”. In: *Zh. Eksp. Teor. Fiz* 8 (1938), p. 89.

[50] Gábor Fülep and Nándor Sieben. “Polyiamonds and polyhexes with minimum site-perimeter and achievement games.” In: *The Electronic Journal of Combinatorics [electronic only]* 17.1 (2010), v17i1r65–pdf.

[51] Alexandre Gaudilliere and Claudio Landim. “A Dirichlet principle for non reversible Markov chains and some recurrence theorems”. In: *Probability Theory and Related Fields* 158.1-2 (2014), pp. 55–89.

[52] Alexandre Gaudillière, Paolo Milanesi, and Maria Eulália Vares. “Asymptotic exponential law for the transition time to equilibrium of the metastable kinetic Ising model with vanishing magnetic field”. In: *Journal of Statistical Physics* 179.2 (2020), pp. 263–308.

[53] Geoffrey R Grimmett. “Random-Cluster Measures”. In: *The Random-Cluster Model* (2006), pp. 1–18.

[54] Berit Grußien. “Isoperimetric Inequalities on Hexagonal Grids”. In: *arXiv preprint arXiv:1201.0697* (2012).

[55] Heng Guo and Mark Jerrum. “Random cluster dynamics for the Ising model is rapidly mixing”. In: *Proceedings of the Twenty-Eighth Annual ACM-SIAM Symposium on Discrete Algorithms*. SIAM. 2017, pp. 1818–1827.

[56] Frank den Hollander, Francesca R Nardi, and Siamak Taati. “Metastability of hard-core dynamics on bipartite graphs”. In: *Electronic Journal of Probability* 23 (2018).

[57] Charles A Hurst and Herbert S Green. “New solution of the Ising problem for a rectangular lattice”. In: *The Journal of Chemical Physics* 33.4 (1960), pp. 1059–1062.

[58] Antonio Iovanella, Benedetto Scoppola, and Elisabetta Scoppola. “Some spin glass ideas applied to the clique problem”. In: *Journal of Statistical Physics* 126.4 (2007), pp. 895–915.

[59] Oliver Jovanovski. “Metastability for the Ising Model on the hypercube”. In: *Journal of Statistical Physics* 167.1 (2017), pp. 135–159.

[60] Mark Kac and John C Ward. “A combinatorial solution of the two-dimensional Ising model”. In: *Physical Review* 88.6 (1952), p. 1332.

[61] Pieter W Kasteleyn. “The statistics of dimers on a lattice: I. The number of dimer arrangements on a quadratic lattice”. In: *Physica* 27.12 (1961), pp. 1209–1225.

[62] Roman Kotecký and Enzo Olivieri. “Droplet dynamics for asymmetric Ising model”. In: *Journal of statistical physics* 70.5 (1993), pp. 1121–1148.

[63] Roman Kotecký and Enzo Olivieri. "Shapes of growing droplets—a model of escape from a metastable phase". In: *Journal of statistical physics* 75.3 (1994), pp. 409–506.

[64] O Kozlov and N Vasilyev. "Reversible Markov chains with local interaction". In: *Multicomponent random systems* 6 (1980), pp. 451–469.

[65] Carlo Lancia and Benedetto Scoppola. "Equilibrium and non-equilibrium Ising models by means of PCA". In: *Journal of Statistical Physics* 153.4 (2013), pp. 641–653.

[66] Carlo Lancia and Benedetto Scoppola. "Ising Model on the Torus and PCA Dynamics: Reversibility, Irreversibility, and Fast Tunneling". In: *Probabilistic Cellular Automata*. Springer, 2018, pp. 89–104.

[67] Joel L Lebowitz, Christian Maes, and Eugene R Speer. "Statistical mechanics of probabilistic cellular automata". In: *Journal of statistical physics* 59.1-2 (1990), pp. 117–170.

[68] Martin Loebl. "A discrete non-Pfaffian approach to the Ising problem". In: (2003).

[69] Francesco Manzo, Francesca R Nardi, Enzo Olivieri, and Elisabetta Scoppola. "On the essential features of metastability: tunnelling time and critical configurations". In: *Journal of Statistical Physics* 115.1 (2004), pp. 591–642.

[70] Francesco Manzo, Francesca R Nardi, Enzo Olivieri, and Elisabetta Scoppola. "On the essential features of metastability: tunnelling time and critical configurations". In: *Journal of Statistical Physics* 115.1-2 (2004), pp. 591–642.

[71] Francesco Manzo and Enzo Olivieri. "Relaxation patterns for competing metastable states: a nucleation and growth model". In: *Markov Proc. Relat. Fields*. Vol. 4. 1998, pp. 549–570.

[72] Francesco Manzo and Enzo Olivieri. "Dynamical Blume–Capel model: competing metastable states at infinite volume". In: *Journal of Statistical Physics* 104.5 (2001), pp. 1029–1090.

[73] Benedek Nagy and Krisztina Barczi. "Isoperimetrically optimal polygons in the triangular grid with Jordan-type neighbourhood on the boundary". In: *International Journal of Computer Mathematics* 90.8 (2013), pp. 1629–1652.

[74] Francesca R Nardi and Enzo Olivieri. "Low temperature stochastic dynamics for an Ising model with alternating field". In: *Markov Proc. Relat. Fields*. Vol. 2. 1996, pp. 117–166.

[75] Francesca R Nardi and Cristian Spitoni. "Sharp asymptotics for stochastic dynamics with parallel updating rule". In: *Journal of statistical physics* 146.4 (2012), pp. 701–718.

[76] Francesca R Nardi and Alessandro Zocca. "Tunneling behavior of Ising and Potts models in the low-temperature regime". In: *Stochastic Processes and their Applications* 129.11 (2019), pp. 4556–4575.

[77] Francesca R Nardi, Alessandro Zocca, and Sem C Borst. "Hitting time asymptotics for hard-core interactions on grids". In: *Journal of Statistical Physics* 162.2 (2016), pp. 522–576.

[78] E Jordao Neves and Roberto H Schonmann. "Critical droplets and metastability for a Glauber dynamics at very low temperatures". In: *Communications in Mathematical Physics* 137.2 (1991), pp. 209–230.

[79] E Jordão Neves and Roberto H Schonmann. "Behavior of droplets for a class of Glauber dynamics at very low temperature". In: *Probability theory and related fields* 91.3-4 (1992), pp. 331–354.

[80] Enzo Olivieri and Elisabetta Scoppola. "Markov chains with exponentially small transition probabilities: first exit problem from a general domain. I. The reversible case". In: *Journal of statistical physics* 79.3 (1995), pp. 613–647.

[81] Enzo Olivieri and Elisabetta Scoppola. "Markov chains with exponentially small transition probabilities: first exit problem from a general domain. II. The general case". In: *Journal of statistical physics* 84.5 (1996), pp. 987–1041.

[82] Enzo Olivieri and Maria Eulália Vares. *Large deviations and metastability*. 100. Cambridge University Press, 2005.

[83] Ludwig Prandtl. "A conceptual model to the kinetic theory of solid bodies". In: *Z. Angew. Math. Mech* 8 (1928), pp. 85–106.

[84] Aldo Procacci, Benedetto Scoppola, and Elisabetta Scoppola. "Probabilistic Cellular Automata for Low-Temperature 2-d Ising Model". In: *Journal of Statistical Physics* 165.6 (2016), pp. 991–1005.

[85] Bernd Schmidt. "Ground states of the 2D sticky disc model: fine properties and N 3/4 law for the deviation from the asymptotic Wulff shape". In: *Journal of Statistical Physics* 153.4 (2013), pp. 727–738.

[86] Roberto H Schonmann. "Slow droplet-driven relaxation of stochastic Ising models in the vicinity of the phase coexistence region". In: *Communications in Mathematical Physics* 161.1 (1994), pp. 1–49.

[87] Roberto H Schonmann and Senya B Shlosman. "Wulff droplets and the metastable relaxation of kinetic Ising models". In: *Communications in mathematical physics* 194.2 (1998), pp. 389–462.

[88] Elisabetta Scoppola. "Metastability for Markov chains: a general procedure based on renormalization group ideas". In: *Probability and Phase Transition*. Springer, 1994, pp. 303–322.

[89] Harold NV Temperley and Michael E Fisher. "Dimer problem in statistical mechanics-an exact result". In: *Philosophical Magazine* 6.68 (1961), pp. 1061–1063.

[90] GA Tomlinson. "CVI. A molecular theory of friction". In: *The London, Edinburgh, and Dublin philosophical magazine and journal of science* 7.46 (1929), pp. 905–939.

[91] Andrea Vanossi, Nicola Manini, Michael Urbakh, Stefano Zapperi, and Erio Tosatti. "Colloquium: Modeling friction: From nanoscale to mesoscale". In: *Reviews of Modern Physics* 85.2 (2013), p. 529.

[92] Alessandro Zocca. "Tunneling of the hard-core model on finite triangular lattices". In: *Random Structures & Algorithms* 55.1 (2019), pp. 215–246.